Development of a Hypoxia-Activated Trehalose Diester for the Treatment of Solid Tumours

By

Amy Jane Foster

2014

A thesis submitted to Victoria University of Wellington
In fulfilment of the requirements for the degree of
Master of Biomedical Science

Abstract

The potential of bacterial cell wall components in the treatment of various cancers was initially realised in the late 1800s during pioneering work with Coley's toxins. Since this preliminary work, efforts have been concentrated on the isolation and identification of bacterial components that lead to tumour regression. Trehalose dimycolates (TDMs) are compounds isolated from the *M. tuberculosis* cell wall and are known to activate macrophages to give a polarised Th1 immune response resulting in reduced tumour burden. Consequently, TDMs have shown great promise in the treatment of solid tumours.

In this thesis, work is presented towards the synthesis of trehalose glycolipid prodrugs that will be specifically activated inside the hypoxic tumour microenvironment, and thereby lead to a more selective form of cancer therapy. These hypoxia-activated trehalose glycolipids incorporate a nitroimidazole trigger that fragments upon enzymatic reduction (in the absence of oxygen) to give the active glycolipid. Throughout the course of this work, it was determined that the nitroimidazole trigger group could not be directly attached to the glycolipid and thus, an alternative carbonate-linker strategy was explored through the use of a reporter fluoroprobe. The validity of this approach was determined in various enzyme and cell-based assays.

Acknowledgments

There have been many people that have contributed to my Masters journey, and without their guidance and support, this thesis would not be what it is. First of all, I would like to extend my most sincere gratitude to Drs Mattie Timmer and Bridget Stocker, who time and time again have gone above and beyond the call of their supervisory duties. Thank you for the endless supply of encouragement. Your unwavering commitment to your work and students does not go unappreciated.

Next, I would like to acknowledge to the past and present members of the immunoglycomics group: Alex, Anna, Ashna, Ben, Janelle, Janice, Jaime, Jessie, Kris, Kristel, Hilary, Rhia, Stefan, and Steph. Every one of you has contributed to making the lab a great place to work. I would specifically like to thank Hilary Corkran and Rhia Stone for their boundless support. I can always count on both of you to laugh at my stupid jokes and to encourage me to keep on going. Additionally, I would like to acknowledge Drs Elsie Williams and Laura Green for all the help with biology related matters.

I would also like to personally acknowledge Jessie Bird. I could not imagine a better person to have gone through this process with. I have had such a memorable 4-5 years with all the junk food runs, late night lab dancing, chess, and squash games. Yours is a friendship I will treasure for life.

Finally, I would like to extend my thanks to my other friends and family that have stuck by me throughout this journey. First and foremost, to my parents who have provided me with unconditional love and support. The perspective you have provided me with has been invaluable. To my brothers, who were always there for a chat and a laugh. To Struan, who has provided me with food, support, and many argumentative discussions on what can only be described as truly unimportant matters. Last but not least, I would like to thank my flatmate, Rachel, who has kept me sane throughout these last few months. Thank you for your compassion and understanding.

Abbreviations

AcOH	Acetic acid
ARNT	Aryl hydrocarbon receptor nuclear translocator
BCG	Bacillus Calmette-Guerin
BMM	Bone marrow-derived macrophages
Calcd.	Calculated
CBP	CREB-binding protein
COSY	Correlated NMR spectrum
CREB	cAMP response element-binding protein
CSA	Camphorsulfonic acid
d	Doublet
dd	Doublet of doublets
DCM	Dichloromethane
DMAP	4-(dimethyl)-aminopyridine
DMEM	Dulbecco's Modified Eagle Medium
DMF	Dimethyl formamide
DMSO	Dimethyl sulfoxide
DNA	Deoxyribonucleic acid
EPO	Erythropoietin
Eq.	Equivalent
ESI	Electron spray ionisation
Et	Ethyl
EtOAc	Ethyl acetate
FDA	Food and drug administration
G-CSF	Granulocyte colony-stimulating factor
GM-CSF	Granulocyte macrophage-colony stimulating factor
HIF-1	Hypoxia-inducible factor 1
HMBC	Heteronuclear multiple quantum coherence
HRE	Hypoxia responsive element
HRMS	High-resolution mass spectrometry
HSQC	Heteronuclear single quantum coherence
Hz	Hertz
IFN	Interferon
IL	Interleukin
IR	Infrared
J	Coupling constant
LPS	Lipopolysaccharide
m	Multiplet
M-CSF	Macrophage colony-stimulating factor
MS	Mass spectral
Me	Methyl
MHz	Megahertz
min.	Minutes
Mincle	Macrophage inducible C-type lectin
MMP	Matrix metalloproteinase
Mp	Melting point

MTP-PE	Muramyl tripeptide phosphatidylethanolamine
m/z	Mass to charge ratio
NAD	Nicotinamide adenine dinucleotide
NMR	Nuclear magnetic resonance
NO	Nitric oxide
Obsd.	Observed
PBS	Phosphate-buffered saline
PCR	Polymerase chain reaction
PE	Petroleum ether
PGE2	Prostaglandin E2
pO_2	Oxygen partial pressure
Pol II	polymerase II
ppm	Parts per million
PRR	Pathogen pattern recognition receptor
r.t.	Room temperature
s	Singlet
t	Triplet
TAM	Tumour-associated macrophage
TBAI	Tetrabutylammonium iodide
TDB	Trehalose dibehenate
TDE	Trehalose diester
TDM	Trehalose dimycolate
TGF	Transforming growth factor
THF	Tetrahydrofuran
TLC	Thin layer chromatography
TLR	Toll-like receptor
TNF	Tumour necrosis factor
TPZ	Tirapazamine
Ub	Ubiquitin
VEGF	Vascular endothelial growth factor
VHL	Von Hippel-Lindau

Table of Contents

1. Introduction

1.1 The war on cancer: A historical perspective

With its recorded history spanning centuries, cancer has emerged as one of the leading causes of death worldwide, accounting for approximately one in every four deaths in the United States, and 30% of all deaths in New Zealand.[1-3] Early attempts at the treatment of cancer were largely centred around the surgical removal of neoplastic tissue, however, due to the metastatic nature of cancerous cells, this approach yielded limited success.[4, 5] After Röntgen's discovery of x-rays, radiation therapy gained popularity, proving successful in the treatment of benign cancers.[4, 6] Like surgical intervention, however, radiotherapy is a localised approach and fails to treat metastatic tissue.

With the realisation that the successful eradication of cancerous tissue would likely require a multi-locational tactic, efforts toward the war on cancer were redirected into drug-mediated therapy.[4, 5] During World War II, Louis Goodman and Alfred Gilman were commissioned by the Federal Government to evaluate the therapeutic potential of a range of compounds originally developed for chemical warfare.[4] Throughout their time with the Department of Defence, they successfully demonstrated the ability of nitrogen mustard to induce tumour regression in a patient with non-Hodgkin's lymphoma and thus, for the first time in recorded history, established the potential of chemotherapy in the treatment of cancer.[4, 7] Since this initial discovery, many topoisomerase inhibitors, DNA alkylating agents, and anti-metabolites have been successfully developed and approved by the Food and Drug Administration (FDA) for the treatment of cancer.[4] By the mid to late 1980s, however, progress in the development of new, more efficacious chemotherapy agents slowed markedly, indicating a need to change strategies. Accordingly, biologists have revolutionised our understanding of cellular processes at the molecular level, identifying signalling pathways, cell-cycle proteins, and other physiological markers unique to cancerous cells. Exploitation of these markers has catapulted the world into the current era of targeted therapy.

1.1 Tumour Hypoxia: A potential target for cancer therapy

Modern day anti-cancer therapeutics predominately employ cytotoxic drugs that target rapidly dividing cells. Therapeutics of this category typically have the capacity to kill large numbers of cancerous cells by altering their DNA. However, as these drugs target dividing cells, rather than a specific marker, they are not overly selective and cause extensive damage to healthy tissue.[8, 9] This lack of selectivity is especially true in tumours which, due to poor vasculature, divide relatively slowly.[8] Tumour hypoxia is a characteristic of solid tumours first established by Thomlinson and Gray while studying the histological structure of human lung cancers.[10, 11] Hypoxia is described by an oxygen deficiency within the tumour microenvironment.[12] This hypoxia can be chronic, due to the limited diffusion capacity of oxygen, or transient, resulting from the temporary occlusion of aberrant blood vessels.[11, 12] Under the stress of hypoxic conditions, cells typically make a series of changes to their metabolic pathways allowing them to thrive in their new environment.

1.1.1 The HIF-1 pathway

A well-documented pathway that is altered in response to hypoxia is the hypoxia-inducible transcription factor one (HIF-1) pathway (Figure 1).[13-15] The HIF-1 complex is a heterodimer comprised of the hypoxic response factor, HIF-1α, and the arylhydrocarbon receptor nuclear translocator (ARNT).[16] Under well-oxygenated conditions, prolyl hydroxylase alters the structure HIF-1α, thereby permitting it to interact with the von Hippel-Lindau (VHL) complex.[17-19] This complex, together with the E2 ubiquitin enzyme, tags HIF-1α for degradation in the proteasome. Alternatively, in hypoxic tissue, prolyl hydroxylase is prevented from modifying HIF-1α, and is consequently translocated into the nucleus where it can interact with other factors such as ARNT, CBP/p300, and DNA polymerase II (Pol II complex), thereby allowing it to bind to the hypoxia responsive elements (HRE).[16] Binding of HRE induces the transcription of genes including vascular endothelial growth factor (VEGF) and erythropoietin (EPO), thereby promoting angiogenesis and vasodilation within the tumour environment.

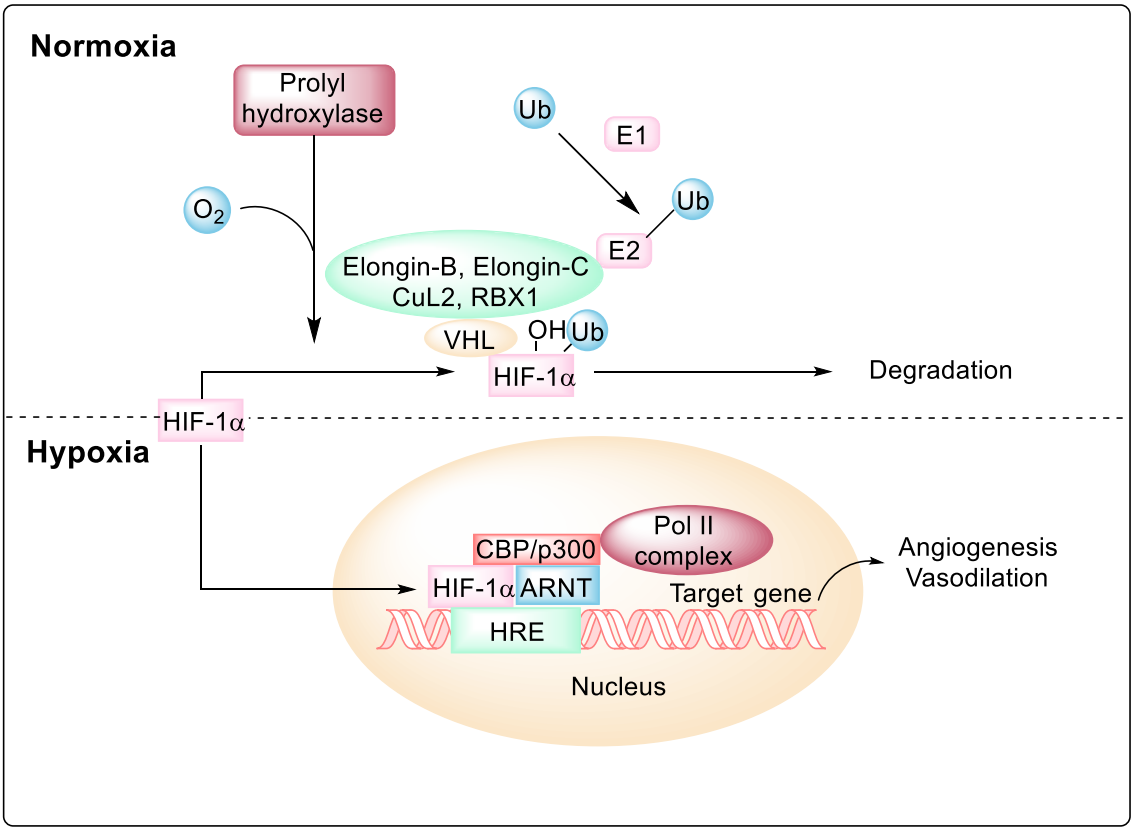

Figure 1: HIF-1 pathway under normoxic (well-oxygenated) and hypoxic conditions.

1.1.2 Hypoxia confers resistance to current treatments

Hypoxia is also known to confer cellular resistance to current cancer treatments. As hypoxic cells are found at a distance to blood vessels, the delivery of chemotherapy agents to the tumour site can be challenging due to low perfusion rates throughout the tumour.[11, 20] Additionally, hypoxia is responsible for the upregulation of genes involved in drug resistance, can select for cells insensitive to p-53-mediated apoptosis, and increases the mutation rate in cancerous cells.[21] Hypoxic cells have also been shown to be resistant to radiotherapy, as the presence of oxygen is required to complete the necessary DNA strand breaks.[22] Although tumour hypoxia represents a major problem in current cancer therapies, it also presents itself as an attractive target for new therapies. The proportion of hypoxic cells within a solid tumour can range from 0.2% to 50% of the tumour's total mass.[23] Well-oxygenated tissues have oxygen partial pressures (pO_2) from 50 mmHg to 80 mmHg, while hypoxic tissues have a reduced pO_2 of 10 to 30 mmHg. This distinction between

normal and cancerous tissue exposes tumour hypoxia as a potential target for selective cancer therapy.

1.3 Hypoxia-activated prodrugs

Hypoxia-activated prodrugs are intended to be innocuous compounds that are only activated when delivered to hypoxic regions of the body.[12] These prodrugs are typically composed of two modules: the trigger and effector components (Figure 2).[8, 12] In some cases, there may also be a linker region to bridge the trigger and effector modules. The effector is responsible for mediating the therapeutic effect of the drug and should rapidly exert its effects and diffuse efficiently throughout the tumour.[20] The 'trigger' dictates the specificity of the therapy and must therefore be selectively metabolised under hypoxic conditions. Finally, the linker attaches the trigger to the effector resulting in an overall inactive compound under normal cellular pO_2.[20] That said, it is not always feasible to separate a prodrug into these distinct modules and the three-component prodrug model is intended to assist with basic prodrug design rather than to be strictly enforced.[12]

Figure 2: Modular design of hypoxia-activated prodrugs

1.3.1 Reductive activation of hypoxia-activated prodrugs

All hypoxia-activated prodrugs are initially reduced by two classes of enzymes.[24] The first of these groups, the one-electron reductases, includes enzymes such as NADH-cytochrome P450 reductase, cytochrome b5 reductase, and Xanthine oxidase.[25] One-electron reductions result in the formation of a radical anion (Figure 3).[20] If molecular oxygen is present, the anion will be re-oxidised to form the original prodrug. However, in a hypoxic environment, the radical anion will be further reduced resulting in activation of the drug.[20] In the case of two-electron reductions, however, formation of the radical anion is bypassed and therefore, these

reductions can occur independently of oxygen concentration.[26] Consequently, if a hypoxia-activated prodrug is a suitable substrate for a two-electron reductase, the prodrug's selectivity towards hypoxia could potentially be compromised. In saying this, in some situations, instead of reversing reduction reactions, molecular oxygen can act as a competitor for the enzyme active site. As a result, the presence of oxygen will inhibit the reduction of the therapeutic allowing for hypoxia selectivity.[12] Although there are limitations with this approach, it is still a very promising therapy and a number of hypoxia-activated prodrugs have reached clinical trials.[12, 27]

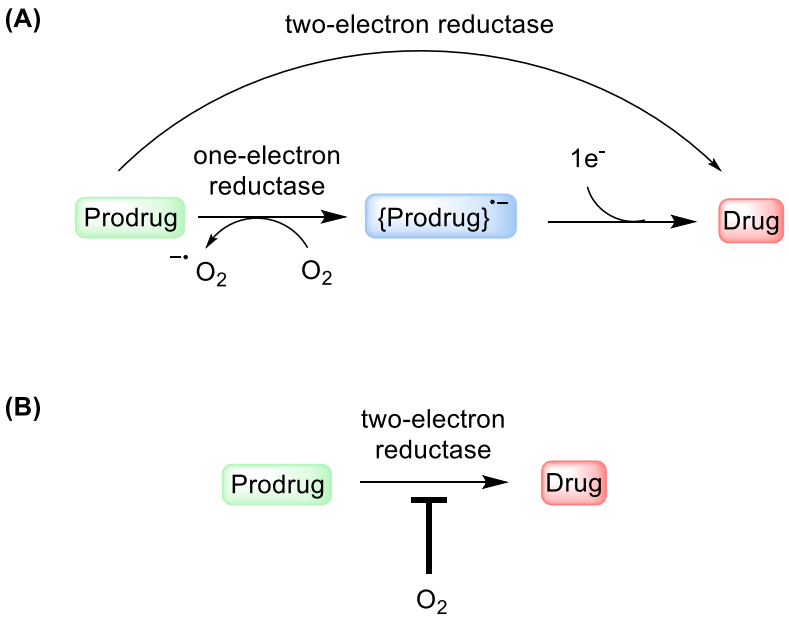

Figure 3: Bioreductive activation of hypoxia-activated prodrugs

1.1.1 Classification of reductively activated prodrugs

There are various ways hypoxia-activated prodrugs can be activated, though in general, these can be categorised into two main groups: intramolecular electron redistribution and intramolecular fragmentations.[28]

i) Intramolecular electron redistribution

Alterations to the electron distribution are commonly used to activate hypoxia prodrugs including nitroaromatic and *N*-oxide containing prodrugs. Installation of electron withdrawing groups, such as nitro-groups, at strategic positions within a suitable molecule can result in a redistribution of electron density.[20] In some cases, this redistribution of electron density results in the inactivation of the therapeutic. The reduction of the nitro-group to a more electron donating group, such as a hydroxylamine or an amine by reductive enzymes however, can result in the activation of that compound.[20] This reduction is often reversed by molecular oxygen so that the activation step will occur selectively in hypoxic conditions. An example of a prodrug from this class is the 4-nitroaniline mustard **1** (Figure 4).[29] Here, the nitro-precursor is reduced by cellular one-electron nitroreductases to the more electron donating species, 4-aminoaniline mustard **2**, which results in a 17,500-fold increase in potency. However, with this particular therapeutic, slow reduction of the nitro-precursor resulted in low hypoxia selectivity and has restricted its clinical use.[30]

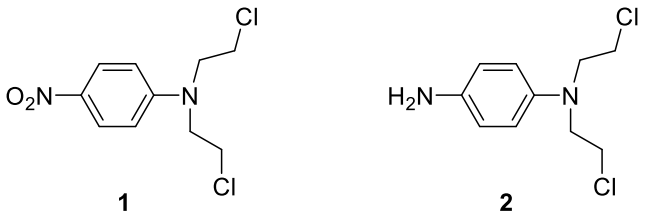

Figure 4: 4-nitroaniline mustard (**1**) and 4-aminoaniline mustard (**2**)

N-Oxides are a common substrate for intramolecular electron redistribution and are best represented by Tirapazamine (TPZ, **3**), which was first reported in the 1980s and is an example of an aromatic *N*-oxide.[31-33] TPZ is first reduced by various cellular reductase enzymes, including Cytochrome P450 reductase, to produce the TPZ radical **4**. In well-oxygenated tissues, radical **4** is re-oxidised by molecular

oxygen to regenerate the original prodrug (Scheme 1).[12, 24] Alternatively, in the absence of oxygen, the TPZ radical **4** can induce both single and double DNA strand breaks, thereby inducing cellular death.[27, 34] TPZ (**3**) has performed well in phase I and II clinical trials when used in combination with cisplatin and thus, the combination therapy was used in a phase III randomised clinical trial in patients with advanced non-small-cell lung cancer.[27, 35-37] The results from this trial indicated that the use of TPZ in conjunction with cisplatin leads to a doubling of the overall response to the treatment. Additionally, TPZ appears to be more selective than other nitroaromatic and quinone-based prodrugs as it maintains its cytotoxic capabilities at lower levels of hypoxia.[38]

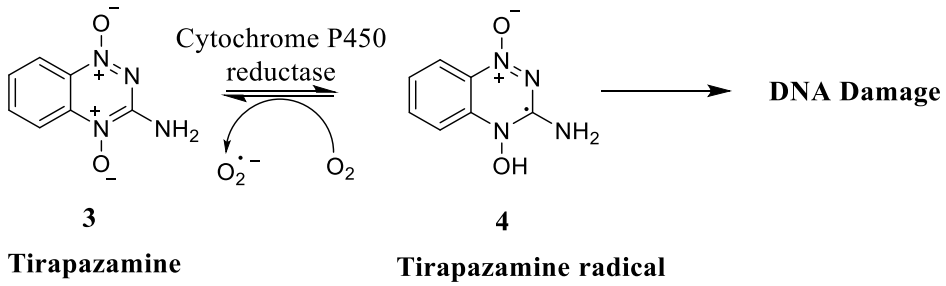

Scheme 1: Conversion of TPZ (**3**) to the oxidising TPZ radical **4**

Quaternary *N*-oxides are often employed to conceal the cationic nature of tertiary amines thereby decreasing binding affinity for DNA and inactivating the prodrug.[24] This category of prodrug is best represented by Banoxantrone (**5**, Figure 5), a hypoxia-activated prodrug that has been evaluated in a clinical setting. Here, Banoxantrone (**5**) is reduced by cytochrome P450's via a two-electron process to give the active drug.[12] However, in well-oxygenated tissue, molecular oxygen competes for the enzyme binding site, thereby inhibiting the reduction process.[20] Once reduced, the active compound **6** can bind directly to DNA and act as a topoisomerase inhibitor. The clinical efficacy of Banoxantrone has been evaluated in several phase I clinical trials.[24, 39-41] In one study, 32 patients with various forms of cancer received treatment with Banoxantrone before surgical intervention.[39] Levels of Banoxantrone and the active drug were measured in 95 tissues and were

then evaluated using Liquid chromatography-tandem mass spectrometry. The results showed the Banoxantrone was selectively activated in hypoxic regions of solid tumours, thus illustrating its potential as a novel anticancer agent.

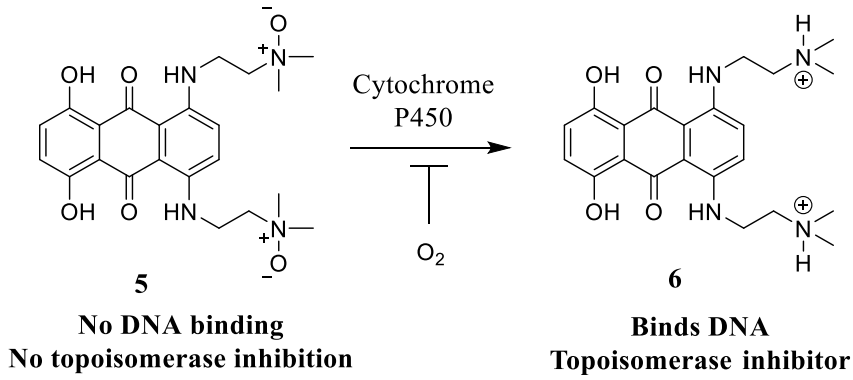

Figure 5: Selective activation of Banoxantrone (**5**) in hypoxic conditions

ii) Molecular fragmentation

The second category of hypoxia-activated prodrugs are activated via molecular fragmentation.[20] Here, the reduction of the prodrug induces molecular fragmentation in order to release the active therapeutic. This phenomenon is observed in varying classes of hypoxia-activated prodrugs including nitroaromatics, quinones, and transition metals.[31, 42]

Nitroaromatic compounds are reduced under hypoxic conditions by specific nitroreductase enzymes.[25] Here, the addition of one electron by the nitroreductase converts the nitro-group into a radical anion (Scheme 2).[20] If molecular oxygen is present, however, the anion will be re-oxidised to form the original prodrug. In a hypoxic environment, the radical anion will be further reduced to the hydroxylamine (or amine) causing the dissociation of the nitroaromatic group from the effector unit.[20]

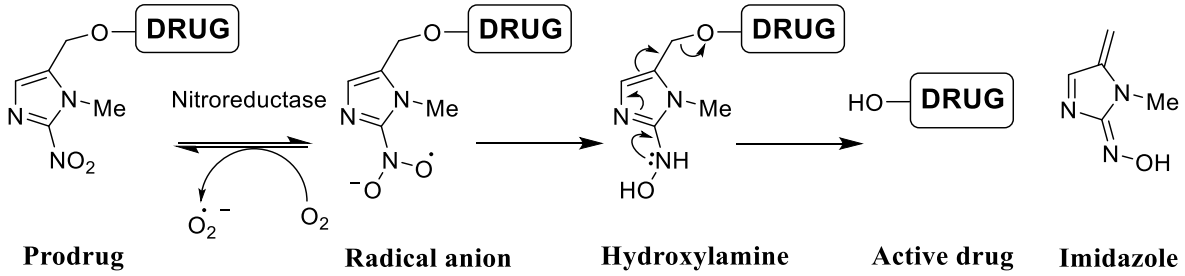

Scheme 2: Reduction of nitroaromatic prodrugs under hypoxic conditions

The nitroimidazoles represent a class of nitroaromatic compounds that has been used extensively as hypoxia-activated prodrugs.[12] The potential of nitroimidazoles as hypoxia-activated prodrugs was realised during studies of the imidazole-based radiosensitiser Misonidazole (**7**) (Figure 6), which was found to be selectively metabolised in a hypoxic environment.[43] Since this initial discovery, nitroimidazoles have been used extensively as hypoxia-activatable prodrugs and much effort has been spent in developing drugs with greater hypoxia selectivity. Nitroimidazoles containing the nitro-group at the 2-position have a higher reduction potential than the corresponding 4- and 5-nitro derivatives and are consequently the preferred nitroimidazole prodrug scaffold.[25] For example, TH-302 (**8**) is an alkylating agent consisting of a phosphoramide mustard group attached to 2-nitroimidazole (Figure 6).[24] TH-302 (**8**) has shown good hypoxia selectivity (up to 300-fold more potent in hypoxic tissue), and has entered phase I clinical trials.

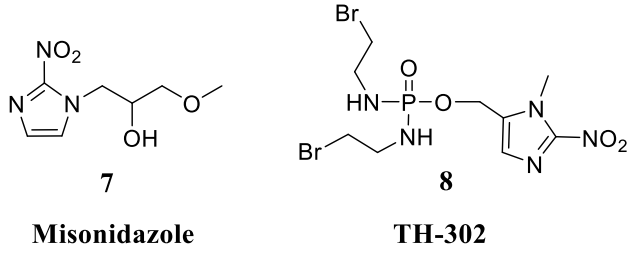

Figure 6. Structures of radiosensitiser Misonidazole (**7**), and hypoxia-activated DNA alkylating agent TH-302 (**8**)

The mode of activation of quinone-containing prodrugs is similar to that of the nitroaromatics. Quinones can undergo one-electron reductions, mediated by reductive enzymes including cytochrome P450 reductase, cytochrome b_5 reductase, and ubiquinone oxidoreductase, which results in the formation of a semiquinone.[20, 24, 43] The semiquinone can then be re-oxidised to form the original prodrug, however, under hypoxic conditions, the semiquinone may be further reduced to generate the active drug.[20, 43] Additionally, quinones can be reduced by two-electron reductases such as DT-diaphorase. DT-diaphorase is found to be overexpressed in various human solid tumours such as breast, ovarian, colon, thyroid, and adrenal cancer and can therefore, result in the selective activation of quinone prodrugs within the tumour microenvironment.[44] That said, DT-diaphorase is also found in healthy tissue and thus, can limit tumour selectivity.[43, 45] Examples of widely used quinones include the anti-cancer agents Mitomycin C (**9**) and its methylated derivative, Porfiromycin (**10**) (Figure 7).[12] Under hypoxic conditions these species undergo fragmentation to release the active alkylating agents **11** and **12**, respectively.[43] The antibiotic Mitomycin C (**9**) provides the first example of a quinone-containing hypoxia-activated alkylating agent.[46] However, in vivo studies of Mitomycin C (**9**) have revealed only minimal hypoxia selectivity.[26] Porfiromycin (**10**), however, has displayed higher hypoxia selectivity and therapeutic index than Mitomycin C (**9**) and has been evaluated in a clinical setting.[43, 46]

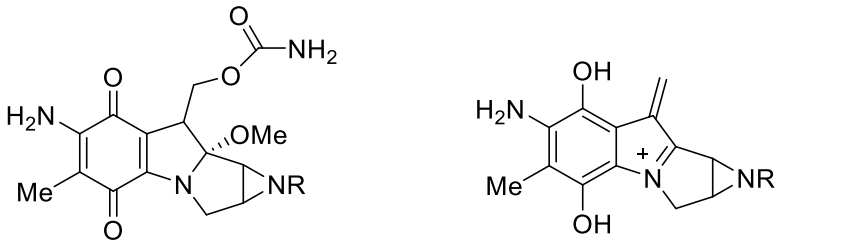

Mitomycin C (**9**): R = H
Porfiromycin (**10**): R = Me

Alkylating agent (**11**): R = H
Alkylating agent (**12**): R = Me

Figure 7: Mitomycin C (**9**), Porfiromycin (**10**), and their respective active drugs

Transition metal complexes have also been employed as prodrugs to selectively target tumour hypoxia.[12] Traditionally, this approach involves the coordination of

an active therapeutic to a metal centre, resulting in an overall inactive metal complex.[47] The viability of this strategy is dependent on the observation that several metal complexes, including Ru(III), Pt(IV) and Co(III) complexes, are found to be relatively stable when in high oxidation states, however once reduced to a lower oxidation state, such as Ru(II), Pt(II) or Co(II), the metal complex becomes more labile, triggering ligand release.[48] The hypoxia selectivity of this class of compounds can be mediated via several mechanisms. The reactivity between molecular oxygen and the biologically reduced metal complex is commonly exploited to give hypoxia selectivity. Under well-oxygenated conditions, the reduced metal complex will rapidly transfer electrons to molecular oxygen, thereby reforming the original prodrug. Under hypoxic conditions, however, the metal complex will not be re-oxidised, and will consequently release the active therapeutic. Alternatively, in some cases, molecular oxygen can compete with the transition metal complex for cellular reductants, resulting in selective activation under hypoxic conditions.[12]

The transition metal prodrug category is well represented by the therapeutic SN-2477 (**13**, Figure 8), a cobalt-mustard complex that exerts its effects through DNA cross-linking.[12, 43] When the drug is attached to cobalt (III), the complex is thought to be relatively stable. However, when the metal centre is reduced to cobalt (II), the metal releases its ligands, which includes the active drug.[43] Molecular oxygen is thought to be a competitive substrate for the active site of the reductive enzyme and therefore, in the presence of oxygen, release of the active therapeutic will be inhibited. SN-2477 has produced promising results in cell culture assays, including significant selectivity towards hypoxia in cell culture assays.[43] Several other metal complexes, including imidazolium tetrachloro (*S*-dimethyl sulfoxide) (imidazole) ruthenate(III) and indazolium tetrachlorobis(indazoleruthenate(III)) have entered phase I clinical trials.[48]

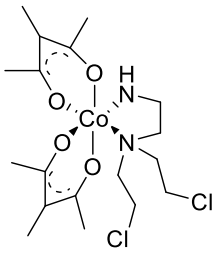

13

Figure 8: SN-24771

1.3.3 Bis-bioreductive drugs

Having investigated bioreductively activated prodrugs, it follows that the introduction of a second trigger group into a hypoxia-activated prodrug would lead to greater selectivity toward hypoxic conditions.[31] This rationale is supported by the biological testing of Nitracrine *N*-oxide (**14**, Figure 9), a DNA intercalating agent, which was found to be 1000 fold more potent in hypoxic cells than in well-oxygenated cells.[38] Nitracrine *N*-oxide contains two bioreductive centres, the *N*-oxide and the nitro-group, which allows for enhanced selectivity. That said, beyond the testing of Nitracrine *N*-oxide (**14**), there has been relatively little investigation into bis-bioreductive prodrugs.

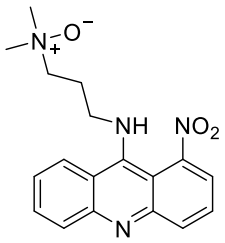

14

Figure 9: Nitracrine *N*-oxide

1.3 Immunomodulators and their potential as cancer therapeutics:

1.3.1 The role of macrophages

Macrophages are a group of fully differentiated myeloid cells with significant roles in both the innate and adaptive arms of the immune system.[49, 50] The common myeloid progenitor is produced in the bone marrow whereby, through the action of various cytokines, it progresses through several stages of development to give rise to monocytes (Figure 10).[49] Monocytes are then released into the blood stream where they can migrate into peripheral tissue and begin the maturation process into a macrophage, of which there are various sub-classes with slightly different functions. The primary function of macrophages in the innate branch of the immune system, however, is to engulf (phagocytose) and destroy invading pathogens and in addition, secrete cytokines and other signalling molecules to activate and recruit other cell types involved in the inflammatory response. Macrophages can also act as scavengers, clearing dead cells and cellular debris.[50]

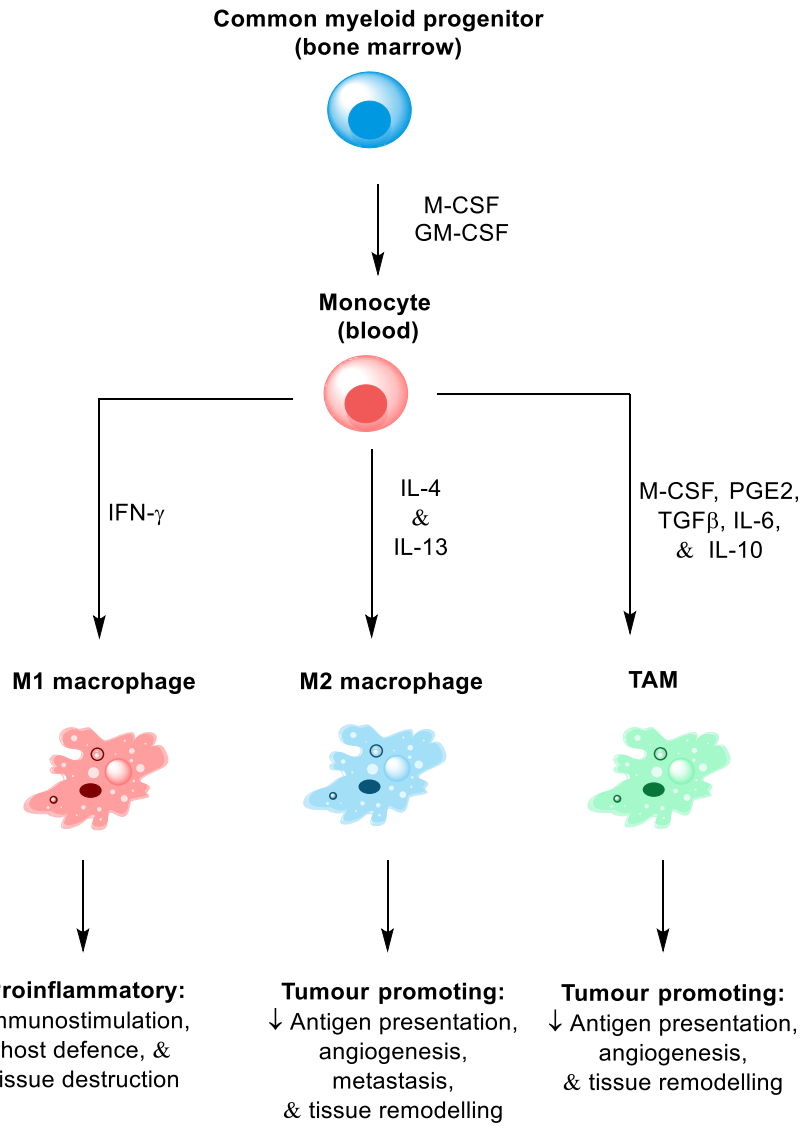

Figure 10: Differentiation of the common myeloid progenitor into M1 macrophages, M2 macrophages, and TAMs

1.3.2 M1/M2 macrophages

Once recruited from the bloodstream, the specific cytokine profile of the tissue environment affects the differentiation of monocytes into mature macrophages expressing a particular functional programme. In accordance with the Th1/Th2 classification system, these macrophages can either be termed M1 or M2.[51, 52] Classically activated, or M1 macrophages, are typically induced in response to

interferon gamma (IFN-γ), lipopolysaacharides (LPS), and cytokines such as tumour necrosis factor (TNF) and granulocyte macrophage colony-stimulating factor (GM-CSF) (Figure 10).[53] M1 macrophages are usually associated with protective functions such as immunostimulation, host defence, and tissue destruction. On the other hand, alternatively activated M2 macrophages can encompass a range of macrophage phenotypes that are not included within the M1 category. M2 macrophages occur in response to interleukin (IL)-4 and IL-13, and while these macrophages display a spectrum of different phenotypes, M2 macrophages are generally considered to be anti-inflammatory.[52] Additionally, M2 macrophages are known to aid parasite clearance, enhance tissue remodelling, and drive tumour progression.[52]

1.3.3 TAMs as a M2 macrophage

It is well known that tumours are heavily infiltrated by various immune cells, with tumour-associated macrophages (TAMs) representing the most abundant population and accounting for up to 50% of the tumour mass.[53-58] Monocytes are typically recruited to the tumour site via the agency of chemokines, including CCL2 and CCL5, which are produced by tumour cells, fibroblasts, endothelial cells, and TAMs.[55, 58, 59] Once in the tumour microenvironment, the monocytes are exposed to macrophage-colony stimulating factor (M-CSF), prostaglandin E2 (PGE2), transforming growth factor beta (TGF-β), IL-6, and IL-10, which in turn, initiates the differentiation of monocytes into mature TAMs (Figure 10). Although TAMs have their own unique phenotype, they typically display a number of M2 functions including the suppression of the inflammatory response, tissue remodelling, poor antigen presentation, metastasis, and the stimulation of angiogenesis.[53, 58] Accordingly, in many tumours, a high level of TAM infiltration has been correlated with poor prognosis.[58, 60]

1.1.2 Altering the phenotype of macrophages

As a cell type, macrophages are known to be ‘plastic’, in that they can readily convert from one phenotype to the other via the agency of different cytokines or combinations thereof.[52, 61] Given that the phenotype of macrophages can influence the progression and regression of solid tumours, it is thought that if the phenotype

of a TAM is transformed to the M1 phenotype, then they could provide protection against tumours.[62] To this end, there have been various studies that target macrophages with the intention of altering their activation state so as to induce tumour necrosis. There are generally two ways that this alteration to the macrophage activation state can be achieved. First, macrophages can be activated *in vivo* via the systemic introduction of a biological response modifier or, alternatively, macrophages can be isolated from the body and then re-injected after *in vitro* activation. Herein, the focus will be on the phenotypic modification of macrophages *in vivo*.

i) MTP-PE

Muramyl tripeptide phosphatidylethanolamine (MTP-PE) is a synthetic analogue of muramyl dipeptide (MDP) and a Toll-like receptor (TLR) 4 agonist that is able to activate monocytes and macrophages to produce inflammatory, M1 type cytokines such as TNF-α, IL-6, IL-8, and IL-1β, as well as other cellular mediators (e.g. nitric oxide [NO]) leading to the enhanced tumouricidal activities of macrophages.[63, 64] MTP-PE has been used in phase I, II, and III clinical trials to treat various advanced forms of cancer including colorectal, melanoma, renal cell carcinoma, lung, breast, stomach, and salivary gland cancers.[64] In particular, one clinical study revealed that when using MTP-PE to treat patients with high-grade osteosarcoma, the risk of reoccurrence decreased by 25% and the six year survival probability increased by 10%.

ii) MMP-9

Matrix metalloproteinases (MMP) are a family of proteinases involved in numerous physiological processes including angiogenesis, bone development, and metastasis. In 2013, Long *et al.*[65] demonstrated that treating human macrophages with adenoviruses carrying the MMP-9 gene resulted in the enhanced production of Th1 cytokines such as IL-1β, IL-6, TNF-α, and IL-8, therefore exemplifying the ability of biological modifiers to induce a phenotypic switch of macrophages.

1.4 Trehalose dimycolates (TDMs) and their immunomodulatory properties

1.4.1 The use of bacteria in the treatment of cancer

By the late 1800s it was well recognised that bacterial infection had the potential to induce tumour regression.[66] This discovery has been largely attributed to the seminal work of William Coley who used whole bacteria to treat cancer patients. Over a period of 40 years, Coley treated over 1000 patients and found that optimal decrease in tumour burden was achieved when using a vaccine containing *Streptococcoal pyogenes* and *Serratia marcescens*, otherwise known as "Coley's toxins".[67] Coley's work, however, was criticised due to its poor documentation, lack of patient follow up, and variability in vaccine preparation and administration.[67, 68] With the introduction of radiotherapy and chemotherapy, interest in Coley's toxins gradually declined and were largely ignored. It was not until late in the 20th century that interest in the potential of bacteria to treat cancer once again came to the forefront of scientific research. For example, Bacillus Calmette-Guerin (BCG), a vaccine containing the attenuated bovine form of *M. tuberculosis*,[69] has been reported to show therapeutic potential when treating acute lymphoblastic leukaemia, and malignant melanoma,[70] and is now the standard therapy for the treatment of superficial bladder cancer.[71] BCG induces immune cells to produce elevated levels of IL-2 and IFN-γ, which is associated with tumour regression.[69, 72] Given the success of BCG to treat some cancer types, efforts are now being directed towards determining the components of *M. tuberculosis* that leads to the Th1 immune response.

1.4.2 The immunomodulatory properties of TDMs

In the 1950s it was determined that *M. tuberculosis* expressed a molecule known as "cord factor" which was essential for the bacteria's pathogenic behaviour.[73] Cord factor, nowadays known as trehalose dimycolate (TDM, **15**, Figure 11),[74, 75] is a glycolipid found on the cell wall mycobacterium species and is composed of a trehalose disaccharide linked to two mycolic acids with a minimum of two chiral centres located α and β to the carboxylic acid.[75, 76] Mycolic acids vary in structural complexity and include oxygenated meromycolates, such as methoxy mycolates (**A**, Figure 11), keto mycolates (**B**), and epoxy mycolates (**C**), as well as non-

oxygenated mycolic acids with *cis* cyclopropanes located in the meromycolate branch (**D**).[75, 77]

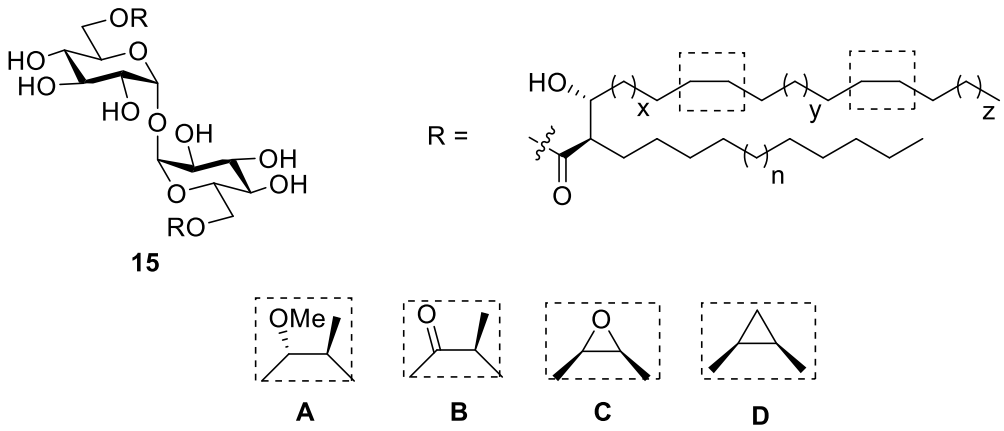

Figure 11: Structure of TDMs

TDMs have been subjected to various biological tests, which have resulted in the discovery of protective activities of these glycolipids including anti-tumour properties, adjuvant activity, anti-bacterial activity, the induction of granuloma formation, and the stimulation of angiogenesis.[75] The anti-tumour properties of TDMs have been determined in various studies, including the work by Pimm *et al.*,[78] whereby the ability of TDMs to induce tumour regression in a hepatoma tumour model was demonstrated *in vivo.* Here, the growth of an ascetic rat hepatoma was suppressed in response to treatment with a TDM emulsion. Similarly, in a separate study conducted by Yarkoni *et al.*,[79] injection of TDM in mice has been shown to suppress the growth of Ehrlich Ascites tumour cells. Other studies have also illustrated the potential of TDMs and related trehalose glycolipids to lead to a reduction in tumour burden.[80-83]

The potential of TDMs to activate macrophages to produce a polarised Th1 response has also been widely studied. Schoenen *et al.*[84] demonstrated the ability of TDM to activate macrophages to produce an inflammatory response, including the production of NO, G-CSF, and IL-1β. Additionally, in a study by Geisel *et al.*,[85] the authors showed that when TDM is delivered to bone marrow-derived murine macrophages (BMMs), it induces the production of the Th1 cytokines IL-1β, IL-6,

and TNF-α, thus illustrating the potential of TDMs to induce an M1 response in macrophages. Finally, in a study by Sakamoto *et al*.[86] the global gene expression of BMMs in response to treatment with TDM was explored. While the authors did not specifically comment on the relative ratios of the different cytokines, on the whole they found that two hours after treatment there was a 5.21-fold increase in IL-1β, a 1.56-fold increase in IL-1, a 1.80-fold increase in IL-10, and a 3.02-fold increase in TNF, which, in general terms, corresponds to a Th1 immune response.

1.4.3 TDB

In addition to TDM, trehalose dibehenate (TDB, **16**) (Figure 12), a C22 synthetic analogue of TDM, has been found to lead to the Th1 activation of macrophages.[84] Like TDM, stimulation of macrophages with TDB induces the production of the Th1 cytokines IL-6, G-CSF, IFN-γ, and IL-17, as well as NO.[84] In a separate study, primed BMMs stimulated with plate-coated TDB were induced to produce TNF-α and MIP-2.[74] Finally, the activation of macrophages with TDB induces higher levels of IL-6 and IL-1β than the other (C4, C7, C10, C18, C20, and C26) TDM analogues.[87]

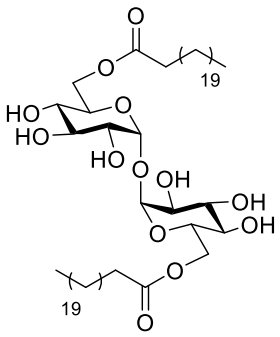

16

Figure 12: Trehalose dibehenate (TDB)

1.4.4 The molecular target of trehalose glycolipids

Trehalose glycolipids have been shown to exert their effects by activating macrophages through two different receptors: the macrophage inducible C-type lectin (Mincle), and the macrophage C-type lectin (MCL).[88, 89] Mincle was first identified as a trehalose glycolipid receptor by Ishikawa *et al.* in 2009.[74] In 2010,

Schoenen *et al.* re-established this fact and additionally, demonstrated that Mincle was vital for the recognition of trehalose glycolipids.[84] More recently, binding to MCL has been found to moderate the activity of TDM.[90] Primarily, trehalose glycolipids bind to Mincle, thereby activating the FcRγ-Syk-Card9 signalling pathway and inducing the production of inflammatory cytokines.[88, 91, 92] In the absence of Mincle, however, this induction of cytokines is not observed. In 2013, the first crystal structures of both bovine and human Mincle complexed to either trehalose or citric acid were reported by Feinberg *et al.* and Furukawa *et al.*, respectively.[88, 93] Structural analysis of the Mincle binding site suggested that trehalose binds to Mincle in a calcium dependent manner, with the 3- and 4-hydroxyls of the trehalose moiety found to be involved in calcium binding, and thus are important for activity (Figure 13). Furthermore, a hydrophobic region located in the surrounding area of the calcium binding site has been identified as the lipid binding pocket.

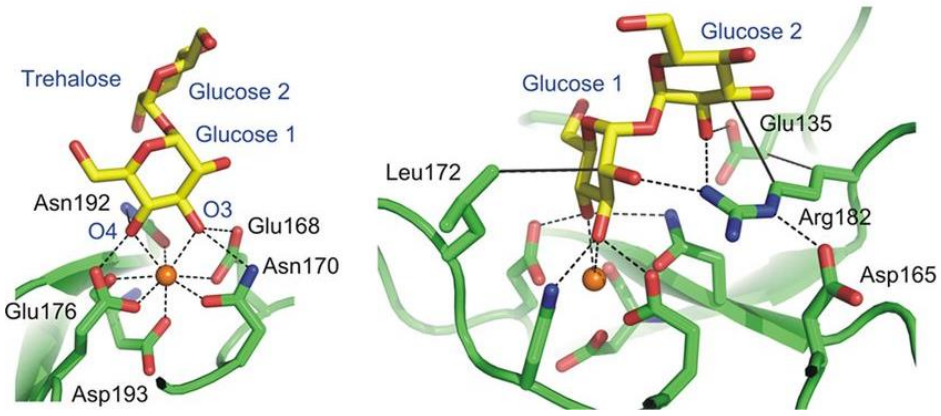

Figure 13: Crystal structure of bovine Mincle complexed with trehalose. Adapted from Feinberg *et al.*[92]

1.5 Objectives

To explore the full potential of TDMs in cancer therapy, the glycolipids must be specifically targeted to TAMs so as to prevent unwanted inflammatory responses. As previously stated, hypoxia is a feature of solid tumours that allows for the specific targeting of drugs to these regions in the body. Current cancer therapeutics such as Mitomycin C, Tirapazamine, and AQ4N are all prodrug examples using the hypoxia-activated prodrug approach as a way of gaining selectivity.[12] Accordingly, it is proposed that the more selective anti-cancer therapy can be achieved by converting TAMs to the M1-tumour suppressive phenotype via the addition of a hypoxia-activated trehalose glycolipid prodrug. To achieve this, a 2-nitroimidazole group will be attached to TDB, so as to form the hypoxia-activatable TDB (H-TDB **17**, Figure 14)). It is expected that the H-TDB (**17**) will be inactive under well-oxygenated cells due to the inability of the prodrug to bind to Mincle. However, once in the tumour microenvironment, the reduced oxygen content will result in the cleavage of the 2-nitroimidazole group thereby releasing the immunomodulatory TDB. Once released, the active TDB is envisioned to revert the TAM phenotype back to Th1. As the 3D protein structure of Mincle has revealed that the 3- and 4-hydroxyls are important for calcium binding, the first objective is to synthesise 3, 3′-bis-nitroimidazolylmethyl trehalose dibehenate, or hypoxia-activatable TDB (H-TDB, **17**), and then to explore the immunomodulatory properties of this compound under hypoxic and well-oxygenated conditions. If successful, this will be the first time that a hypoxia-activated immunomodulatory prodrug approach has been developed. Accordingly, this strategy represents a new approach for the treatment of solid tumours.

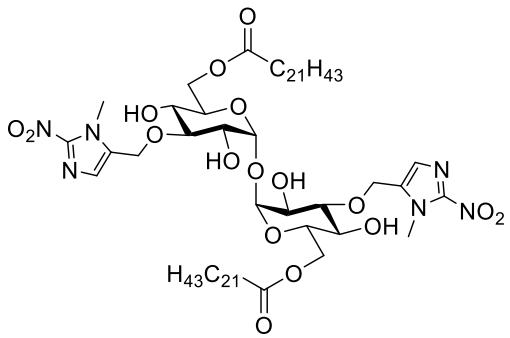

H-TDB **17**

Figure 14: Hypoxia-activatable TDB (H-TDB) **17**

2. Results and Discussion

2.1 Synthetic strategy

To synthesise H-TDB **17**, a retrosynthetic strategy was proposed whereby the nitroimidazole moiety could be installed on the C-3 hydroxyls of trehalose (**21**) via alkylation of benzylidene protected trehalose **18** with nitroimidazole derivatives **19** or **20** (Scheme 3A).[94] Benzylidene protected trehalose **18** could, in turn, be prepared in one step from α,α′-trehalose (**21**) according to a literature procedure.[95] The synthesis of nitroimidazole halides **19** and **20** was envisaged to occur in four steps from amino ester **22** (Scheme 3B). To this end, the oxidation of the amino-group in **22** to the corresponding nitro-group, hydrolysis of the ester, subsequent reduction of the carboxylic acid to the alcohol, and finally, bromination or chlorination was proposed to yield target compounds **19** and **20**, while amino ester **22** itself could be made via a cyclisation reaction of α-formylated sarcosine ester **23** with cyanamide. Finally, the synthesis of α-formylated sarcosine ester **23** was envisioned to require three steps from sarcosine (**24**).

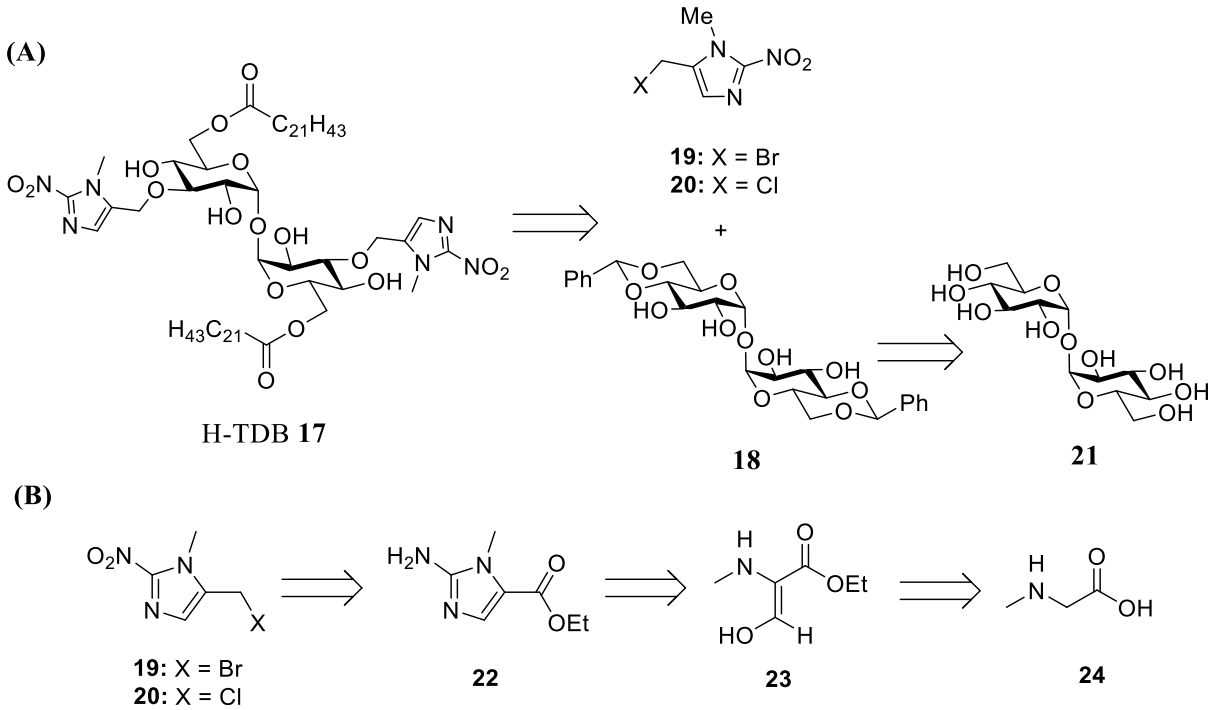

Scheme 3. Retrosynthesis of H-TDB **17**

2.2 Synthesis of the Nitroimidazole Halides

In order to synthesise the hypoxia-activated trehalose glycolipid, the nitroimidazole prodrug triggers **19** and **20** first needed to be prepared. To this end, an 8-step patented procedure by Matteucci *et al*. (2007)[96] for the preparation of **19** and **20** was used as a guide and adapted where necessary to improve on yields. The first step in the synthesis of the nitroimidazole trigger involved the esterification of sarcosine (**24**) with methanol (Scheme 4). This reaction proceeded smoothly to give sarcosine methyl ester (**25**) in 95% yield. Next, sarcosine ester **25** was treated with sodium hydride and ethyl formate in an attempt to form the di-formylated sarcosine ester **27**. Here, it is important to note that ethanol is liberated throughout the course of this reaction, which, in the presence of NaH, results in the transesterification of the methyl ester to produce the ethyl ester of **27**. Initial attempts at this formylation, were largely unsuccessful and only the *N*-formylated sarcosine ester **28** was produced in exceedingly poor yield (entries 1 & 2, Table 1). Here, the ^{1}H NMR spectrum of the isolated material revealed pairs of singlets at 8.12 ppm and 4.10 ppm, which are diagnostic of the formamide and α-protons, respectively (Figure 15). Furthermore, the singlet at 4.1 ppm integrated for two protons, which is indicative of the formation of the *N*-formylated ester **28**. The absence of a second formyl proton signal, which would be expected downfield of 8 ppm, further supported this assignment. In the ^{1}H NMR spectrum of *N*-formylated ester **28**, it is also interesting to observe the paired nature of the singlets at 8.12 and 8.04, 4.10 and 3.97, and 3.04 and 2.93 can be attributed to the *E*- and *Z*-amide rotamers (Figure 15). While the assignment of the major rotamer could not be readily achieved, the relative ratios of the isomers changed depending on solvent, with a 1:1.4 isomeric ratio being observed in $CDCl_3$, while a 1:1.1 ratio of rotamers was observed in CD_3OD.

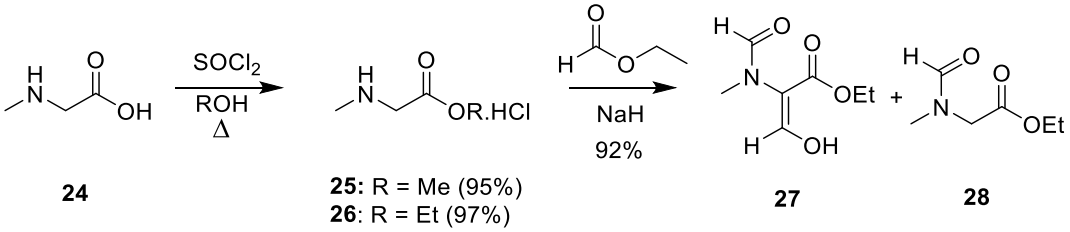

24 **25:** R = Me (95%) **26**: R = Et (97%) **27** **28**

Scheme 4. Synthesis of di-formylated sarcosine ethyl ester **27**

Table 1: Optimisation of the di-formylation of sarcosine esters **25-26**

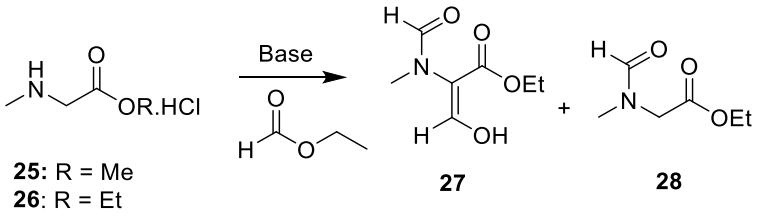

25: R = Me
26: R = Et

27 **28**

Entry	substrate	Scale (g)	Base	Equivalents of base	Time (hours)	Temp. (°C)	Yield (%) 28	27
1	**25**	4.1	NaH	2.3	18	r.t.	~5	-
2	**25**	2.1	NaH	3.5	24	r.t.	~5	-
3	**25**	0.2	NaOEt	1	62	r.t.	9	-
4	**26**	5	NaOEt	2.5	48	55	-	-
5	**26**	5	NaH[1]	3.5	18	r.t.	4	61
6	**26**	8.5	NaH[1]	3.9	24	r.t.	4	75
7	**26**	9	NaH[1]	4.2	60	r.t.	1	92

[1] Newly purchased ethyl formate used

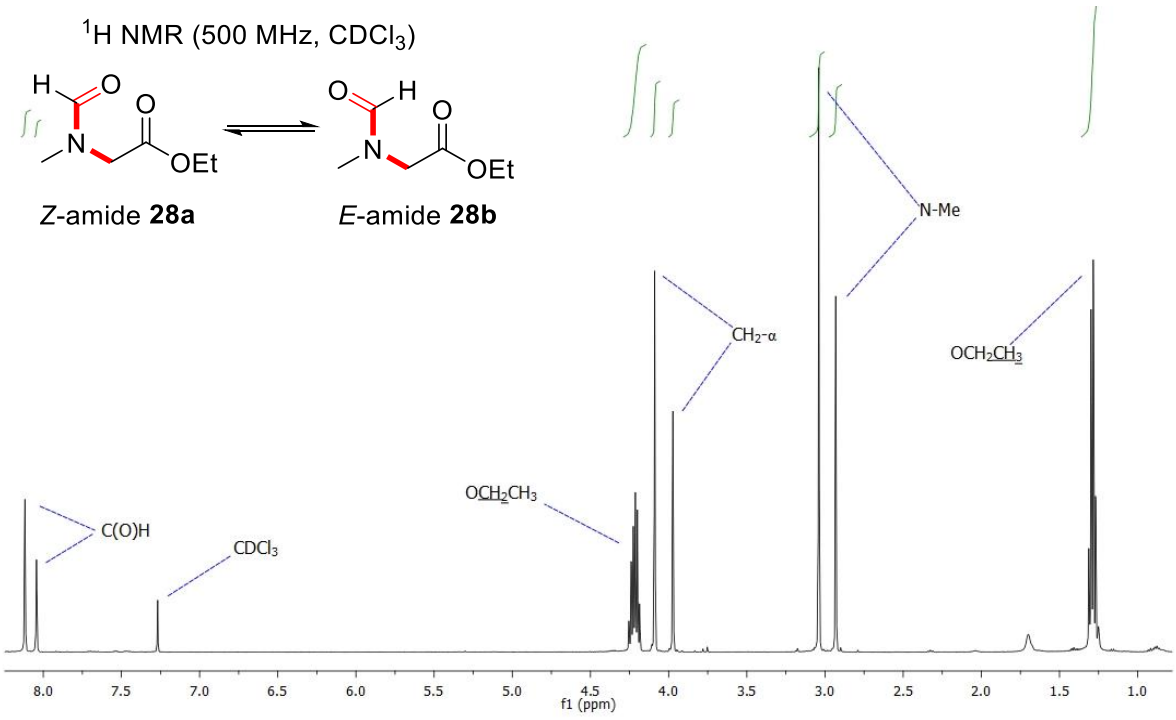

Figure 15. ^{1}H NMR of *N*-formylated sarcosine ethyl ester (**28**)

In an attempt to produce the desired di-formylated product **27** from sarcosine ester **25**, an alternative base, sodium ethoxide, was then used (entry 3, Table 1). Unfortunately, this made little difference to the outcome of the reaction and only a small amount (9% yield) of the undesired *N*-formylated ester **28** was obtained. With limited success in achieving the desired transformation of sarcosine methyl ester (**25**) into the di-formylated ester **27**, it was then decided to use sarcosine ethyl ester (**26**), which was synthesised from sarcosine (**24**) in 97% (Scheme 4). While sarcosine esters **25** and **26** would, in theory, lead to the formation of the di-formylated product **27**, the use of the ethyl ester meant that the transesterification reaction was not required. Throughout the course of these experiments, it became apparent that the sarcosine esters were poorly soluble in ethyl formate, and in an attempt to increase the solubility of the reagent, the reaction was then performed under reflux conditions (Entry 4, Table 1). Unfortunately, these conditions did not fare any better and only starting material was isolated. In an attempt to determine why the transformation of the sarcosine esters to the di-formylated product was unsuccessful, the quality of the ethyl formate was then brought into question. Accordingly, the ethyl formate was dried over P_2O_5 and freshly distilled before use, and when this measure yielded no success, new ethyl formate was purchased. The reaction was then performed again with the newly purchased ethyl formate and NaH as the base, and gratifyingly, the di-formylated ester **27** was formed in 61% yield (Entry 5). The reaction was further optimised by exploring different reaction times and scales (Entries 6–7), whereby it was determined that those reactions that had long reaction times (~60 hours) and were performed on a large scale (>5g) were the highest yielding. The optimal conditions produced the di-formylated product **27** in 92% yield (Entry 7).

The successfully prepared di-formylated ester **27** was then treated with ethanol and concentrated hydrochloric acid, which led to the cleavage of the formamide group to give α-formylated sarcosine ester **29** (Scheme 5A). The reaction mixture was filtered over activated carbon, concentrated, and used without further purification for the subsequent cyclisation with cyanamide to form amino ester **22**. Here, cyclisation to amino ester **22** is proposed to occur via the attack of the amide nitrogen of cyanamide onto the aldehyde of **29** to give intermediate **30**, which with

the loss of water produces imine **32** (Scheme 5B). Intramolecular cyclisation of imine **32** then results in the formation of imidazole backbone **33**. Finally, deprotonation of the ester α-proton (in **34**) results in aromatisation, and formation of the target amino ester **22**. Although this reaction appears practicable, the patented procedure lacked key synthetic details and as initial attempts at the cyclisation were poor yielding, the reaction required some optimisation.

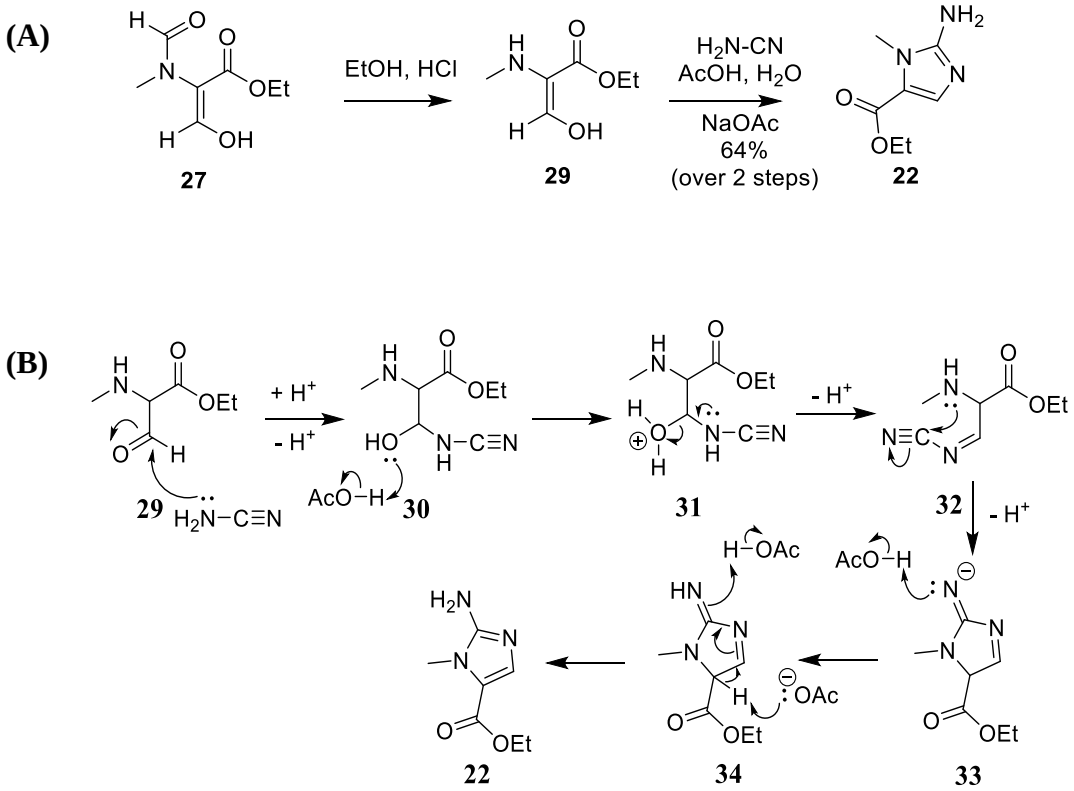

Scheme 5. (A) Synthesis of amino ester **22 (B)** Proposed mechanism for the formation of amino ester **22**

As described in the patent, the conversion of α-formylated sarcosine ester **29** into amino ester **22** was first attempted by refluxing ethanolysis product **29**, cyanamide, and sodium acetate in acetic acid and water for 90 minutes (Entry 1, Table 2). Unfortunately, this resulted in the formation of the desired product in remarkably

low yields (15% from **26**), despite performing the reaction multiple times. To improve the yields, a series of reactions were then performed at reduced temperatures (Entries 2-4), and in slightly more acidic buffers (Entries 3 & 4). While the use of a more acidic buffer resulted in marginally increased yields (24% from **26**, as compared to 15%), the pivotal condition that led to a greatly increased yield was from an alteration to the work-up protocol. The patented procedure detailed a work-up whereby the reaction mixture was acidified, concentrated, basified, and then extracted with ethyl acetate.[96] It was initially thought that the acidification step would prevent the reaction mixture from becoming too basic during concentration, which could lead to ester hydrolysis, however, when this step was removed from the work-up procedure a 59% yield of the desired amino ester **22** was obtained (Entry 4). Accordingly, the acidification step may have actually resulted in acid catalysed ester hydrolysis and degradation of the product, thereby decreasing the yield of the desired product.

Table 2. Optimisation of cyclisation reaction

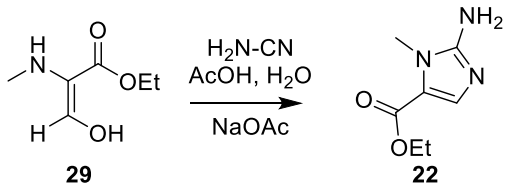

29 **22**

Entry	Buffer pH[1]	Temp. (°C)	Reaction Time (hours)	Acidified before concentration	Yield (%) from 26
1	4.83	100	1.5	Yes	15%
2	4.83	50	1.5	Yes	14%
3	4.63	50	1.5	Yes	24%
4	4.63	50	1.5	No	59%

[1]Buffer pH was estimated using the Henderson-Hasselbalch equation

To confirm that amino ester **22** had been synthesised, standard spectroscopic techniques were used. For example, diagnostic peaks in the ^{1}H NMR spectrum include the singlets at 3.60 ppm and 7.32 ppm for the *N*-Me and H-4 resonances, respectively (Figure 11). Although most ^{1}H NMR assignments could be made on

the basis of chemical shift and coupling patterns, 2D-NMR was required to fully assign the ^{13}C NMR spectrum. Specifically, an HSQC between the carbon at 134.4 ppm and the proton at 7.32 ppm, allowed for the assignment of C-4 to this resonance. Additionally, mass spectral analysis was consistent with the expected mass [HRMS(ESI) *m/z* calcd. for $[C_7H_{12}N_3O_2+H]^+$: 170.0930, obsd.: 170.0925].

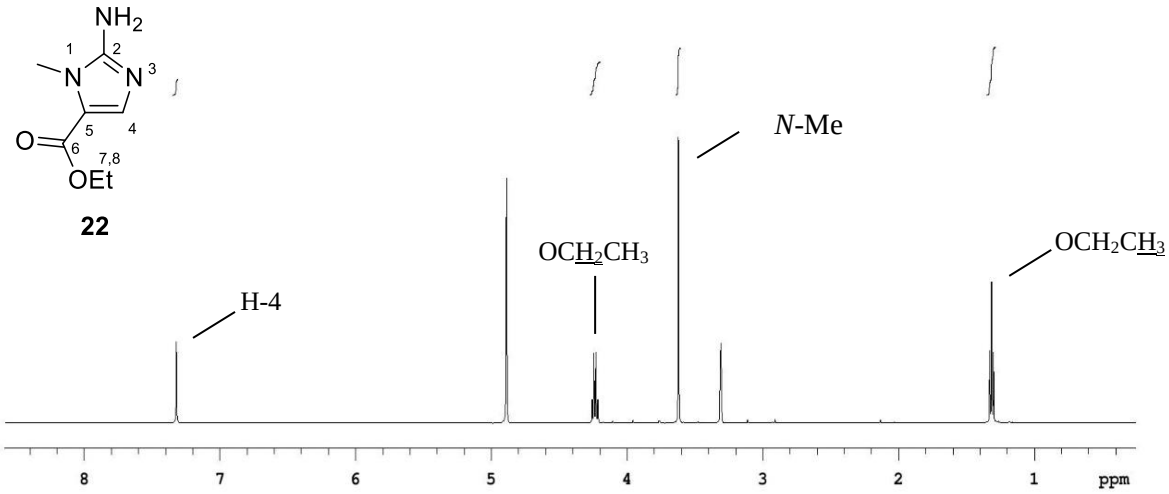

Figure 11. ^1H NMR of amino ester **22** (CD_3OD, 500 MHz)

Having successfully prepared amino ester **22**, oxidation of the amino group in **22** was undertaken to give the corresponding nitroimidazole **35** in 44% yield (Scheme 6). Here, the ^1H NMR spectrum of nitroimidazole **35** revealed a downfield shift of all proton signals, which is consistent with the oxidation of the amine to the electron withdrawing nitro group. Mass spectral analysis also confirmed the formation of the desired product [HRMS(ESI) *m/z* calcd. For $[C_7H_9N_3O_4+H]^+$: 200.0667, obsd.: 200.0671]. Ethyl ester **35** was then hydrolysed using NaOH in water to give carboxylic acid **36** in quantitative yield. The absence of the ethyl ester signals at 4.40 ppm and 1.39 ppm in the ^1H NMR spectrum clearly indicated that the desired product **36** had been formed.

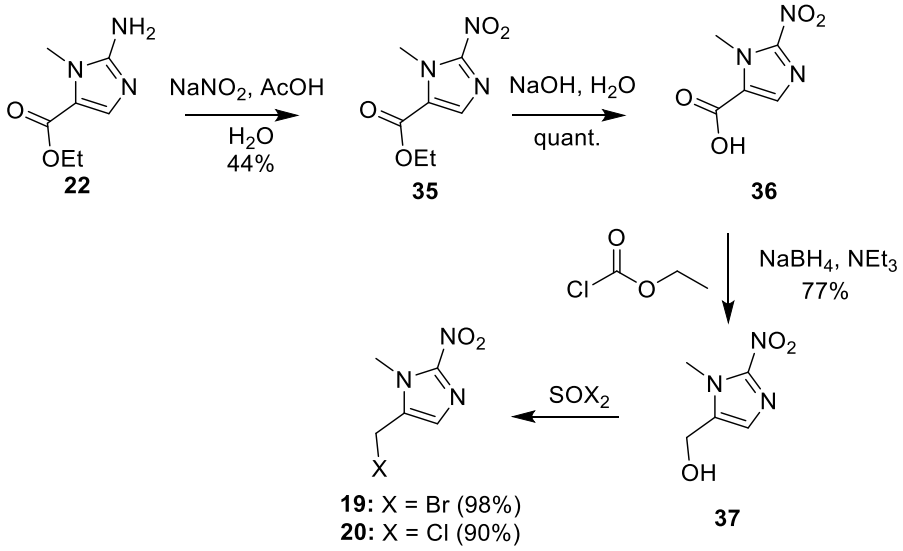

Scheme 6. Synthesis of nitroimidazolylmethyl halides **19** and **20**

Next, carboxylic acid **36** was reduced to the corresponding alcohol **37** using a sodium borohydride ($NaBH_4$) mediated reduction. Reductions of carboxylic acids to primary alcohols are traditionally carried out using borane, rather than sodium borohydride, as a reducing agent.[97] Although these reagents appear to be extraneously alike, they differ in their electronic nature. Generally speaking, the negative charge on borohydride reducing agents enhances their reactivity towards electrophilic carbonyls, thereby reducing their reactivity towards electron rich carbonyls, such as deprotonated carboxylic acids.[97] On the contrary, borane is an excellent Lewis Acid and its reactivity is largely driven by its preference to accept electrons into its unoccupied p-orbital. Accordingly, for the reduction of **36** using sodium borohydride, the carboxylic acid is first deprotonated to give **38** and then reacted with ethyl chloroformate to form the mixed anhydride **39** (Scheme 7), thereby greatly enhancing the electrophilicity of the carbonyl and facilitating its reduction by $NaBH_4$. The reduction is further enhanced by the elimination of carbon dioxide during the course of the reaction, to give intermediate aldehyde **40**, which is subsequently reduced to the alcohol. Initially, the reduction of carboxylic acid **36** proceeded in modest (56%) yield to give 5-hydroxymethyl-1-methyl-2-nitroimidazole (**37**). To optimise the reaction, the amount of ethyl chloroformate

added was therefore increased from 1.0 to 2.3 equivalents, which resulted in the formation of nitroimidazole **37** in 77% yield. Satisfied with this result, the alcohol in **37** was then converted into a bromide or chloride using thionyl bromide or thionyl chloride, respectively (Scheme 6). Both transformations proceeded smoothly to give imidazolylmethyl bromide **19** and imidazolylmethyl chloride **20** in excellent yields.

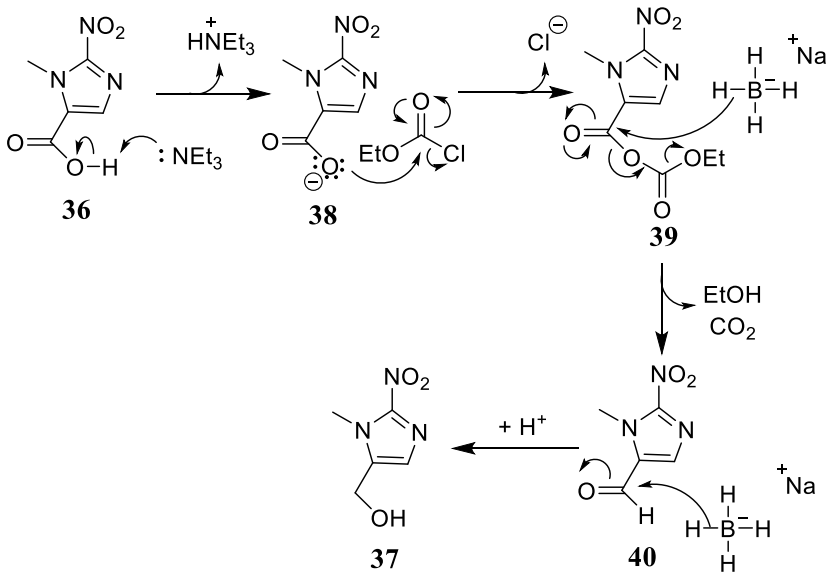

Scheme 7. Mechanism for the sodium borohydride mediated reduction of carboxylic acid **36**

2.2.1 Summary of synthesis of nitroimidazole halides 19 and 20

In summary, a 7-step patented procedure by Matteucci *et al*.[96] was used with some modifications to produce nitroimidazolylmethyl bromide **19** and nitroimidazoylmethyl chloride **20** (Scheme 8). Key amendments to the published protocols included the use of sarcosine, in contrast to sarcosine methyl ester **25**, as the starting material, with sarcosine being esterified to give ethyl ester **26**, which was used in subsequent steps. During the formylation reaction of ethyl ester **26**, the quality of the ethyl formate proved crucial, as the use of substandard solvent in this reaction resulted in the isolation of only *N*-formylated product **28** in low yield. Throughout the course of the optimisation process, it was also determined that

longer reactions times and a larger reaction scale (*ca.* 10 g) enhanced the yield of the desired di-formylated sarcosine ethyl ester **27**.

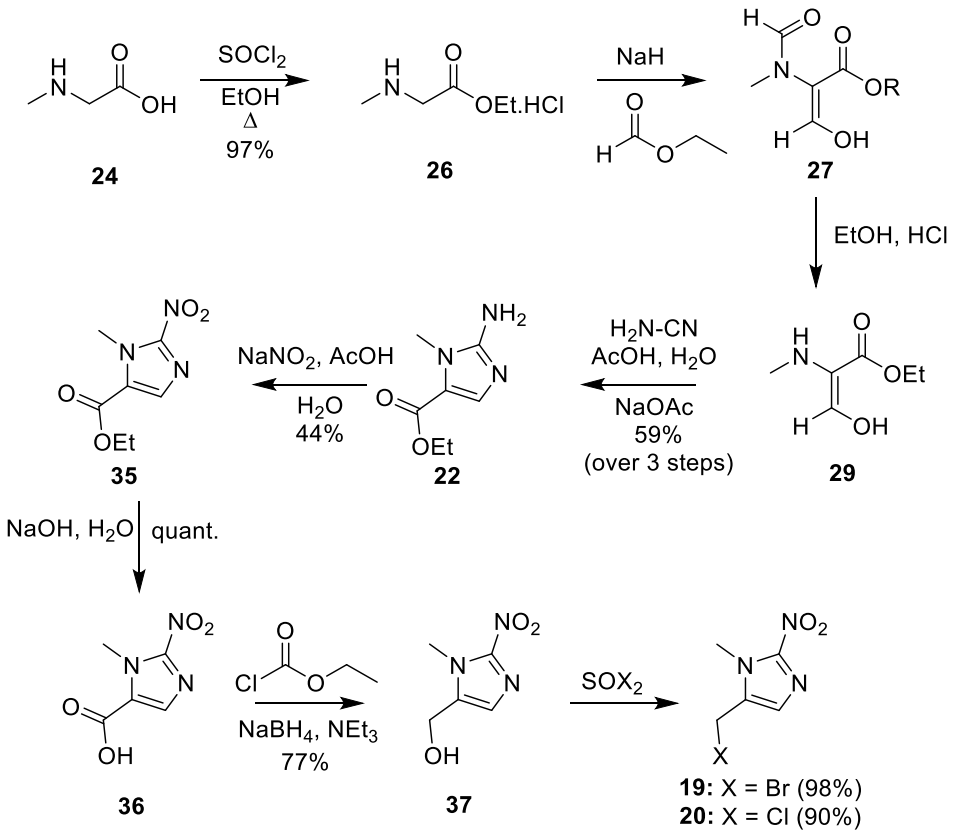

Scheme 8. Summary of synthesis of nitroimidazole halides **19** and **20** from sarcosine (**24**)

After acid hydrolysis of **27**, the α-formylated sarcosine ester **29** was then subjected to a cyclisation reaction with cyanamide to produce amino ester **22**. A noteworthy adaptation to the suggested procedure was the removal of the acidification step in the work-up which resulted in a 35 pp (percentage points) increase in yield. Amino ester **22** was then oxidised to the corresponding nitroimidazole **35**, with **35** then being reduced to give alcohol **37**. Finally, alcohol **37** was reacted in the presence of either thionyl bromide or thionyl chloride to give nitroimidazolylmethyl bromide **19** and nitroimidazolylmethyl chloride **20** in overall yields of 18% and 17%, respectively (8 steps). The syntheses are comparable to, if not better than, the

patented procedure which produced nitroimidazolylmethyl bromide **19** in 8% yield over 7-steps.[96]

2.3 Attempted synthesis of H-TDB (17):

Having successfully prepared the nitroimidazole prodrug triggers **19** and **20**, the next step in the synthesis involved the conjugation of these compounds to a suitably protected trehalose derivative. Accordingly, a benzylidene protecting group was installed at the C-4 and C-6 hydroxyls of α,α′-trehalose (**21**) using the protocol of Baddeley and Wardell (2009).[95] The reaction proceeded smoothly to produce benzylidene protected trehalose **18** in 78% yield as a white crystalline product. ^{1}H NMR spectral data was consistent with the reference spectra,[95] in particular, aromatic signals between 7.1 and 7.3 ppm and the benzylidene acetal signal at 5.6 ppm confirmed that the benzylidene protecting group had been successfully installed. Additionally, an HMBC between H-6 and the benzylidene methylene confirmed that the benzylidene protecting group was indeed installed on the C-4 and C-6 positions. Next, it was proposed that alkylation of the more reactive 3- and 3′- hydroxyls of benzylidene-protected trehalose **18** with nitroimidazolylmethyl halides **19** or **20** would give bis-nitroimidazolylmethyl-di-*O*-benzylidene-trehalose **41**, which could be subsequently converted to H-TDM **17** via removal of the benzylidene protecting groups and regioselective esterification with behenic acid at the 6- and 6′-positions.

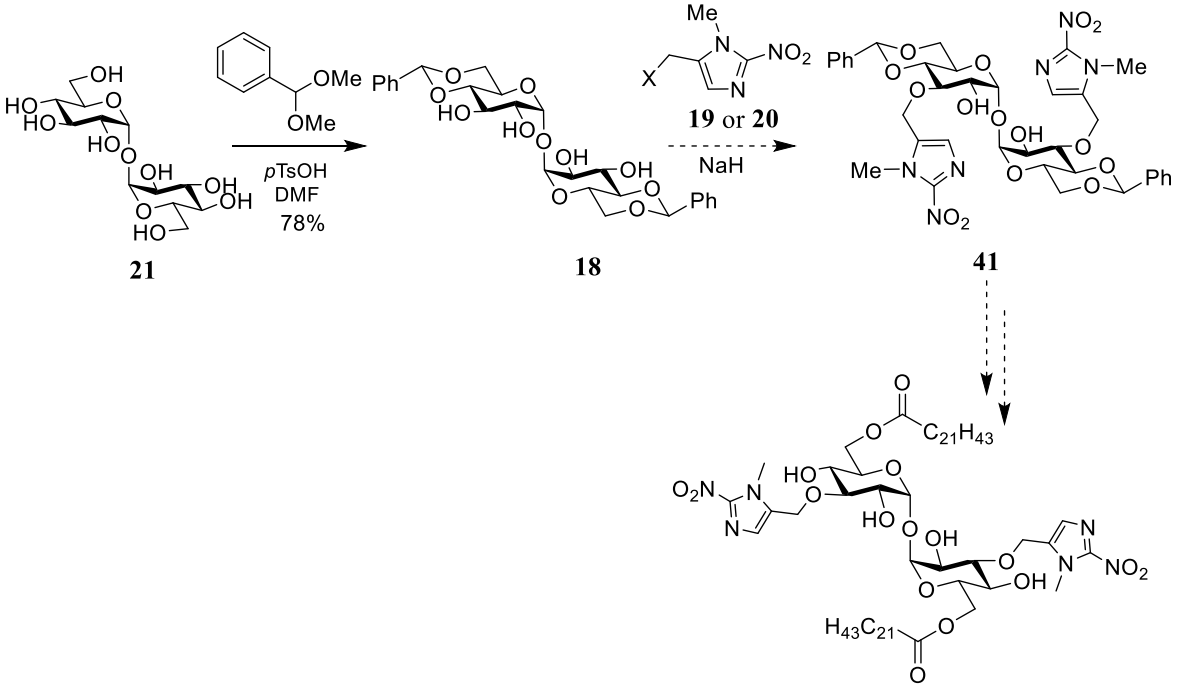

Scheme 9. Proposed synthetic strategy for synthesis of H-TDB **17**

A number of conditions were used in an attempt to alkylate benzylidene protected trehalose **18** with the nitroimidazole halide (Table 3). First, the imidazolylmethyl chloride **20** was added dropwise to a solution of protected trehalose **18** and NaH in DMF (at 0 °C), and the reaction was warmed to room temperature and then stirred for one hour (Entry 1, Table 3). Unfortunately, only starting materials were isolated from the reaction mixture. The reaction was then repeated with warming to 70 °C (Entry 2). Once again, benzylidene protected trehalose **18** was recovered, however the imidazole had degraded, highlighting its lack of stability at high temperatures. It was then proposed that imidazolylmethyl chloride **20** might not be reactive enough, and thus the imidazolylmethyl bromide **19** was employed instead (Entry 3).The use of bromide **19** however, made little difference to the reaction outcome and only starting material were recovered.

Table 3 Attempts at the alkylation with nitroimidazolylmethyl halides (**19-20)**

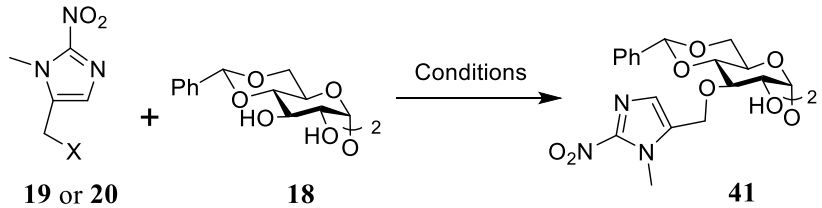

19 or **20** **18** **41**

Entry	X	Conditions	Isolated compound
1	Cl	NaH, TBAI, DMF, r.t.	**18** + **20**
2	Cl	NaH, TBAI, DMF, 70 °C	**18** only
3	Br	NaH, TBAI, DMF, 0-70 °C	**18** only

At this point, the carbohydrate substrate was changed from a benzylidene protected derivative to the more robust, isopropylidene protected galactose **42** in order to explore the parameters of the alkylation reaction (Table 4). In this way, the chemistry could be optimised using a more reactive substrate before continuing on with the planned synthetic route. As degradation of imidazolylmethyl bromide **19** was observed during test reactions with NaH (Entry 3, Table 3), milder reaction conditions were attempted. First, different bases were used (Entries 1-4, Table 4),

however, neither caesium carbonate, 1.1 M sodium hydroxide, 6.3 M sodium hydroxide, or 10 M sodium hydroxide led to the desired transformation and only starting materials were recovered. Satisfied that these bases were not strong enough to deprotonate the alcohol a stronger base, potassium *tert*-butoxide, was used and a variety of reaction conditions were explored including changes to the solvent (DMF, *t*-BuOH, or toluene) and temperature (25 °C – 70 °C) (Entries 5-7). Finally, the reaction was performed in the presence of silver(II) oxide and TBAI (Entry 9), however, this approach yielded no success and once again, starting material was isolated.

Table 4. Attempts at the alkylation of galactose **42** with nitroimidazole bromide **19**

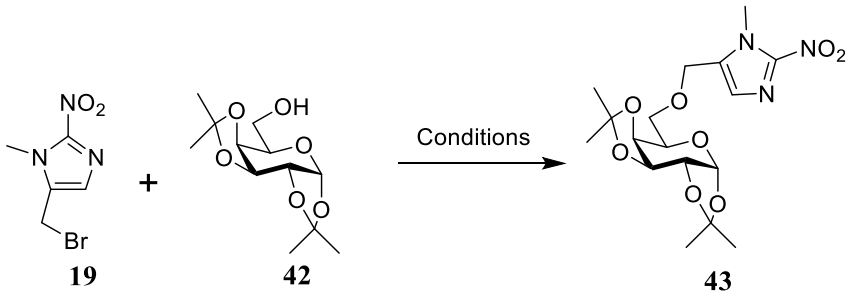

Entry	Conditions	Isolated compound
1	Cs_2CO_3, TBAI, DMF, r.t.	**19** + **42**
2	1.1 M NaOH, DCM, r.t.	**19** + **42**
3	6.3 M NaOH, DCM, r.t.	**19** + **42**
4	10 M NaOH, DCM, r.t.	**19** + **42**
5	*t*-BuOK, TBAI, DMF, r.t.	**19** + **42**
6	*t*-BuOK, TBAI, DMF, 70 °C	**19** + **42**
7	*t*-BuOK, TBAI, *t*-BuOH, 25 °C	**19** + **42**
8	*t*-BuOK, Toluene, r.t.	**19** + **42**
9	Ag_2O, TBAI, DMF, r.t.	**19** + **42**

Frustrated by the lack of success in the alkylation reactions when using nitroimidazolylmethyl halide **19** or **20** and either a primary or secondary aliphatic alcohol, a further search of the literature was conducted in order to understand more about the reactivity of this prodrug trigger. The result of this search suggested that no primary aliphatic, secondary aliphatic, or non-aromatic alcohols have been used in alkylation reactions when using nitroimidazolylmethyl halides **19** or **20**. However, nitroimidazolyl bromide **19** has been reported to be used successfully in a number of alkylation reactions with aromatic alcohols.[98] It was therefore hypothesised that nitroimidazolylmethyl bromide **19** was only a suitable alkylating agent for aromatic, rather than aliphatic, alcohols. To test this theory, a test reaction was conducted using phenol (**44**) as the model alcohol, and imidazolylmethyl bromide **19** as the alkylating reagent. The reaction proceeded uneventfully to give the corresponding imidazole-phenol conjugate **45** in 61% yield (Scheme 10).

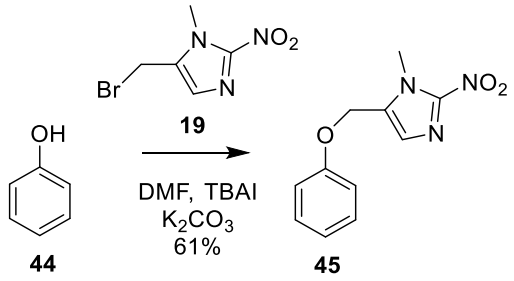

Scheme 10. Alkylation of phenol (**44**) with nitroimidazole bromide **19**

In order to understand the lack of reactivity observed in the alkylation reactions with aliphatic alcohols, the factors dominating S_N2 reactions must be considered. When a nucleophile attacks a saturated carbon, the nucleophile must donate its electrons from its non-bonding orbital into the σ*-antibonding orbital of the C-X bond, where X is the leaving group.[97] Typically, the σ*-antibonding orbital of the electrophile is higher in energy than the non-bonding orbital of the nucleophile. Because good orbital overlap is critical for orbital controlled reactions, the closer in energy the non-bonding and σ*-antibonding orbitals, the more favourable the

reaction (Figure 12). It is for this reason that softer nucleophiles (with higher energy non-bonding orbitals), react more favourably in S_N2 reactions. In the context of the imidazole alkylation reaction, the nucleophile is charged and basic, and would thus be considered to be a hard nucleophile. Therefore, it is possible that the lack of reactivity between the imidazole bromide **19** and galactose **42** is due to insufficient orbital overlap between the highest occupied molecular orbital (HOMO) of the galactose nucleophile and the lowest unoccupied molecular orbital (LUMO) of the imidazole bromide **19**. In the case of phenolic alcohols, however, the electron density is delocalised over the aromatic system, which results in a considerably softer nucleophile. Consequently, the orbital overlap between the HOMO of the phenol and the LUMO of the imidazole bromide **19** would be much greater, resulting in enhanced reactivity between the two substrates.

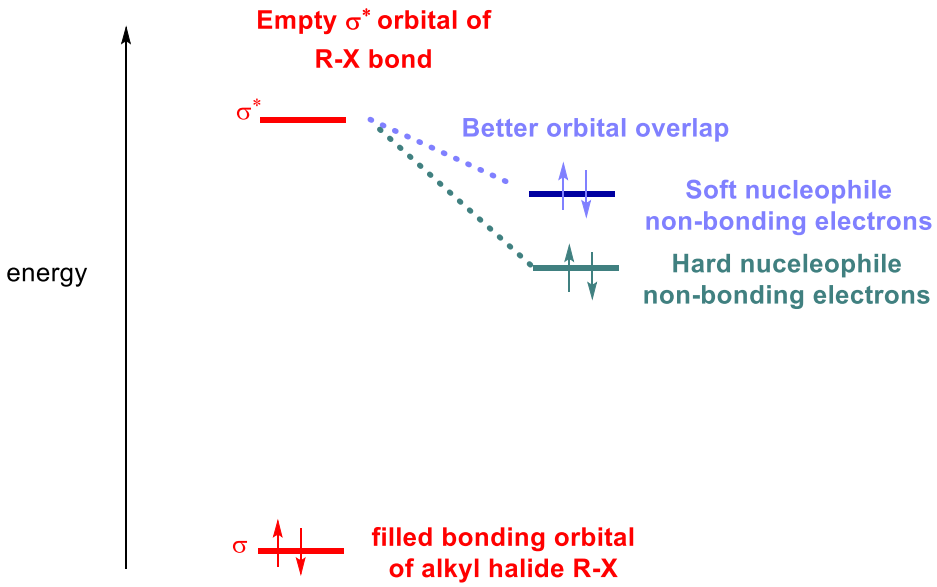

Figure 12. Orbital interactions during S_N2 alkylation reactions

2.3.1 Summary of attempted synthesis of H-TDB 17:

In this section of work, benzylidene protected trehalose **18** was successfully synthesised to be used in an alkylation reaction with nitroimidazole halides **19** and **20**. A number of reaction conditions were employed for the alkylation reaction, including several different solvents, bases, and reaction temperatures. Unfortunately, none of these conditions led to the formation of the desired product, and only starting materials were recovered. A thorough literature review revealed that no primary aliphatic, secondary aliphatic, or non-aromatic alcohols had ever been successfully used in alkylation reactions when using nitroimidazole halides **19** and **20**. Successful synthesis of phenol imidazole conjugate **45** suggested that there are serious issues of reactivity between imidazole bromide **19** and non-aromatic alcohols and therefore, a new method of attaching the imidazole trigger to the trehalose effector needs to be developed.

2.4 Development of a new carbonate linker strategy

As it seemed unfeasible to directly alkylate protected trehalose **18** using nitroimidazole bromide **19** or chloride **20**, the modular design of the prodrug was revisited. As previously discussed, hypoxia-activated prodrugs are typically divided into two domains, the trigger and the effector, with the option of a linker to connect the two essential units.[99] To alleviate the difficulties associated with the direct alkylation of trehalose **18**, it was thus proposed that a linker could be positioned between the nitroimidazole trigger and the trehalose effector (Figure 13). Any linker that is to be used in this setting must satisfy a specific set of criteria. First, the linker must fragment in a manner similar to that of the original prodrug design while remaining stable to various categories of cellular enzymes. Additionally, the linker must be readily attached to both the trigger and effector moieties.

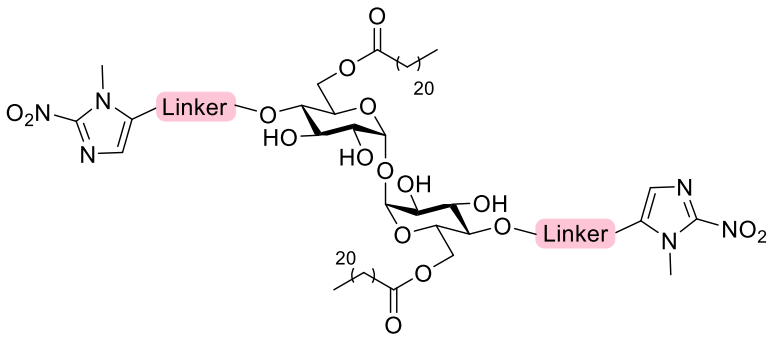

Figure 13. Generic design of a hypoxia-activated prodrug using a linker strategy.

In an attempt to meet the aforementioned criteria for a suitable linker strategy, a number of linker units were considered (Figure 14). The 1-6 spacer developed by Carl *et al.* has proven promising and has been used in the development of paclitaxel prodrugs (Figure 14a).[100, 101] Upon liberation of the phenol moiety, the group becomes electron donating, which leads to 1-6 elimination of the effector molecule. Elongated spacers, such 1-8 and 1-10 spacers, developed by Scheeren *et al.*, can be used in a similar manner (Figure 14b, 14c, and 14d), whereby 1-8 or 1-10 elimination produces the effector moiety.[101] Finally, the selectivity of prodrugs derived from parent drugs incorporating a hydroxyl group is often improved by the

integration of a bis-amine cyclisation spacer (Figure 14e).[101] Here, 1-6 elimination liberates the bis-amine spacer, which readily cyclises, thereby eliminating the effector molecule. That said, these linker strategies would be challenging synthetic targets, and adding numerous steps to the overall synthetic route. The use of a carbonate linker, however, would provide simple synthetic targets, adding only two additional steps to the synthetic route (Figure 14f). Therefore, it was proposed that the imidazole trigger **47** could be attached through a carbonate linker to TDB so as to form the H-TDB **46** (Figure 15A). It was hypothesised that the trigger-carbonate linker combination would dissociate in an analogous pattern to that of the original design, with the production of carbon dioxide providing a supplementary driving force for the fragmentation process (Figure 15B), and that the carbonate linkage would be relatively stable to non-specific degradation. Carbonate linkages are considered to be relatively stable to hydrolysis in aqueous buffers at physiological pH, and have been shown to hydrolyse three-fold slower than their ester-linked counterparts.[102] It is important to note, however, that there has been insufficient investigation into the broad enzymatic stability of carbonate linkages and consequently, the chemo-enzymatic stability of this linker system will need to be evaluated.

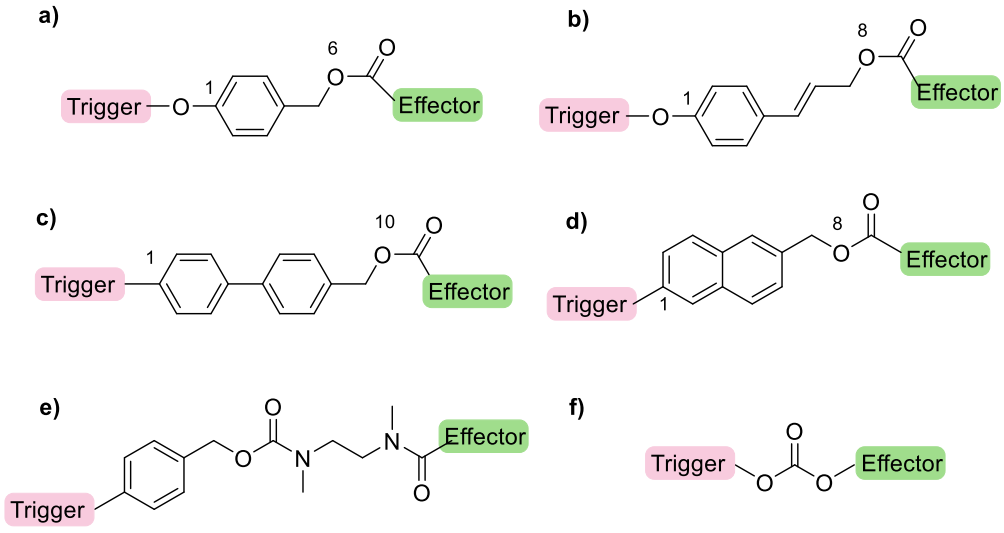

Figure 14. Potential linker strategies

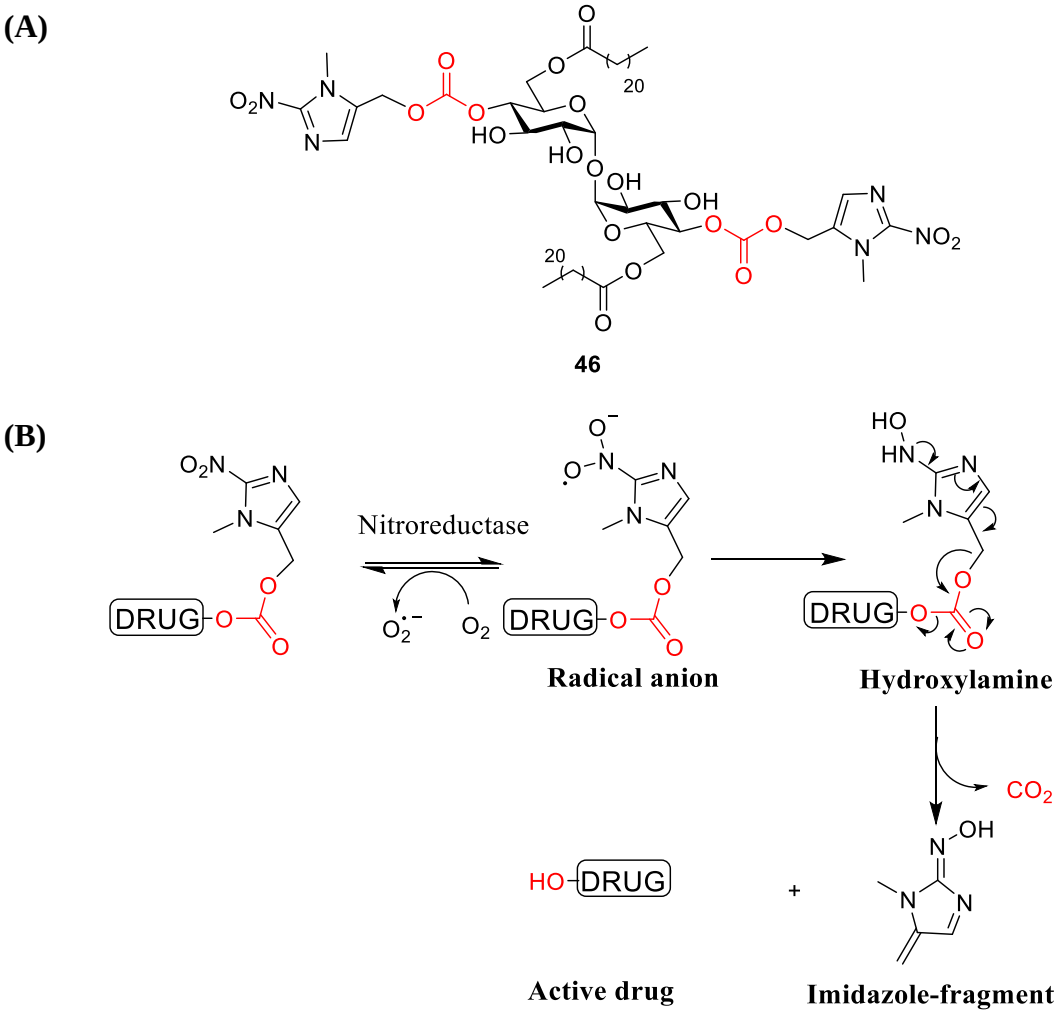

Figure 15. (A) New prodrug target (H-TDB **46**)
(B) Predicted fragmentation patter of the carbonate linker.

2.4.1 Determining the validity of the carbonate linker

For the carbonate-linker strategy to be useful in the design of the trehalose prodrug **46**, it was first necessary to demonstrate that the carbonate functionality could be successfully installed onto the nitroimidazole trigger **37** and linked to an aliphatic alcohol. To this end, it was proposed that nitroimidazole **37** first be reacted with triphosgene to yield the chloroformate **47** (Scheme 11),[103] and that aliphatic alcohols could then be reacted with chloroformate **47** to produce a range of hypoxia-activatable compounds. To determine the validity of the carbonate linker in

the context of carbohydrate chemistry, isopropylidene protected galactose **42** was selected as the model alcohol to be reacted with chloroformate **47** (to give **48**) due to the ease of its synthesis.

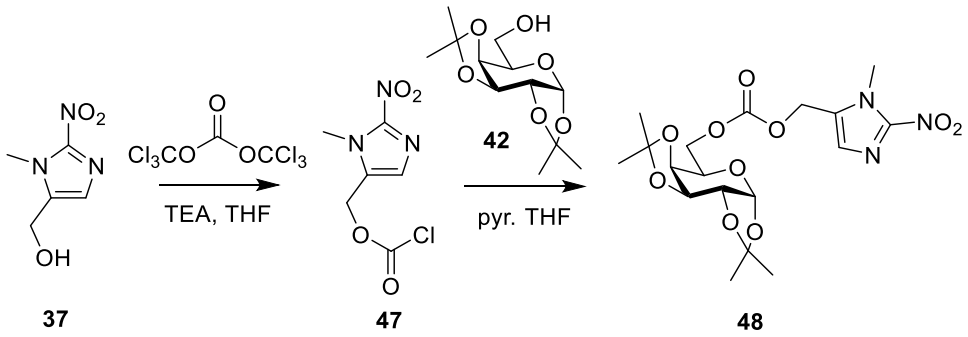

Scheme 11. Proposed synthetic strategy for galactose-imidazole conjugate **48**

To synthesise chloroformate **47**, the nitroimidazole-trigger **37** was first reacted with triphosgene in THF at room temperature. Unfortunately, these conditions led to the formation of a chlorinated adduct, which was tentatively assigned as imidazolylmethyl chloride (**20**) on the basis of HRMS analysis [HRMS(ESI) *m/z* calcd. For $[C_5H_6ClN_3O_2+H]^+$: 176.0221, obsd.: 176.0218]. Here, the chloride ion liberated in the first step of the reaction attacks the electrophilic carbon of chloroformate **47**, displacing a molecule of carbon dioxide and a further chloride ion to give the chlorinated by-product **20** (Scheme 12). Indeed, similar chlorinated by-products have been observed when treating alcohols with triphosgene.[104] In an attempt to reduce the rate of this side reaction, the reaction time was decreased and the reaction temperature was lowered. Unfortunately, neither of these approaches was met with success.

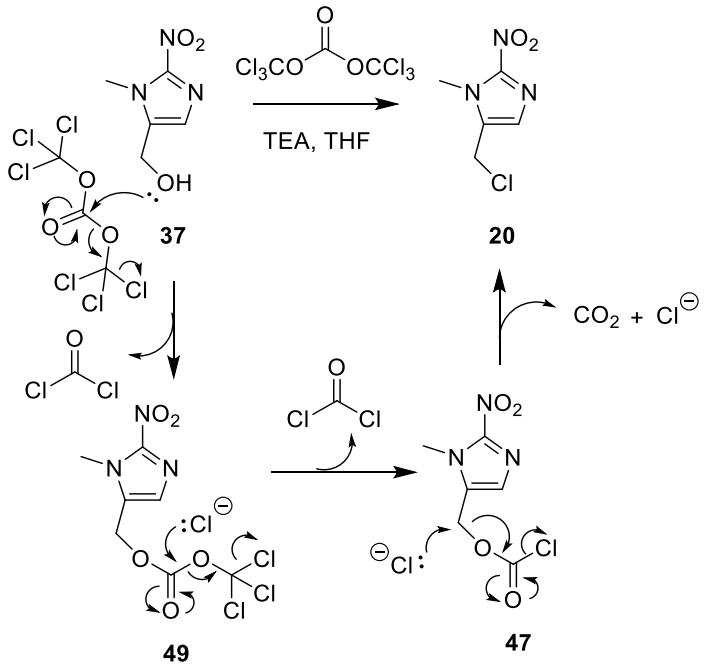

Scheme 12 Attempts to synthesise acid chloride **47**

Due to the difficulties accompanying the synthesis of chloroformate **47**, an alternative strategy was proposed. Here, isopropylidene protected galactose **42** was first reacted with triphosgene to produce the chloroformate **51** (Scheme 13). Gratifyingly, this reaction proceeded smoothly to yield the desired chloroformate **51** in excellent yield (92%), as evidenced by ^{13}C NMR spectral data which included a resonance signal at 150.8 ppm indicative of the chloroformate. Furthermore, an HMBC between this carbon and the protons at 4.40 ppm confirmed the chloroformate was installed at the 6-hydroxyl of galactoside **42**. Chloroformate **51** was promptly carried through to the next step where it was reacted with nitroimidazole **37** to give the desired galactose-imidazole conjugate **52** in a modest 35% yield. A downfield shift of the imidazole methylene protons from 4.67 ppm to 5.18 ppm was consistent with formation of the carbonate linkage. Moreover, an HMBC between the carbonate carbon at 154.3 ppm and H-6a and H-6b on galactose (4.29 ppm) as well as the methylene protons on the nitroimidazole (5.18 ppm) confirmed that the desired imidazole conjugate had been synthesised. The low yield of this reaction can be attributed to the reaction of chloroformate **51** with its hydrolysed counterpart **42** to yield a galactosyl carbonate dimer as a major byproduct of the reaction (*ca*. 50% yield). In an attempt to optimise this reaction,

the number of equivalents of chloroformate **51** used was increased, however this resulted in the isolation of a greater amount of galactosyl carbonate dimer. In the interest of time, further optimisation was left to a later date in order to continue with the synthetic scheme. Additionally, it should also be noted that galactose **42** gave the desired chloroformate in good yield, yet the similar reaction with nitroimidazole **37** was unsuccessful. While it is difficult to conclusively account for the different reactivities of the two alcohols with triphosgene, the result does suggest that the 6-position in the nitroimidazole intermediate **50** is far more electrophilic than the corresponding centre in the galactose chloroformate **51**.

2.4.2 Development of a new carbonate linker: summary

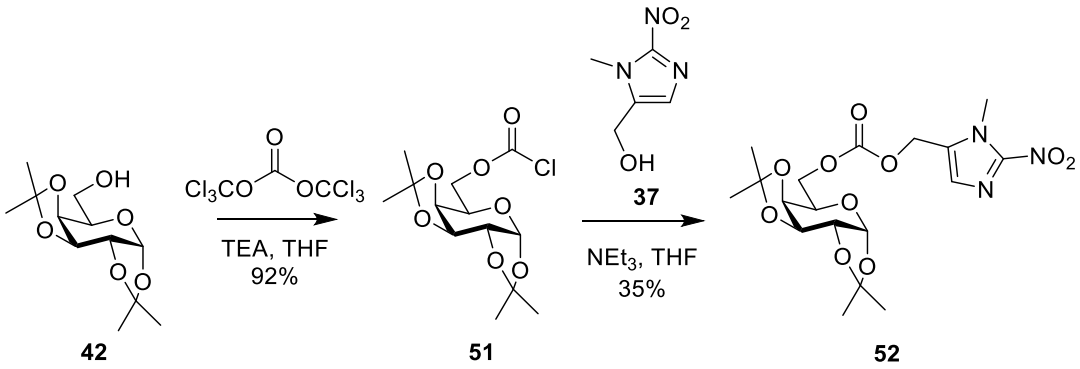

Scheme 13. Synthetic strategy for galactose-imidazole conjugate **52**

In this section, the choice of a carbonate group as a suitable linker strategy to connect the TDB to the nitroimidazole trigger was discussed. It was envisioned that the nitroimidazole trigger **37** could be reacted with triphosgene to produce chloroformate **51**, which could then be further reacted with a suitable carbohydrate, thus demonstrating the validity of this approach. The reaction of **37** with triphosgene, however, resulted only in the isolation of nitroimidazole chloride **20**, and the synthetic strategy was therefore re-evaluated. To circumvent this issue, chloroformate **51** was synthesised in excellent (92%) yield and was subsequently reacted with **37** to successfully produce galactose imidazole conjugate **52**, albeit in 35% yield, thereby demonstrating the validity of the carbonate linker in this setting.

2.5 Design of a reporter fluoroprobe

Having successfully demonstrated that the carbonate linker can be used to connect imidazole trigger **37** to a model carbohydrate, the next step was to establish that the new prodrug trigger would fragment in the expected manner under reductive conditions. For this reason, a reporter fluoroprobe **53** containing the nitroimidazole trigger **37** attached through a carbonate linker to the highly fluorescent 7-hydroxy-4-methylcoumarin (**55**), also commonly known as 4-methylumbelliferone, was designed (Figure 16A). Coumarins that have an electron donating group, such as a hydroxyl, at the 7-position are typically highly fluorescent, however, if an electron-withdrawing group, such as an ester or carbonate, is located at the 7-position, the molecule becomes practically non-emissive.[105] In this way, the reporter fluoroprobe **53** should be non-fluorescent while intact, however, upon reduction of the nitroimidazole and fragmentation of the linker, the fluorescent 4-methylumbelliferone (**55**) would be reformed (Figure 16B). This particular reporter fluoroprobe approach has been previously implemented to investigate the activity of various enzymes such as carboxylesterases and sulfatase.[106, 107] In this work, the ability of fluoroprobe **53** to fragment under reductive conditions will be explored using two-electron nitroreductases to reduce the nitroimidazole to the corresponding hydroxylamine, and also using cell-based hypoxic conditions, where one-electron reductases will be employed to reduce the nitroimidazole to the radical anion.

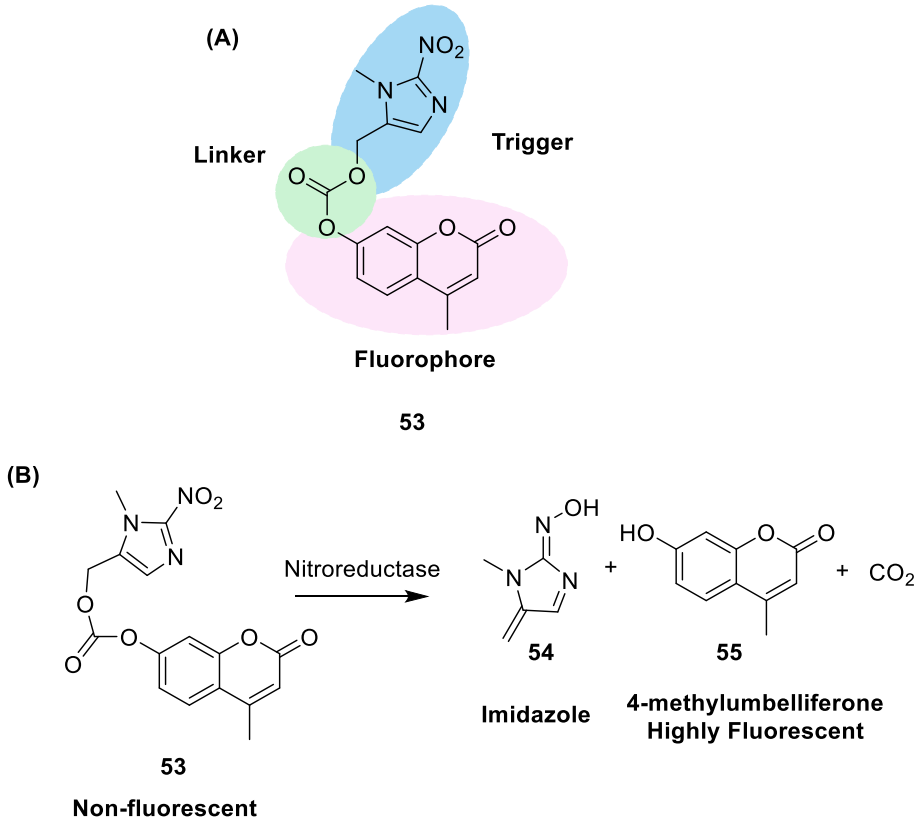

Figure 16. (A) Modular design of reporter fluoroprobe **53 (B)** Predicted fragmentation pattern of reporter fluoroprobe **53** to produce 4-methylumbelliferone (**55**) and imidazole fragment **54**

2.5.1 Synthesis of the reporter fluoroprobe

The synthetic strategy used to prepare reporter fluoroprobe **53** is illustrated in Scheme 14. First, 4-methylumbelliferone (**55**) was treated with triphosgene to produce the corresponding chloroformate **56** in 77% yield. Following purification by silica gel flash chromatography, chloroformate **56** was then immediately added to a solution of the imidazole trigger **37** in pyridine at 70 °C. After stirring for four hours, TLC analysis revealed the formation of a lower running spot (R_f = 0.2, 1:1, PE:EtOAc), and mass spectral analysis indicated the desired product had been formed [HRMS(ESI) *m/z* calcd. For $[C_{16}H_{13}N_3O_7+H]^+$: 360.0826, obsd.: 360.0836]. The reaction mixture was then concentrated under reduced pressure and purified by

silica gel flash chromatography to give the target probe **53** in 25% yield. Due to the labile nature of chloroformate **56**, formation of a 4-methylumbelliferone carbonate dimer (*ca*. 65% yield) resulted in a relatively low yield of **53** for this step. A downfield shift of the imidazole methylene protons from 4.29 ppm to 5.30 ppm in the ^{1}H NMR suggested that the carbonate linkage had been formed.

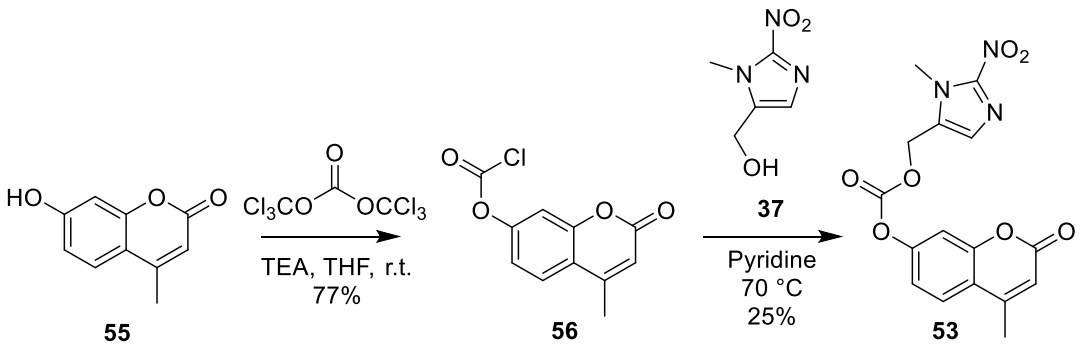

Scheme 14. Synthesis of reporter fluoroprobe **53**

2.5.2 Enzymatic assay of the reporter fluoroprobe [1]

A bacterial enzymatic assay was used to assess the activity of reporter fluoroprobe **53**. Here, bacterial candidates either overexpressing a selected 2-electron nitroreductase or with all known nitroreductases knocked out, were challenged with the reporter fluoroprobe **53**.[108] Such bacterial two electron nitroreductases reduce similar nitro-triggers to the corresponding hydroxylamine in an oxygen-independent manner,[109] and according, it was proposed that reporter fluoroprobe **53** would be reduced via a two-electron process to give the hydroxylamine intermediate, which would fragment via the loss of CO_2 to give the highly fluorescent 4-methylumbelliferone (**55**) (Scheme 15). If the carbonate linker does not fragment, however, there will be no overall change in fluorescence.

[1] All enzymatic assay work was carried out with assistance from Dr Elsie Williams in the Ackerley lab, Victoria University of Wellington

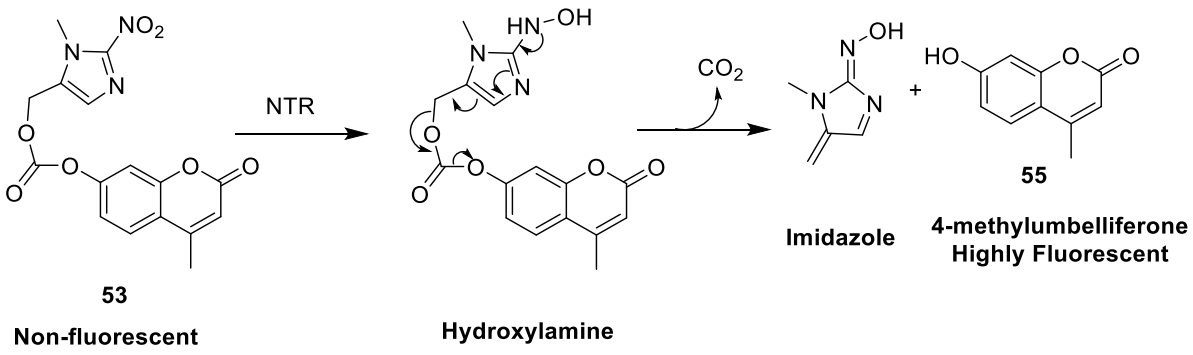

Scheme 15. Predicted fragmentation pattern of reporter fluoroprobe **53** to produce 4-methylumbelliferone (**55**) after reduction by a bacterial nitroreductase

To commence these studies, five nitroreductase overexpression strains known to reduce other nitroaromatic hypoxia-activated prodrugs were selected.[108] These overexpression strains (NemA_Ec, NfsA_Li, NfsB_Vv, NfsB_Ec, and NfsA_Ec), as well as the nitroreductase knockout strain, were incubated with fluoroprobe **53** at various concentrations (0, 3.13, 6.25, 12.5, 25, 50, and 100 µM) for 120 minutes, during which fluorescence measurements were made at 15 minute intervals. At lower concentrations (0-50 µM), there was very little difference in fluorescence between the overexpression and control strains (Figure 17A), however, at 100 µM, an increase in mean fluorescence intensity was observed when using the overexpression strains, which is indicative of the successful reduction and fragmentation of the nitroimidazole trigger to produce the highly fluorescent 4-methylumbelliferone (**55**). Because all candidate overexpression strains reduced the nitroimidazole trigger at 100 µM concentration, further analysis was simplified by only considering two enzymes, NfsB_Ec and NfsA_Ec. Herein, it should also be noted that, albeit to a lesser extent, the addition of the reporter fluoroprobe **53** to the *E. Coli* knockout strain also resulted in an increase in mean fluorescence intensity over time (Figure 17B). This increase in fluorescence may be due to non-enzymatic hydrolysis of the carbonate causing an increase in abundance of 4-methylumbelliferone (**55**), however, as carbonate linkages are known to be relatively stable in an aqueous environment,[102] it is more likely that there is some

non-specific enzymatic cleavage of the carbonate linker. Nonetheless, the increase in mean fluorescence intensity over time is greater in the overexpression strains than in the knockout strain, thus indicating that the nitroreductases contribute to the fragmentation of the prodrug.

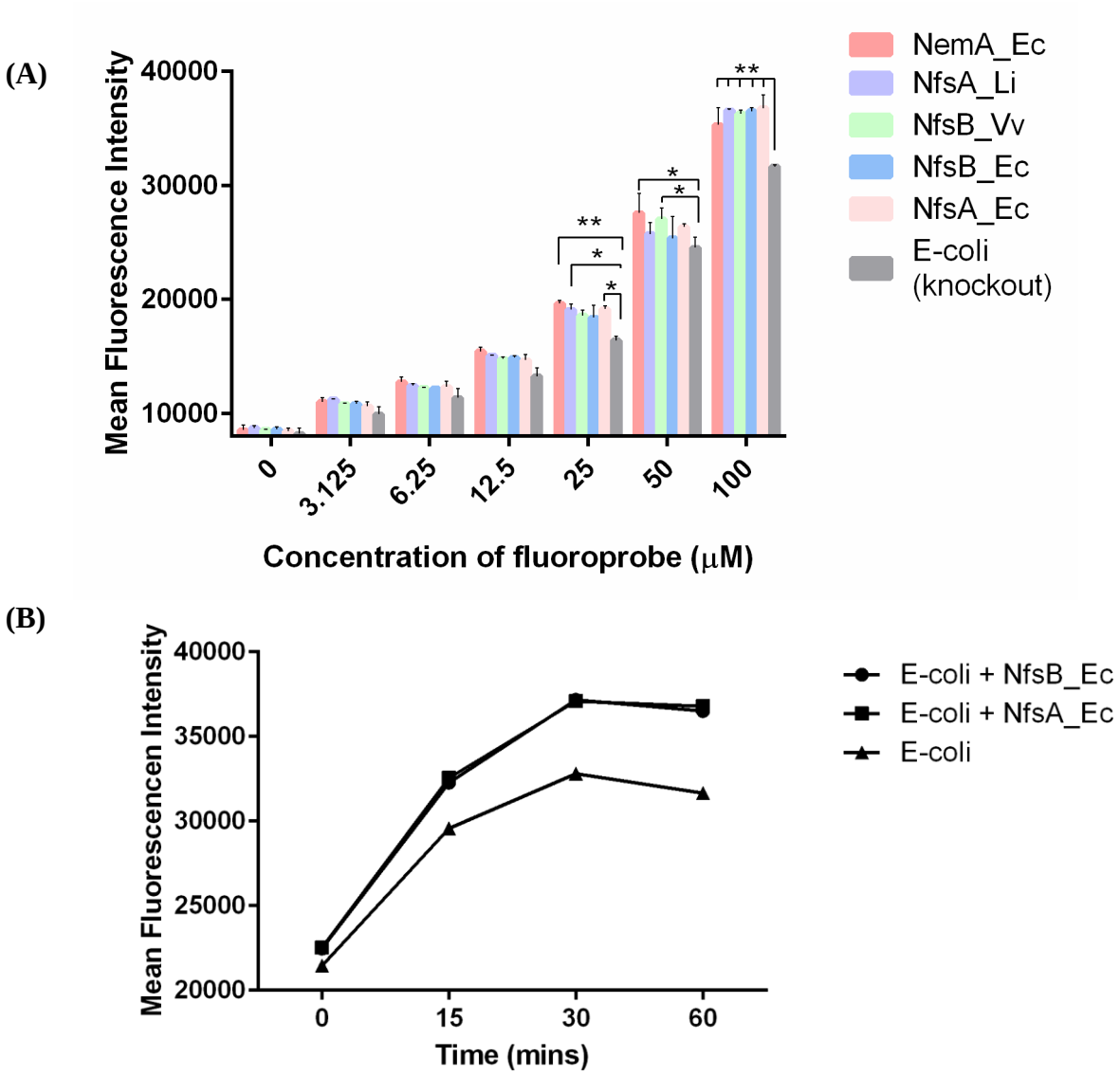

Figure 17. (A) Mean fluorescence intensity (λ_{em} = 460 nm) measured 60 minutes after the addition of reporter fluoroprobe **53** (at 0, 3.125, 6.25, 12.5, 25, 50, or 100 μM) to *E. Coli* nitroreductase overexpression strain (NemA_Ec, NfsA_Li, NfsB_Vv, NfsB_Ec, or NfsA_Ec) or *E. Coli* knockout strain [*E. Coli* (knockout)]. Error bars represent the SEM across two replicates. $^{**}p < 0.01$, $^{*}p < 0.05$ **(B)** Mean fluorescence measured 0, 15, 30, and 60 minutes after addition of reporter fluoroprobe **53** (100μM) to *E. Coli* nitroreductase overexpression strains (NfsB_Ec and NfsA_Ec) or *E. Coli* knockout strain [*E. Coli* (knockout)]. Fluorescence averaged across two replicates.

Having established that the fragmentation of fluoroprobe **53** occurs under the agency of several nitroreductases, the assay was then repeated using a wider fluoroprobe **53** concentration range (0-500 μM). As illustrated (Figure 18), in the absence of fluoroprobe **53**, there is no difference in mean fluorescence intensity between the knockout and overexpression strains ($p > 0.05$). However, upon addition of fluoroprobe **53** (at 15.75, 31.25, and 62.5 μM) there is a small but statistically significant increase in fluorescence between the knockout strain and the NfsB_Ec strain ($p < 0.05$). Interestingly, there is no difference in mean fluorescence intensity between the knockout and NfsA_Ec strains at these concentrations, which suggests that fluoroprobe **53** is a better substrate for the NfsB_Ec nitroreductase compared to the NfsA_Ec nitroreductase. At the higher concentrations (125, 250, and 500 μM), however, there is a statistically significant increase in fluorescence between the knockout strain and both overexpression strains [$p < 0.01$ (125 μM), $p < 0.05$ (250 μM), and $p < 0.01$ (500 μM)]. Taken as a whole, these results demonstrate that *E. Coli* overexpression strains NfsA_Ec and NfsB_Ec successfully reduce fluoroprobe **53**, with the probe being a slightly better substrate for NfsB_Ec.

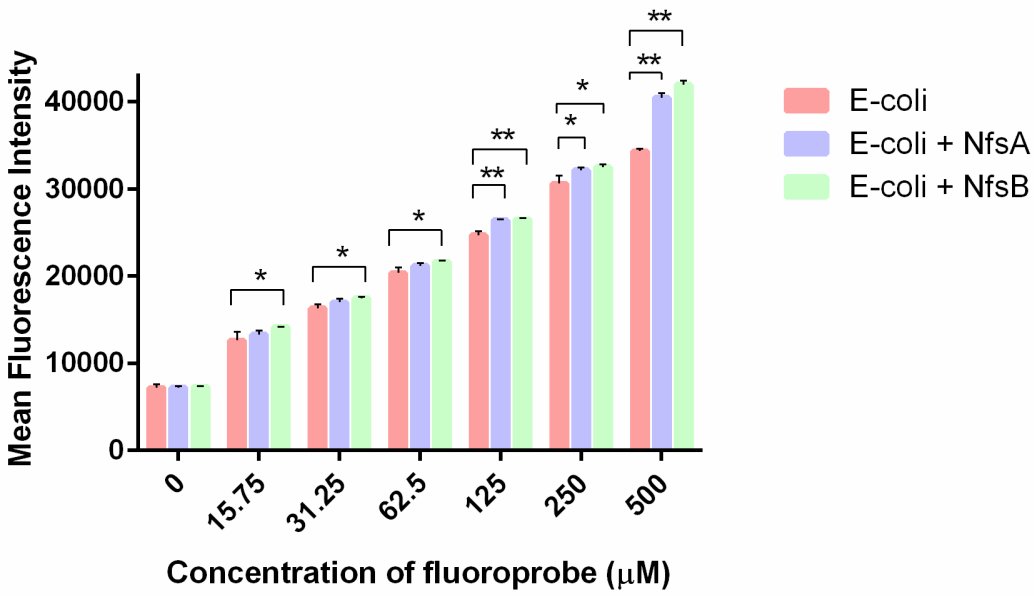

Figure 18. Mean fluorescence intensity (λ_{em} = 460 nm) measured 120 minutes after addition of reporter fluoroprobe **53** (at 0, 15.75, 31.25, 62.5, 125, 250, or 500 μM) to *E. Coli* nitroreductase overexpression strains (NfsA_Ec or NfsB_Ec) or *E. Coli* knockout strain (*E. Coli*). Error bars represent the SEM across three replicates. $^{**}p < 0.01$, $^{*}p < 0.05$.

The time course for the fragmentation of fluoroprobe **53** at a concentration of 500 μM is illustrated in Figure 19A. As shown, the mean fluorescence intensity of fluoroprobe **53** in the presence of any of the bacterial overexpression strains reaches a plateau at approximately 120 minutes. When compared to the positive control, 4-methylumbelliferone (**55**), the mean fluorescence intensity after a 120 minute incubation time reached approximately 60% of the theoretical intensity (Figure 19B), which suggests that not all of fluoroprobe **53** is being converted to 4-methylumbelliferone **(55)**. This difference in mean fluorescence intensity could arise because fluoroprobe **53** is a poor substrate for two electron nitroreductases, or alternatively, fluoroprobe **53** could be sequestered into other cellular compartments before it can be reduced by nitroreductases.

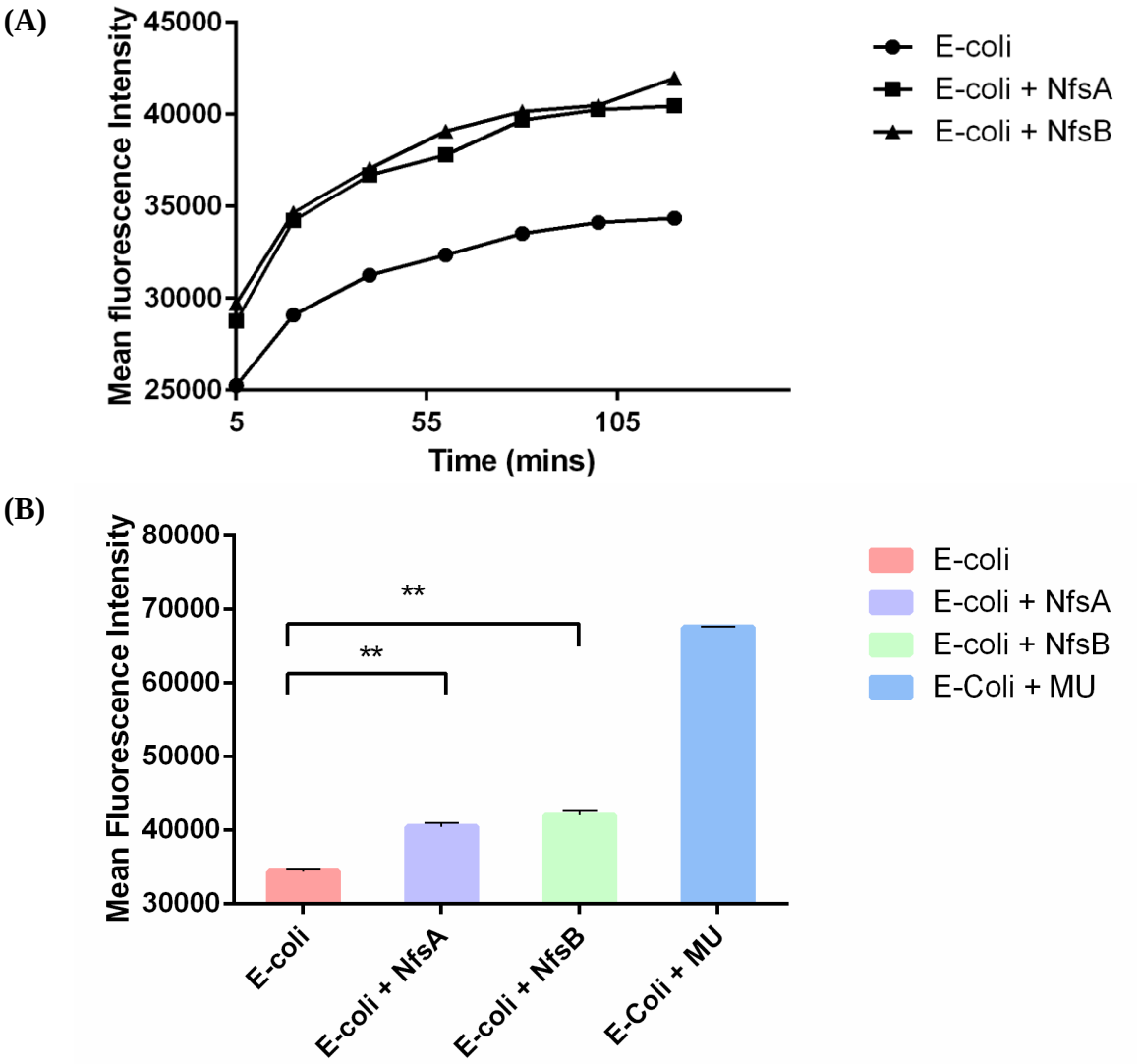

Figure 19. (A) Mean fluorescence intensity (λ_{em} = 460 nm) measured 0, 20, 40, 60, 80, 100, and 120 minutes after addition of reporter fluoroprobe **53** (500 µM) to *E. Coli* nitroreductase overexpression strains (NfsA_Ec or NfsB_Ec) or *E. Coli* knockout strain (*E. Coli*). **(B)** Mean fluorescence intensity measured 120 minutes after addition of reporter fluoroprobe **53** (500 µM) or 4-methylumbelliferone (MU) (500 µM) to *E. Coli* overexpression strains (*E. Coli* + NfsA_Ec or *E. Coli* + NfsB_Ec) or *E. Coli* knockout strain (*E. Coli*). Error bars represent SEM across 3 replicates. $^{**}p < 0.01$, $^{*}p < 0.05$.

To gain some understanding about how the reduction and fragmentation of the carbonate-linked fluoroprobe **53** compared to the more typical ether-linked prodrug design, the analogous ether-linked probe **57** was synthesised via the alkylation of 4-methylumbelliferone (**55**) with nitroimidazole bromide (**19**) (Scheme 16). The synthesis of ether-linked probe **57** proceeded uneventfully and in a good yield for

these types of alkylation reactions (55%). Once again, standard spectroscopic techniques were employed to confirm that the expected product had been successfully prepared.

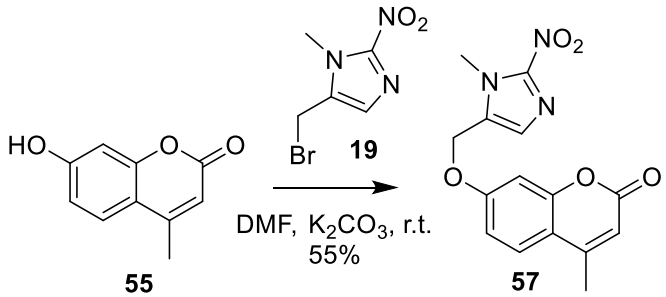

Scheme 16. Alkylation of 4-methylumbelliferone (**55**) with nitroimidazole bromide **19**

The ether-linked probe **57** and fluoroprobe **53** were then tested in the bacterial enzymatic assay, whereby the data sets were normalised to allow for comparison between the two probes which displayed markedly different background fluorescence. To illustrate this, fluorescence emission spectra were obtained for 4-methylumbelliferone (**55**) and fluoroprobes **53** and **57**. When excited at 372 nm, the λ_{em} for 4-methylumbelliferone (**55**) and fluoroprobes **53** and **57** was 466 nm (Figure 20A). Although the emission of carbonate-linked fluoroprobe **53** was significantly quenched in comparison to 4-methylumbelliferone (**55**), it is still much more emissive than its ether-linked counterpart (**57**). This result explains the comparably high levels of background fluorescence observed in the enzymatic assay. In addition to fluorescence emission spectra, quantum yields provide a good approximation of the fluorescence of a given compound. With this in mind, quantum yields were determined for both the carbonate- and ether-linked nitroimidazole fluoroprobes **53** and **57** (Φ_f = 0.26 and 0.06, respectively) and 4-methylumbelliferone (**55**, Φ_f = 0.41), which corroborated the conclusions made from the fluorescence emission spectra. As illustrated below (Figure 20B), the increase in mean fluorescence intensity of the ether-linked fluoroprobe **57** is much greater than that of the carbonate-linked fluoroprobe **53** when exposed to the actions of NfsA_Ec, thus suggesting that the ether-linked fluoroprobe **57** is a better substrate for the two-electron bacterial nitroreductases than the carbonate-linked

fluoroprobe **53**. That said, the target enzyme in a hypoxic setting is a one-electron nitroreductase and these reductases will have different specificities to this bacterial model. Accordingly, the relative specificities of nitroimidazole prodrugs need to be determined in a more advanced *in vitro* model, using the cell type that will be targeted.

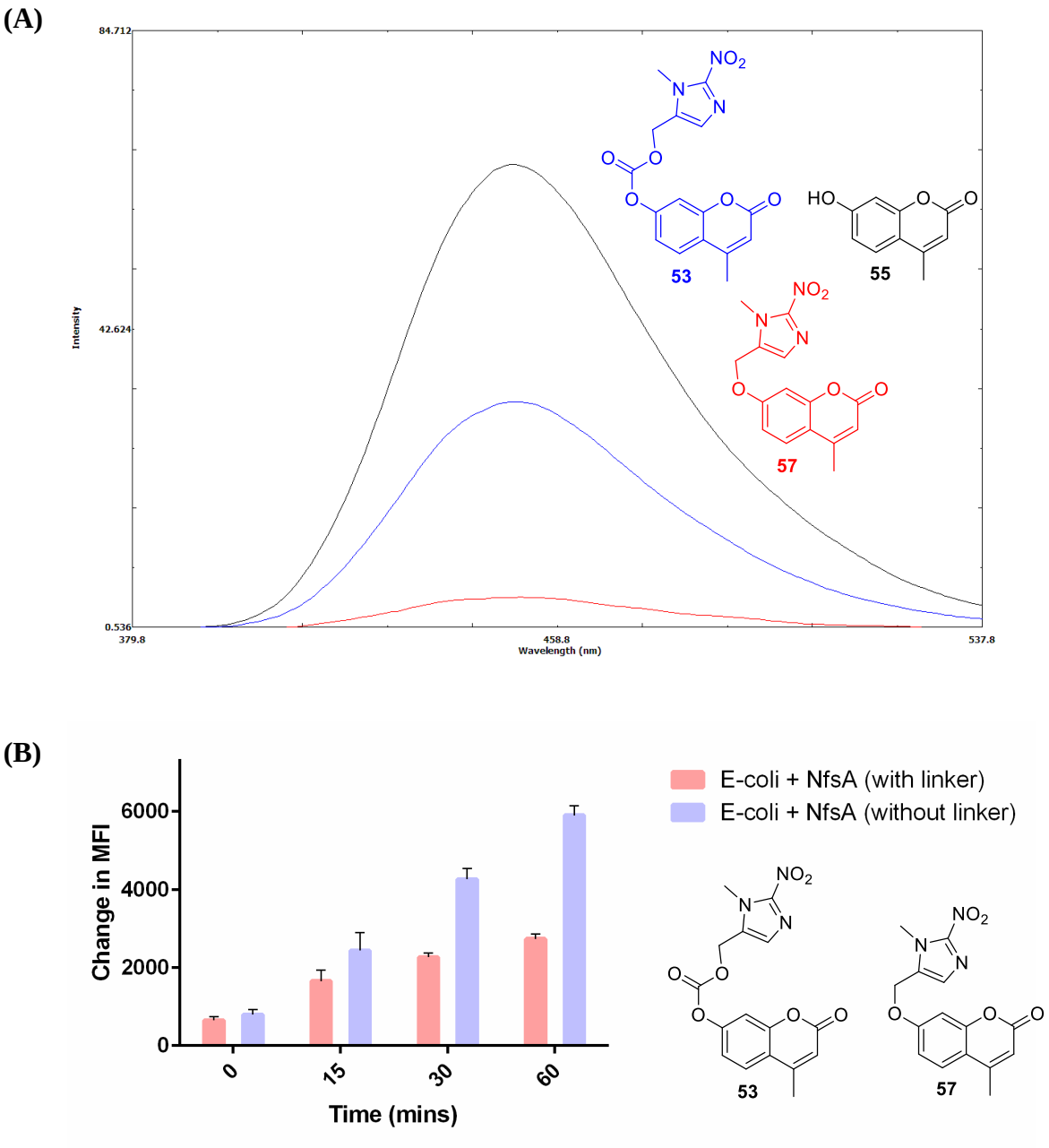

Figure 20. (A) Fluorescence emission spectra for 4-methylumbelliferone (**55**) (0.05 mg/mL, blue line) and fluoroprobe **53** (0.05 mg/mL, black line). Excitation wavelength = 372 nm. **(B)** Mean fluorescence intensity measured 0, 15, 30, and 60 minutes after the addition of reporter fluoroprobes **53** (with carbonate linker) and **57** (ether-linked) (at 25 µM) to *E. Coli* nitroreductase over expression strain (*E. Coli* + NfsA). Data normalised by the subtraction fluorescence values of *E. Coli* knockout strain from fluorescence values of the *E. Coli* nitroreductase overexpression strain. Error bars represent SEM across 2 replicates.

2.5.3 Summary of design and enzymatic assay of reporter fluoroprobe 53

In this piece of work, carbonate-linked reporter fluoroprobe **53** was synthesised in two steps from 4-methylumbelliferone (**55**) and nitroimidazole trigger **37**. The ability of reporter fluoroprobe **53** to fragment upon reduction was assessed via the use of a bacterial enzymatic assay. Here, it was shown that two-electron nitroreductases could successfully reduce reporter fluoroprobe **53** to the corresponding hydroxylamine, resulting in fragmentation of the carbonate linker and liberation of 4-methylumbelliferone (**55**). It must be noted, however, that the two-electron nitroreductases were more efficient at reducing the analogous ether-linked fluoroprobe **57**. In any case, to truly assess the potential of the carbonate-linked fluoroprobe **53**, a more advanced *in vitro* model needs to be employed.

2.6 Development of a macrophage assay for reporter fluoroprobes

After successfully demonstrating that reporter fluoroprobe **53** can be reduced by 2-electron bacterial nitroreductases to give 4-methylumbelliferone (**55**), the next step was to investigate whether fluoroprobe **53** could be selectively activated under hypoxic conditions. As the overall objective of this research is to use a hypoxia-activated TDB prodrug for the activation of macrophages, it was thus determined that an appropriate cellular assay would involve macrophages incubated under both hypoxic and normoxic conditions.[23, 112, 113] Accordingly, an assay was designed whereby RAW 264.7 murine macrophages would be used as a cellular source of one-electron nitroreductases. In this way, incubation of the reporter fluoroprobe **53** with RAW 264.7 cells under either hypoxic or normoxic conditions would result in the reduction of fluoroprobe **53** to the radical anion **58** (Scheme 17). Under hypoxic conditions, the radical anion **58** should be further reduced to give the hydroxylamine **59**, which will subsequently fragment to provide the highly fluorescent 4-methylumbelliferone (**55**). Under normoxic conditions, however, molecular oxygen will reverse the first reductive step, thereby reforming the original prodrug. In this manner, it is expected that there will be a greater increase in fluorescence over time when using fluoroprobe **53** under hypoxic conditions, than when using the same prodrug under normoxic conditions.

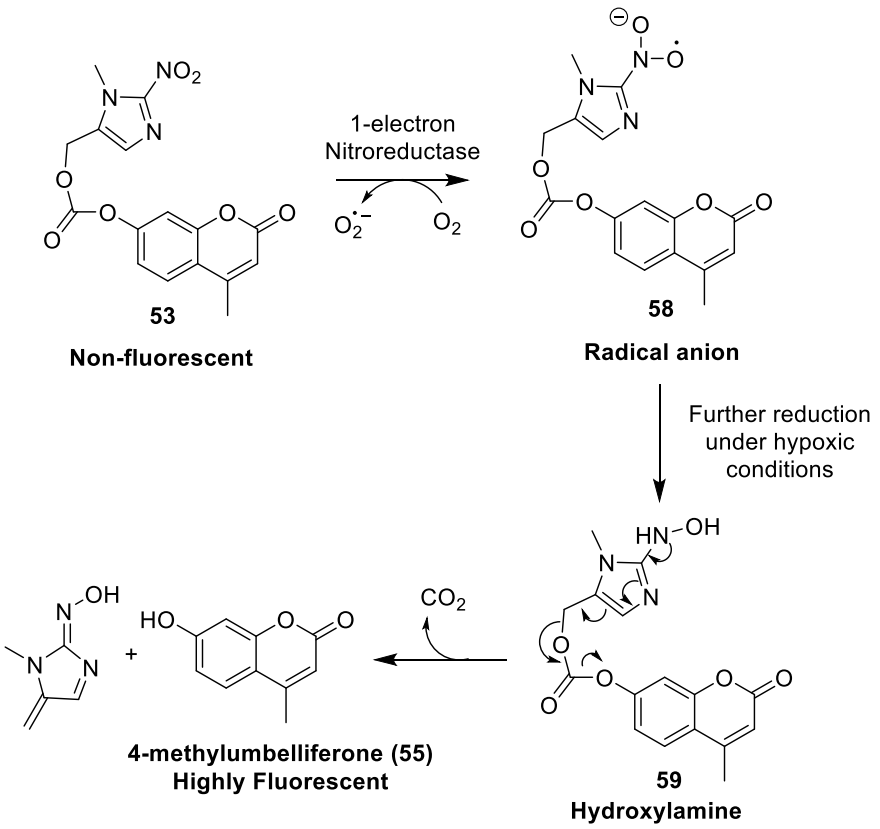

Scheme 17. Predicted fragmentation pattern of reporter fluoroprobe **53** under hypoxic conditions. Macrophages will be used to provide the source of one-electron nitroreductases.

2.6.1 RAW 264.7 hypoxia assay optimisation

Before testing fluoroprobe **53** under hypoxic conditions, the appropriate assay conditions for a well-oxygenated environment needed to be established. To this end, acetylated fluoroprobe **60** was synthesised (Scheme 18), as this probe would serve as a control to determine the degree of non-specific (esterase or media-induced) cleavage of fluoroprobe **53** and hence, the level of background fluorescence in the cell-based assays. Here, the addition of an acetate protecting group to the 7-hydroxy of 4-methylumbelliferone (**55**) would create a practically non-emissive compound,[105] while non-specific hydrolysis would generate 4-methylumbelliferone (**55**) and result in increased fluorescence.

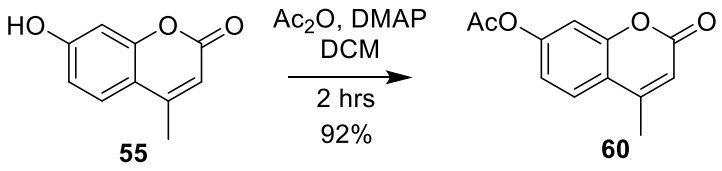

Scheme 18. Synthesis of acetylated probe **60**

With the control probe **60** in hand, the assay conditions were then determined. To this end, RAW 264.7 macrophages were seeded in a 96-well plate at 3×10^5, 2.4×10^5, and 1×10^5 cells/mL (in complete Dulbecco's Modified Eagle's Medium [CTCM]), and the following day, titrated concentrations (0, 7.8, 15.6, 31.3, 62.5, 125, and 250 μM) of acetylated probe **60** and 4-methylumbelliferone (**55**) were added and the cells incubated for a further 3 hours. Fluorescence measurements were made at 0, 30, 80, and 180 minutes. As illustrated (Figure 21), the replicates contained large SEM, and the mean fluorescence intensity of the positive control, 4-methylumbelliferone **55**, was not consistent across all time points. Moreover, the fluorescence of the acetylated probe **60** was found to increase over time, which is indicative of acetate cleavage by cellular esterases. Upon further investigation, it was determined that the media used contained a dye, phenol red, and that the presence of this dye may be interfering with the fluorescent measurements. Accordingly, the assay was repeated, this time in Phosphate Buffered Saline (PBS) rather than CTCM. Gratifyingly, at all three cell concentrations, the acetylated probe **53** was gradually converted to 4-methylumbelliferone (**55**), with complete conversion occurring approximately three hours after the addition of the probe (Figure 21B). Furthermore, the mean fluorescence intensity of 4-methylumbelliferone was consistent and with low SEM over the course of the experiments. Here, it should also be noted that there is a slight decrease in the mean fluorescence intensity of 4-methylumbelliferone (**55**) over time. This may be due to macrophages metabolising 4-methylumbelliferone (**55**) into a non-fluorescent derivative, or other chemical forms of decomposition (*e.g.* photo bleaching). This effect, however, appears to be minor.

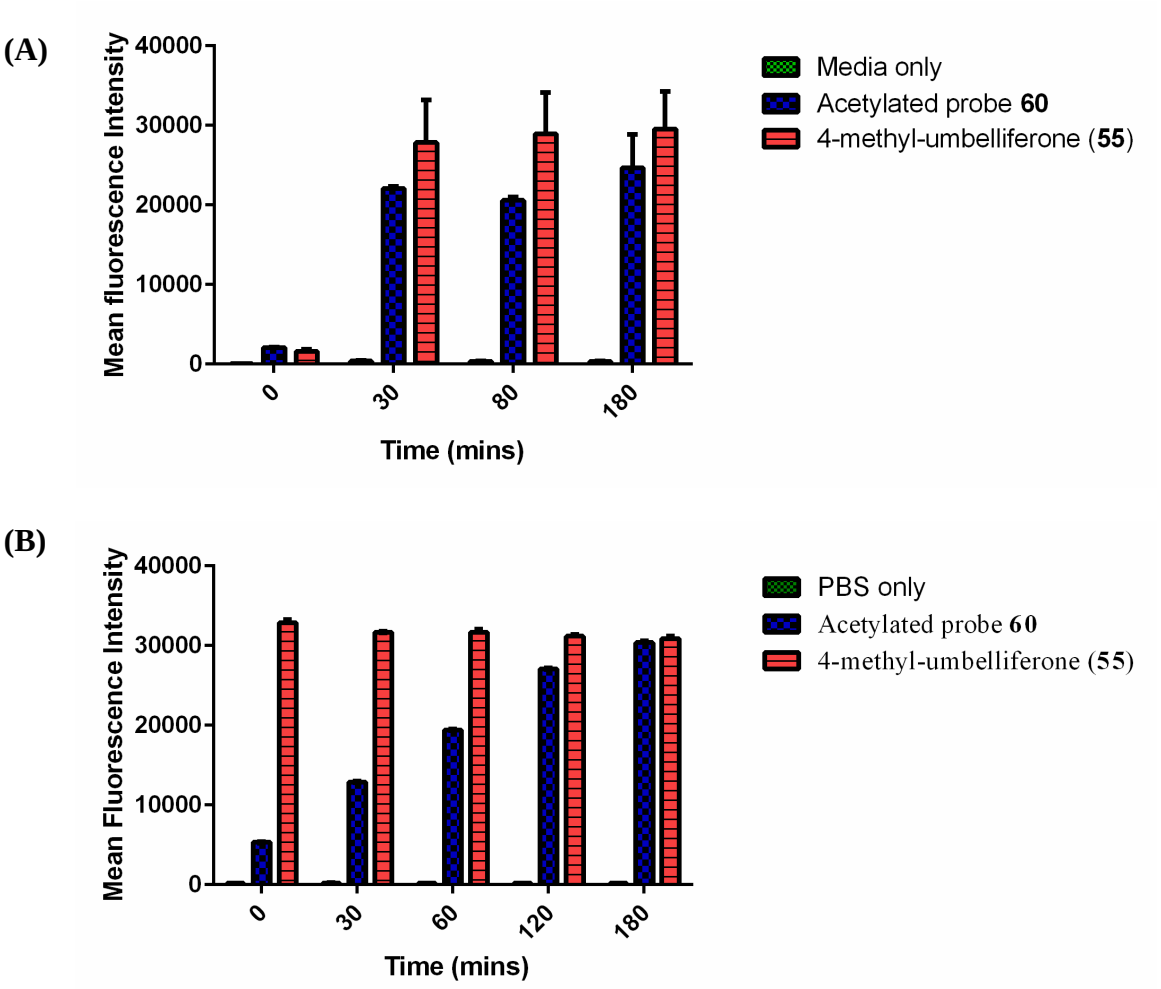

Figure 21. (A) Mean fluorescence intensity measured at 0, 30, 80, and 180 minutes after the addition of acetylated probe **60** and 4-methylumbelliferone (**55**) (at 125 μM) to RAW 264.7 cells plated at 2.4×10^5 cells/mL. Error bars represent SEM across 2 replicates. **(B)** Mean fluorescence intensity measured at 0, 30, 60, 120, and 180 minutes after the addition of acetylated probe **60** (125 μM) or 4-methylumbelliferone (**55**) 125 (μM) to RAW 264.7 cells in PBS (2.4×10^5). Error bars represent SEM over two replicates.

Next, the stabilities of probes **53** and **60** to aqueous hydrolysis were determined. To this end, the probes were added to PBS at a variety of concentrations (0, 7.8, 15.6, 31.3, 62.5, 125, and 250 μM) and the fluorescence measured over a period of three hours. As illustrated (Figure 22), the mean fluorescence intensity was relatively consistent for both 4-methylumbelliferone (**55**) and reporter fluoroprobe **53**, which indicates that both the fluorescent dye and the carbonate-linked reporter probe **53** are stable in an aqueous environment. In the case of acetylated probe **60**, however, a

slight increase in fluorescence was observed over time, which suggests that this probe is marginally sensitive to aqueous hydrolysis. That said, the cleavage of the acetylated probe **60** by aqueous hydrolysis is almost negligible when compared to the esterase mediated cleavage. Accordingly, most of the cleavage of acetylated probe **60** can be attributed to cell based activities.

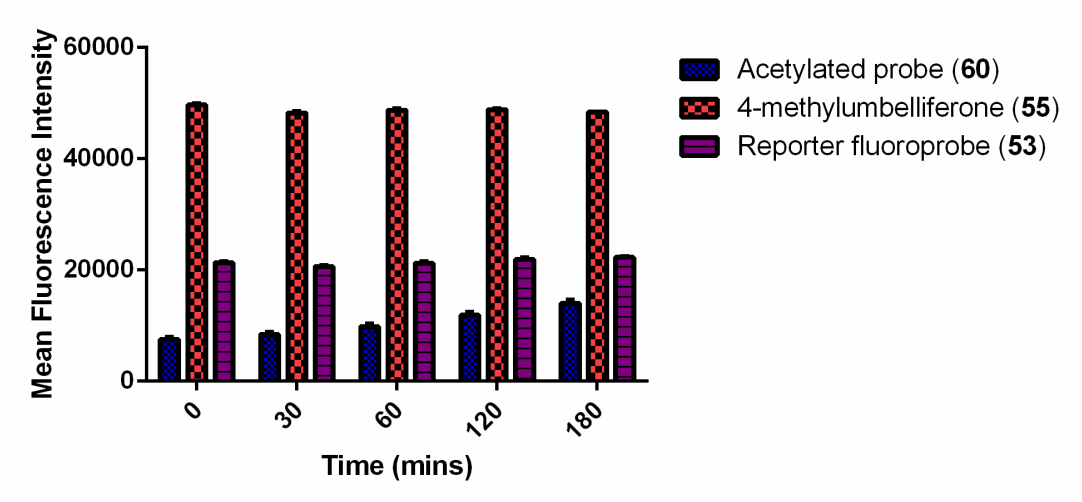

Figure 22. Mean fluorescence intensity measured 0, 30, 60, 120, and 180 minutes after the addition of either acetylated probe **60** (250 μM), 4-methylumbelliferone (**55**, 250 μM), or reporter fluoroprobe **53** (250 μM) to PBS. Error bars represent SEM across three replicates.

Having determined the parameters of the macrophage assay and the associated esterase mediated cleavage of probe **60**, the next step was to determine the stability of carbonate-linked probe **53**. Accordingly, fluoroprobe **53** and control probe **60** were added to pre-plated RAW 264.7 macrophages in PBS and then incubated for three hours. Fluorescence measurements were made at regular intervals. As illustrated (Figure 23), the mean fluorescence intensity of acetylated probe **60** increases over time, which indicates that the cells are viable and that cleavage of the acetate group is cell mediated. In the case of fluoroprobe **53**, however, there appears to be no increase in mean fluorescence intensity over time, which suggests that

fluoroprobe **53** is stable to cellular cleavage at this concentration of RAW 264.7 macrophages.

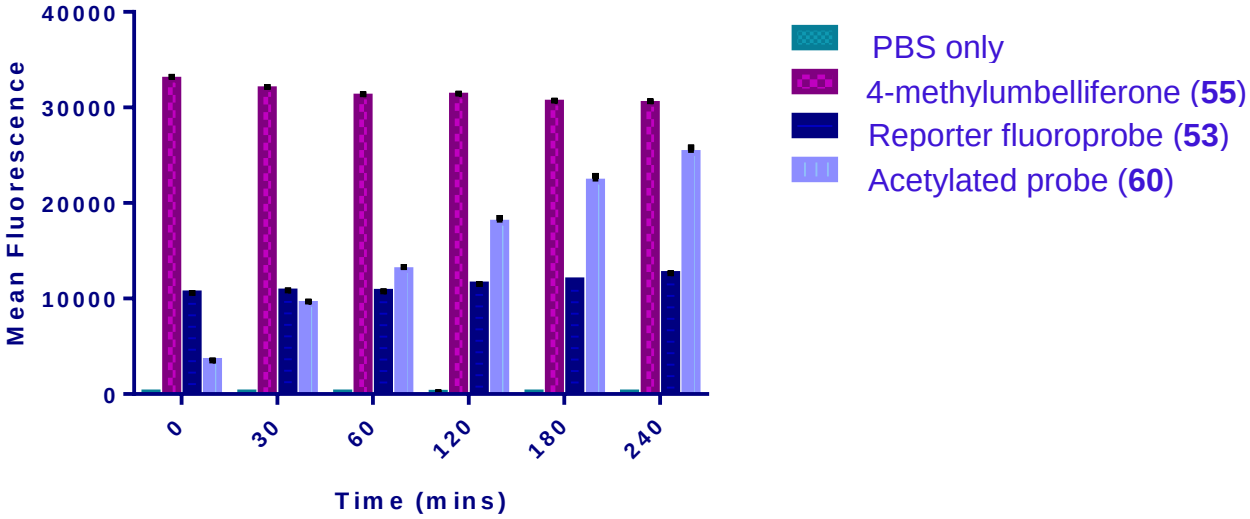

Figure 23. Mean fluorescence intensity measured at 0, 30, 60, 120, and 180 minutes after the addition of either the acetylated probe **60** (125 μM), reporter fluoroprobe **53** (125 μM), 4-methylumbelliferone **55** (125 μM), or PBS to RAW 264.7 cells (2.4×10^5 cells/mL). Error bars represent SEM across three replicates.

2.6.2 Hypoxia experiments

With the assay parameters established under normoxic conditions, the next step was to determine the biological activity of the carbonate-linked fluoroprobe **53** in a hypoxic setting. Typically, hypoxia-activated prodrugs for the treatment of solid tumours are cytotoxic compounds and are thus tested against an appropriate cancerous cell line under either well-oxygenated or hypoxic conditions.[23, 101, 102] Physiological hypoxia induces many metabolic and physical alterations within a cell, [103, 104] and to best mimic the hypoxic environment within a solid tumour, it is therefore important to target cells that are representative of those found inside a tumour. Accordingly, the cancerous cells are typically pre-incubated under hypoxic conditions to allow the cells time to adjust to the oxygen depleted environment. [101, 102] In the case of fluoroprobe **53**, however, only the presence or absence of molecular oxygen and one-electron nitroreductases were deemed important for the

fragmentation of the prodrug into a potential immunomodulator and accordingly, the RAW 264.7 macrophages were not pre-incubated under hypoxic conditions.

Before considering the effect of hypoxia on the reduction and fragmentation of fluoroprobe **53**, it was first important to establish the effect of hypoxia on the survival of RAW 264.7 cells. Several studies have shown that after a single exposure to hypoxic conditions, apoptosis of RAW 264.7 macrophages is increased by up to 20%.[110] To determine whether this effect was also applicable under the assay conditions proposed in this thesis, RAW 264.7 cells were plated into a 12-well microplate at a concentration of 2.4×10^5 cells/mL (in PBS) to a total of 2 mL/well. The cells were then incubated for 3 hours under either hypoxic (1.2% O_2)[23] or well-oxygenated (20% O_2) conditions. The number of live cells were subsequently counted using trypan blue staining as a measure of cellular viability. As illustrated below (Figure 24), exposure to hypoxic conditions induced a 20% increase in death (as compared to well-oxygenated conditions), which is consistent with previously reported results.[110]

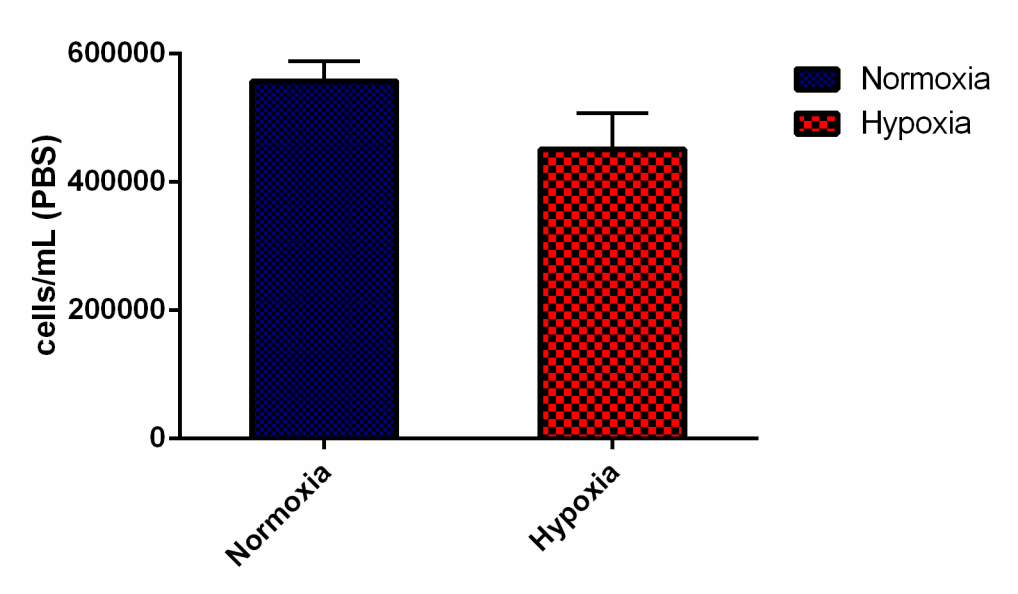

Figure 24. RAW 264.7 cell counts after incubation in normoxic (20% O_2) or hypoxic (1.2%) conditions for 3 hours. Cells were plated out at a concentration of 1×10^6 cells/mL (2 mL/well). Error bars represent SEM across three replicates.

Next, the reporter fluorprobe **53** was tested for its ability to fragment selectively under hypoxic conditions. To this end, RAW 264.7 cells were added to a 96-well microplate and incubated overnight in PBS. The following morning, the macrophages were challenged with range of concentrations of reporter fluoroprobe **53**, acetoxy probe **60**, and 4-methumbelliferone (**55**) (0, 7.8, 15.6, 31.3, 62.5, 125, and 250 μM in PBS) and were subsequently incubated for three hours under either well-oxygenated or hypoxic conditions. The mean fluorescence intensity was measured both prior to and after incubation and there was no significant difference between the change in mean fluorescence intensity of reporter probe **53** when incubated in either well-oxygenated or hypoxic conditions. One possible explanation for this result is that the RAW 264.7 cell culture had matured passed its optimal state for nitroreductase activity and accordingly, the experiment was repeated with a new culture of RAW 264.7 macrophages. Unfortunately, once again, no significant increase in mean fluorescence intensity resulting from the incubation of fluoroprobe **53** under hypoxic conditions was observed (Figure 25A). It is interesting to note, however, that after 3.5 hours of incubation in a hypoxic environment, acetylated probe **60** was not completely converted to 4-methylumbelliferone (**55**). One possible explanation for this observation is that due to hypoxia-induced cellular death, there were not enough macrophages, and hence enzyme activity (*e.g.* esterases), to complete the transformation of **60** to **55**. Alternatively, the oxygen-depleted environment may potentially induce metabolic transformations resulting in reduced enzyme activity. To determine whether an increase in macrophage number would have an effect on potential nitroreductase activity, the experiment was repeated, this time with an increased seeding concentration of macrophages from 2.4×10^5 cells/mL to 1×10^6 cells/mL. As illustrated (Figure 25B), the increase in macrophage concentration did result in an increase in mean fluorescence intensity of fluoroprobe **53** over time, however, this change in fluorescence is present under both normoxic and hypoxic conditions, which indicates that it may result from non-specific enzymatic activity.

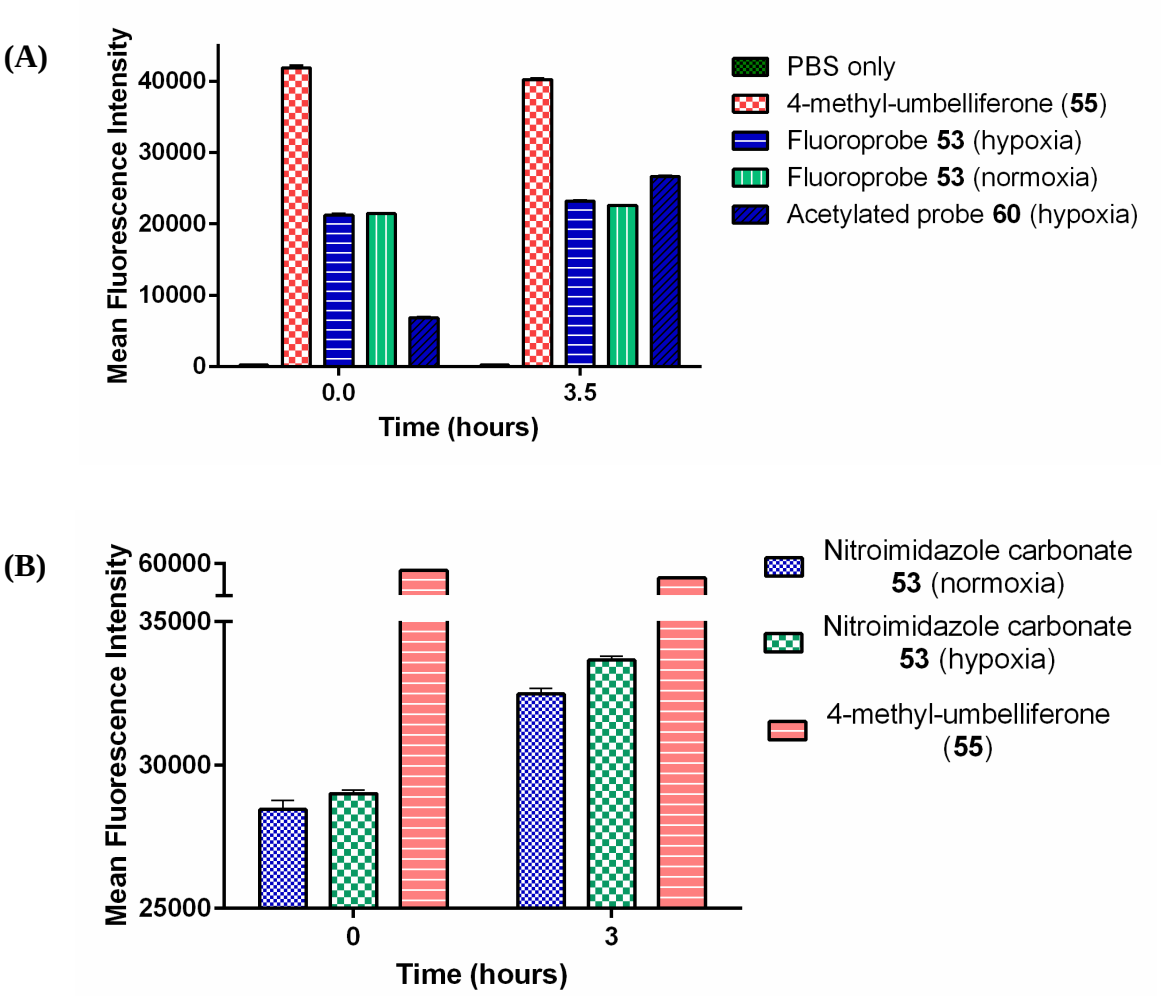

Figure 25. **(A)** Mean fluorescence measured before and after 3.5 hour incubations of either 4-methylumbelliferone (**55**, 250 μM) or reporter fluoroprobe **53** (250 μM) with RAW 264.7 cells (3×10^5 cells/mL) under either hypoxic (1.2% O_2, 5% CO_2) or normoxic (20 O_2%, 5% CO_2) conditions. Error bars represent SEM across three replicates. **(B)** Mean fluorescence measured before and after 3 hour incubations of either 4-methylumbelliferone (**55**, 250 μM) or reporter fluoroprobe **53** (250 μM) with RAW 264.7 cells (1×10^6 cells/mL) in either hypoxic (1.2% O_2, 5% CO_2) or normoxic (20 O_2%, 5% CO_2) conditions. Error bars represent SEM across three replicates.

Due to the lack of adequate positive controls, it was unclear whether there was no selective fragmentation of fluoroprobe **53**, or whether there was a problem with the assay set-up, resulting in diminished nitroreductase activity. In order to clarify this, an extended set of hypoxia-activated fluoroprobes were synthesised (Figure 26), which include *p*-nitrobenzyl carbonate fluoroprobe **63** and *p*-nitrobenzyl ether-linked fluoroprobe **64**, as well as the previously synthesised nitroimidazole carbonate fluoroprobe **53** and nitroimidazole ether-linked fluoroprobe **57**. Ether-

linked nitrobenzyl probe **64** was synthesised via the alkylation of 4-methylumbelliferone (**55**) with nitrobenzyl bromide **62** to give the desired product **64** in 87% yield. Similarly, the addition of nitrobenzyl alcohol (**61**) to chloroformate **56** gave the carbonate-linked fluoroprobe **63** in modest (24%) yield. The nitroimidazole probe **57** contains a well-documented ether-linked trigger group that has been shown to be selectively activated under hypoxic conditions and thus, would serve as an excellent positive control,[111-113] while nitrobenzyls (e.g. **63** and **64**) are a further class of nitroaromatic prodrug triggers that undergo nitroreductase mediated reduction to give the corresponding radical anion, and which would be useful as additional controls.[24, 114, 115]

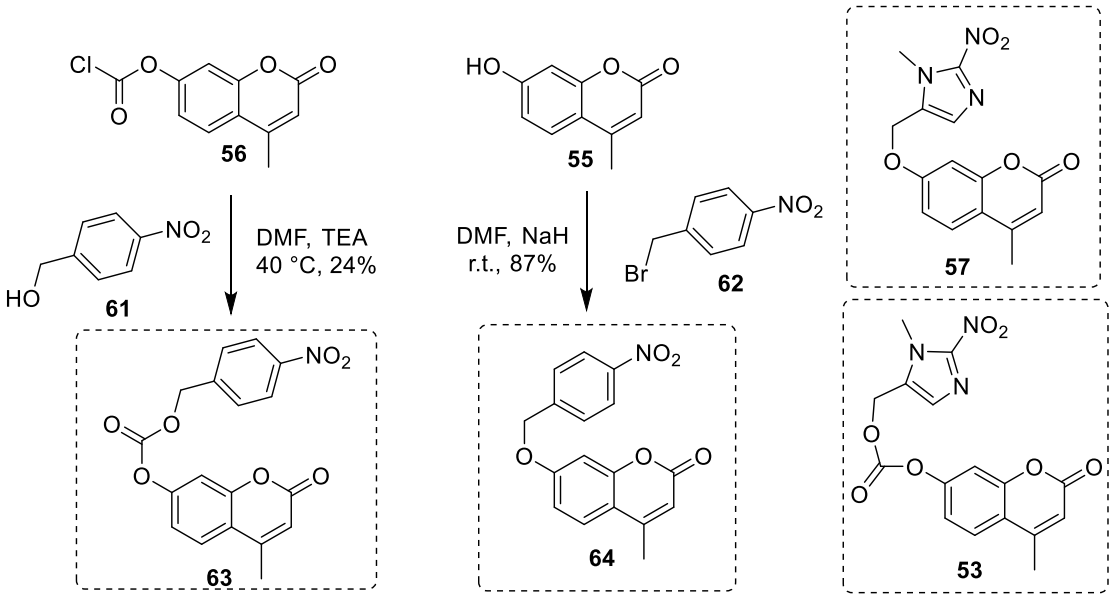

Figure 26. Expanded fluoroprobe set

Accordingly, reporter fluoroprobes **53**, **57**, **63**, and **64** were tested in the macrophage assay in order to determine whether they could be selectively activated under hypoxic conditions. As illustrated (Figure 27), there is no hypoxia-selective activation of any of the fluoroprobes, which indicates that there is a problem with the assay design. It is interesting to note, however, that for the probes with the carbonate linker (**63** and **53**), there is hypoxia-independent activation of the fluoroprobe, which is most likely due to the non-specific cleavage of the carbonate

linkage by cellular enzymes. This result suggests that a carbonate-linker may not be sufficiently robust for use in an H-TDB, and consequently, it would be valuable to explore other linker-strategies.

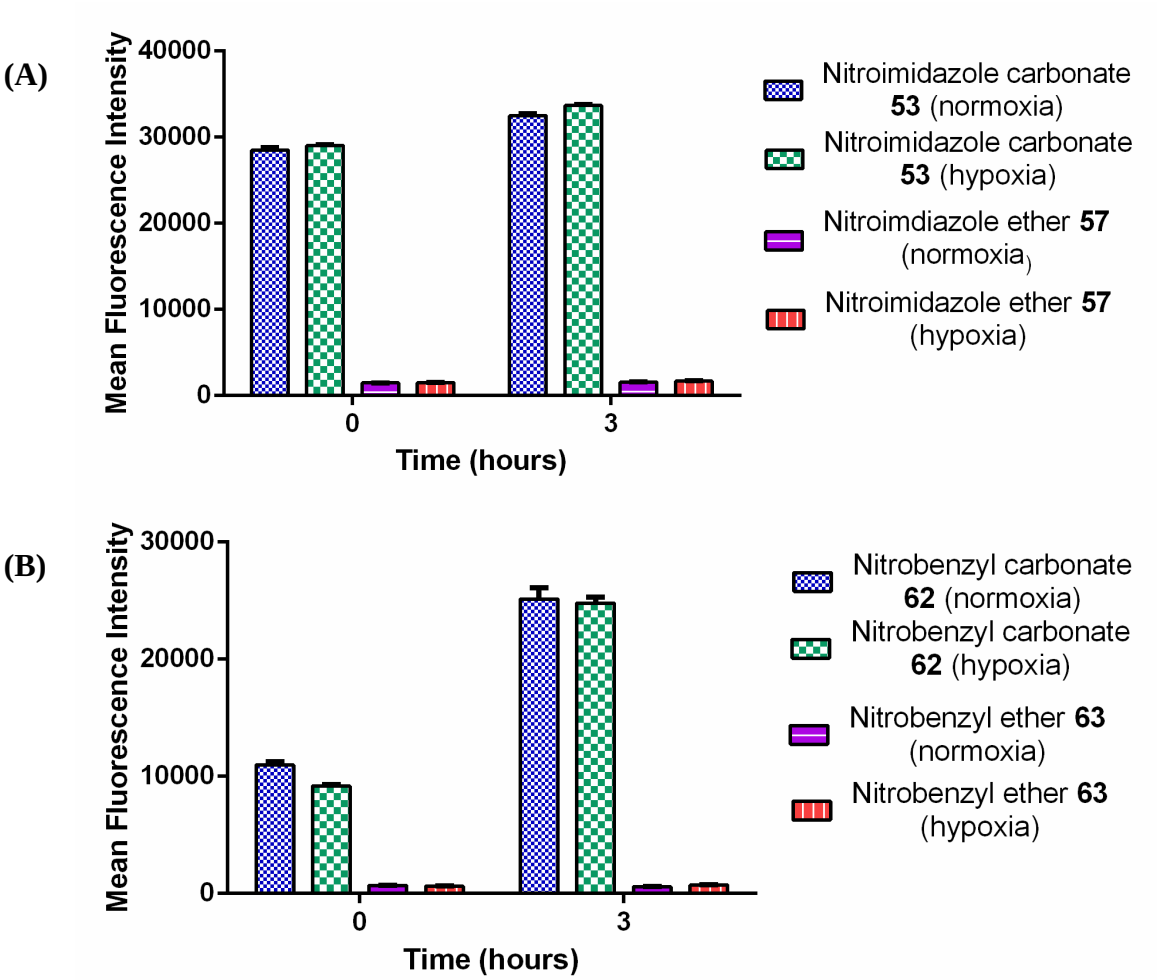

Figure 27. (A) Mean fluorescence intensity measured before and after 3.5 hour incubations of either nitroimidazole carbonate fluoroprobe (**53**, 250 μM) or ether-linked nitroimidazole fluoroprobe **57** (250 μM) with RAW 264.7 cells under either hypoxic (1.2% O_2, 5% CO_2) or normoxic (20 O_2%, 5% CO_2) conditions. Error bars represent SEM across three replicates. **(B)** Mean fluorescence intensity measured before and after 3 hour incubations of either nitrobenzyl carbonate **63** (250 μM) or ether-linked nitrobenzyl fluoroprobe **64** (250 μM) with RAW 264.7 cells (1×10^6 cells/mL) in either hypoxic (1.2% O_2, 5% CO_2) or normoxic (20 O_2%, 5% CO_2) conditions. Error bars represent SEM across three replicates.

2.6.3 Summary of macrophage assay

As described, a macrophage assay was developed in an attempt to assess the selective-activation of reporter fluoroprobe **53** in a hypoxic setting. Throughout the course of these experiments, it was determined that although carbonate-linked fluoroprobe **53** was stable to aqueous hydrolysis, it was susceptible to non-specific enzyme-mediated cleavage in the presence of macrophages and thus, the carbonate linker strategy may need to be re-evaluated. In addition to fluoroprobe **53**, the newly synthesised positive controls **57** and **63** were also not selectively-activated under the determined assay conditions, indicating may be a problem with the assay or compound design and a new assay will need to be developed to explore the activity of H-TDBs in a biological setting.

3. Conclusions and Future Prospects

The findings of this Masters project can be divided into four main sections. In the first section, a 7-step patented procedure was used as a guide and amended where necessary to produce nitroimidazolylmethyl halides **19** and **20**. Key findings include the need to use high quality ethyl formate to ensure the successful formylation of sarcosine ester **26**, and moreover, longer reaction times and larger reaction scales enhanced the yield of the desired di-formylated ester **27**. Additionally, in the cyclisation reaction of α-formylated ester **29** to give amino-ester **22**, the removal of an acidification step in the work-up proved crucial for the successful isolation of **22** in good yield. Finally, the yields of the overall synthetic route were improved so as to give nitroimidazole halides **19** and **20** in 18% and 17%, respectively, over 8 steps. This is significantly better than the published protocol, which produced nitroimidazole bromide **19** in 8% yield over 7 steps.

The second part of this thesis focused on the attempted synthesis of H-TDB **17**. Here, several different solvents, bases, and reaction temperatures were used in an attempt to alkylate benzylidene protected trehalose **18** with nitroimidazole halides **19** or **20**, however, none of these reaction conditions led to the formation of the desired product. A subsequent literature search revealed that no aliphatic or non-aromatic alcohols had ever been used in an alkylation reaction with the nitroimidazole halides **19** or **20**. Upon the successful synthesis of the phenol imidazole conjugate **45**, it was therefore postulated that the energy gap between the reactive orbitals of imidazole bromide **19** and a secondary aliphatic alcohol was too large for the substitution reaction to proceed.

As the direct alkylation of benzylidene protected trehalose **18** using nitroimidazole halides **19** and **20** seemed unlikely, the third section of this thesis explored the use of a carbonate group as a suitable linker to connect the TDB effector group to the nitroimidazole trigger. Here, it was successfully demonstrated that nitroimidazole trigger **37** could be attached to a model carbohydrate through the carbonate linker.

The final section of this Masters project explored the validity of the carbonate-linker strategy in a biological context. To this end, the reporter fluoroprobe **53** was

synthesised and evaluated in two distinct biological systems. First, fluoroprobe **53** was tested in a bacterial enzymatic assay, where two-electron nitroreductases were shown to successfully reduce the nitroimidazole trigger to the hydroxylamine, resulting in fragmentation of the carbonate linker and liberation of the fluorescent umbelliferone (**55**). Next, a macrophage assay was developed in an attempt to assess the hypoxia-selective cleavage of fluoroprobe **53**. Although this assay proved to be unsuccessful for the hypoxia-selective reduction of fluoroprobe **53**, valuable information was nonetheless obtained from the macrophage experiments. For example, it was determined that the presence of a carbonate group in the reporter fluoroprobe resulted in an increase in non-specific cleavage of said carbonate group. This effect was found to be conserved across both nitroimidazole and nitrobenzyl based fluoroprobes, which suggests that a more enzymatically stable linker strategy may be needed. An example of such a linker is the previously discussed cyclisation linker (see section 2.4) found in fluoroprobe **65** (Figure 28). The development of a shorter carbamate or thiocarbonate linker (*e.g.* fluoroprobes **66** and **67**) as well as a probe with a structure closer resembling that of the target H-TDB may also be worth exploring.

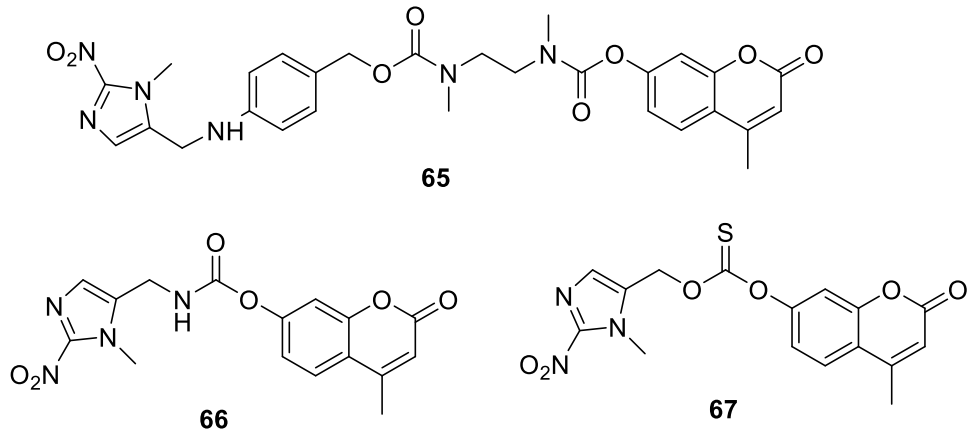

Figure 28. Proposed structure of a fluoroprobe including a cyclisation linker

In addition to the development of a more robust linker-strategy, the macrophage assay needs to be further optimised so that the positive controls **57** and **64** are successfully reduced under hypoxic conditions. The next step in the process will be

to explore the relative levels of nitroreductase expression in RAW 264.7 cells, which can be better evaluated through the use of quantitative reverse-transcription polymerase chain reaction (RT-PCR),[116] or alternatively, a mixed cell culture assay, more akin to the tumour environment, could be explored.

4. Experimental

4.1 General chemical methods

Unless otherwise stated, all reactions were performed under an atmosphere of argon, using dry solvents. DCM and THF were freshly distilled over phosphorus pentoxide and sodium, respectively. D-(+)-Trehalose dehydrate (Sigma Aldrich), benzaldehyde dimethyl acetal (Sigma Aldrich), toluene (Panreac), camphorsulfonic acid (Sigma Aldrich), sodium carbonate (PROLABO), ethyl acetate (Fischer Scientific), DMF (Acros), sarcosine (Merck), ethyl formate (Sigma Aldrich), sodium hydride (Sigma Aldrich), ethanol (Panreac), hydrochloric acid (Panreac), petroleum ether (Panreac), cyanamide (Sigma Aldrich), sodium acetate (Riedel-de Haën), potassium carbonate (Pure Science), acetic acid (Sigma Aldrich), sodium nitrite (Merck), dichloromethane (Panreac), sodium hydroxide (Pure Science), THF (Sigma Aldrich), triethylamine (Sigma Aldrich), ethyl chloroformate (Sigma Aldrich), sodium borohydride (Riedel-de Haën), sulfuric acid (Panreac), thionyl chloride (Roth), methanol (Fischer Scientific), thionyl bromide (Sigma Aldrich), phenol (BDH), triphosgene (Sigma Aldrich), 4-methylumbelliferone (Eastman Organic Chemicals), pyridine (Panreac), tetrabutylammonium iodide (Riedel-de Haën), 4-(Dimethylamino)pyridine (Merck), *p*-nitrobenzyl alcohol (Merck), *p*-nitrobenzyl bromide (BDH), quinine sulphate (Sigma Aldrich), and acetic anhydride (Acros) were used as received. Solvents were removed *in vacuo*. TLC analysis was employed to monitor reactions using Macherey-Nagel silica gel coated plastic sheets (0.20 mm, Polygram SIL G/UV254). TLC visualisation was achieved by dipping in 10% H_2SO_4 in EtOH followed by charring at 150 °C or UV visualisation. High resolution mass spectra were obtained on a Waters Q-TOF Premier^{TM} Tandem Mass Spectrometer using positive electrospray ionisation. Optical rotations were recorded on a Perkin-Elmer 241 polarimeter or Autopol II (Rudolph Research Analytical) at 589 nm (sodium D-line). Infrared spectra were recorded on a Bruker Tensor 27 FTIR spectrometer equipped with an Attenuated Total Reflectance (ATR) sampling accessory. Nuclear magnetic resonance spectra were recorded at 20 °C in CD_3OD or $CDCl_3$ using a Varian INOVA operating at 500 MHz. Chemical shifts are given in ppm calibrated to residual solvent. NMR

peak assignments were made using COSY, HSQC, and HMBC 2D experiments. Melting points were determined using a Gallenkamp Melting Point Apparatus.

Determination of Quantum yields

Quantum yields were determined using the comparative method. UV/vis absorption spectra were measured on an Agilent 8453 spectrophotometer. The corrected fluorescence emission spectra were recorded on a Shimadzu RF-5301PC spectrofluorophotometer. Both absorption and fluorescence spectra were recorded at 20 °C in 1 cm quartz cells. Quinine sulphate (Φ = 0.55 in 1 M H_2SO_4) was used as a reference.[117] Solutions with increasing concentrations of fluoroprobe in methanol or quinine sulphate in 1 M H_2SO_4 were prepared and their absorption and fluorescence emission spectra were measured. Re-absorption effects were minimised by keeping the absorbance low and slit width was kept to 1.5 nm in all cases. The relative quantum yields were obtained using the following equation:

$$\Phi_f = \Phi_R(I/I_R)(A_R/A)(n^2/n^2_R)$$

Where Φ is the quantum yield, I is the integrated emission spectrum, A is the absorbance at the excitation wavelength, and n is the refractive index of the solvents used. Finally Φ_R refers to the quantum yield of the reference fluorophore.

4.2 Chemical synthesis

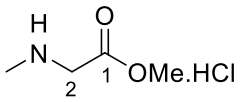

25

Sarcosine methyl ester hydrochloride (25): Sarcosine (1 g, 11.2 mmol) in methanol (10 mL) was added to a 50 mL round bottom flask, fitted with a condenser, and cooled to 0 °C. To this suspension, thionyl chloride (3.4 mL, 4.60 mmol) was added down the condenser, and the resulting mixture was left to stir for 30 minutes. The solvent was removed *in vacuo* yielding a white solid, which was recrystallised from methanol to give the sarcosine methyl ester hydrochloride (**25**) as white crystals (1.46 g, 95%). R_f = 0.125 (MeOH:EtOAc, 1:5, *v/v*); Mp = 115.0-117.4 °C, lit.[118] Mp = 115–117 °C; IR (film): 2957, 2643, 1733 cm^{-1}; ^1H NMR (500 MHz, CD_3OD): δ 3.97 (s, 2H, H-2a & H-2b), 3.84 (s, 3H, OMe), 2.76 (s, 3H, N-Me); ^{13}C NMR (125 MHz, CD_3OD): δ 166.8 (C-1), 52.1 (OMe), 48.1 (C-2), 32.1 (N-Me); HRMS(ESI) *m/z* calcd. for $[C_4H_9NO_2+H]^+$: 104.0706, obsd.: 104.0705.

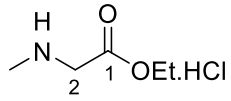

26

Sarcosine ethyl ester hydrochloride (26): Sarcosine (12.5g, 0.140 mol) in ethanol (50 mL) was heated to 50 °C. To this mixture, thionyl chloride (11.2 mL, 0.154 mol) was added in small portions and the resulting solution was left to stir for 1.5 hours, after which point the solvent was removed *in vacuo* to yield the title compound (**26**) as a white solid (20.8 g, 97%). R_f = 0.23 (MeOH:EtOAc, 1:5, *v*/*v*); Mp = 119.0–122.2 °C; lit.[119] Mp = 122-123 °C; IR (film): 2984, 2692, 1742 cm^{-1}; ^1H NMR (500MHz, CD_3OD): δ 4.31 (q, J_{OEt} = 7.1 Hz, 2H, CH_2 OEt), 3.96 (s, 2H; H-2a & H-2b), 2.76 (s, 3H, N-Me), 1.32 (t, J_{OEt} = 7.0 Hz, 3H, CH_3 OEt); ^{13}C NMR (125 MHz, CD_3OD): δ 166.3 (C-1), 62.1 (OEt CH_2), 48.3 (C-2), 31.9 (N-Me), 12.9 (OEt CH_3); HRMS(ESI) *m/z* calcd. for $[C_5H_{11}NO_2+H]^+$: 118.0863, obsd.: 118.0863.

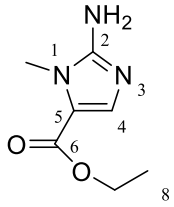

22

2-Amino-5-ethoxycarbonyl-1-methyl imidazole (22): Sarcosine ethyl ester hydrochloride (10 g, 65.1 mmol) was dissolved in ethyl formate (60 mL) and cooled to 0 °C. To this solution, sodium hydride (60% oil suspension, 10 g, 0.25 mol) was added and the resulting suspension was stirred at room temperature for 30 hours. The reaction mixture was diluted with 20 mL of water and washed with ethyl acetate (3 × 50 mL). The aqueous layer was acidified to pH 1 using concentrated HCl and extracted with ethyl acetate (5 × 50 mL), which was subsequently dried over $MgSO_4$, filtered, and concentrated under reduced pressure to yield a pale brown solid. The resulting solid was dissolved in ethanol (100 mL) and concentrated HCl (45 mL), and left to stir at 50 °C for 1.5 hours. The reaction mixture was cooled, filtered over carbon, and concentrated to give a green oil, which was dissolved in 10% aqueous acetic acid (90 mL). To this solution, cyanamide (5.3 g, 0.126 mol), and sodium acetate (10.36 g, 0.126 mol) were added and the resulting mixture was left to stir at 50 °C for 1.5 hours. The solution was then adjusted to pH 8 via the addition of K_2CO_3, and extracted with ethyl acetate (5 × 50 mL). The combined fractions were dried over $MgSO_4$, filtered, and concentrated to yield 2-amino-5-ethoxycarbonyl-1-methyl imidazole (**22**) as a brown solid (5.3 g, 59%), which was used without further purification. R_f = 0.40 (EA); Mp = 162.5-164 °C; IR (film):= 3388, 2361, 1647 cm^{-1}; ^1H NMR (500 MHz, CD_3OD): δ 7.32 (s, 1H; H-4), 4.24 (q, $J_{7,8}$ = 7.4 Hz, 2H, H-7a & H-7b), 3.63 (s, 3H,

N-CH_3), 1.32 (t, J = 7.1 Hz, 3H, OEt CH_3).^{13}C NMR (125 MHz, CD_3OD): δ 160.5 (C-6), 153.9 (C-2), 134.4 (C-4), 117.9 (C-5), 59.4 (C-7) 29.4 (N-Me), 13.3 (C-8); HRMS(ESI) *m/z* calcd. for $[C_7H_{12}N_3O_2+H]^+$: 170.0930, obsd.: 170.0925.

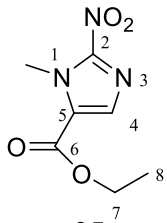

35

5-Ethoxycarbonyl-1methyl-2-nitroimidazole (35): A solution of amino ester **22** (0.14 g, 0.81 mmol) dissolved in acetic acid (0.14 mL) was added drop wise to a solution of sodium nitrite (0.37 g, 5.35 mmol) in water (2.2 mL) and stirred at -5 °C for 15 minutes. The solution was warmed to room temperature and allowed to stir for 14 hours. The reaction mixture was extracted with dichloromethane (5 × 50 mL), dried over $MgSO_4$, filtered, and concentrated *in vacuo* to yield an orange-red oil. The resulting oil was purified by column chromatography on silica gel (PE/EtOAc, 75:25, *v/v*) to yield the title compound as a pale orange solid (0.071 g, 0.36 mmol, 45%). R_f = 0.78 (EA); IR (film): = 2984, 1719, 1551 cm^{-1}; ^{1}H NMR (500 MHz, CD_3OD): δ 7.74 (s, 1H, H-4), 4.40 (q, $J_{7,8}$ = 7.0 Hz, 2H, H-7a & H-7b), 4.31 (s, 3H, N-Me), 1.39 (t, $J_{7,8}$ = 7.0 Hz, 3H, CH_3-8); ^{13}C NMR (125 MHz, CD_3OD): δ 158 (C-6), 147.6 (C-2), 133.2 (C-4), 126.6 (C-5), 61.4 (C-7), 34.7 (N-Me), 13.3 (C-8); HRMS(ESI) *m/z* calcd. For $[C_7H_9N_3O_4+H]^+$: 200.0667, obsd.: 200.0671.

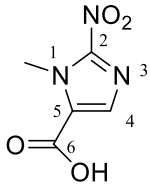

36

1-Methyl-2-nitroimidazole-5-carboxylic acid (36): A solution of the nitro ester **35** (50 mg, 0.2 mmol) in 1 M NaOH (0.6 mL) and water (0.25 mL) was left to stir overnight to give a brown solution. The reaction mixture was adjusted to pH 1 via the addition of concentrated HCl, extracted with ethyl acetate (5 × 50 mL), dried over $MgSO_4$, filtered, and concentrated under reduced pressure to give 1-methyl-2-nitroimidazole-5-carboxylic acid as pale pink solid (34 mg, 0.2 mmol, quant.). R_f = 0.35 (EtOAc); Mp = 161.8-162.9 °C, lit.[120] Mp = 160-161 °C; IR (film): 2851, 2361, 1849, 1710 cm^{-1}; H NMR (500 MHz, CD_3OD): δ 7.72 (s, 1H, H-4), 4.41 (s, 3H, N-Me); ^{13}C NMR (125 MHz, CD_3OD): δ 160.1 (C-6), 147.5 (C-2), 133.3 (C-4), 127.0 (C-5), 34.4 (N-Me); HRMS(ESI) *m/z* calcd. $[C_5H_5N_3O_4+H]^+$: 172.0353, obsd.: 172.0347.

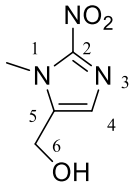

37

5-Hydroxymethyl-1-methyl-2-nitroimidazole (37): Carboxylic acid **36** (230 mg, 1.34 mmol) was dissolved in anhydrous THF (30 mL) and triethylamine (0.27 mL, 1.94 mmol) and cooled to -10 °C. Ethyl chloroformate (0.29 mL, 3.0 mmol) was added dropwise over a period of 10 minutes and the mixture was left to stir at -10 °C for 30 minutes, after which point the temperature was increased to -5 °C, and stirring was continued for a further 30 minutes. Sodium borohydride (0.27 g, 7.2 mmol) was added followed by dropwise addition of water (6 mL) over a period of 30 minutes. The reaction mixture was warmed to 0 °C, filtered over a pad of anhydrous sodium sulfate, and the residue was washed with THF. The combined filtrates were concentrated *in vacuo* to give a yellow solid. The resulting solid was purified by column chromatography on silica gel (PE:EtOAc, 3:1, *v/v*) to yield a yellow solid (210 mg, 1.3 mmol, 77%). R_f = 0.25 (EA); Mp. = 142.2–142.8 °C, lit.[120] Mp = 142.2-142.8 °C; IR (film): 3252, 2917, 2420 cm^{-1}; ^1H NMR (500 MHz, CD_3OD): δ 7.1 (s, 1H, H-4), 4.7 (s, 2H, H-6a & H-6b), 4.0 (s, 3H, N-Me); ^{13}C NMR (125 MHz, CD_3OD) δ 145.8 (C-2), 137.9 (C-5), 126.0 (C-4), 53.1 (C-6), 33.4 (N-Me); HRMS(ESI) *m/z* calcd. for $[C_5H_7N_3O_3+H]^+$: calcd.: 158.0560, obsd.: 158.0554.

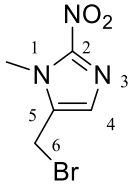

19

5-Bromomethyl-1-methyl-2-nitroimidazole (19): Nitroimidazole **37** (241 mg, 1.53 mmol) was dissolved in $SOBr_2$ (1.6 mL, 20.7 mmol) and the solution was stirred at room temperature. After 15 minutes, the reaction was quenched by the addition of ice, and extracted with EtOAc (5 × 20 mL). The organic layer was washed with water and brine, dried over $MgSO_4$, filtered, and evaporated to yield the title compound as brown crystals (331 mg, 1.5 mmol, 98%). R_f = 0.30 (EtOAc); Mp = 97.1–97.9 °C; IR (film): 3030, 1746, 1363, 660 cm^{-1}; ^1H NMR (500 MHz, $CDCl_3$): δ 7.15 (s, 1H, H-4), 4.47 (s, 2H, H-6a & 6b), 4.00 (s, 3H, N-Me); ^{13}C NMR (125 MHz, $CDCl_3$): δ 146.4 (C-2), 133.3 (C-5), 128.5 (C-4), 34.2 (N-Me), 19.2 (C-6); HRMS(ESI) *m/z* calcd. For $[C_5H_6BrN_3O_2+H]^+$: 219.9716, obsd.: 219.9716.

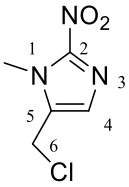

20

5-Chloromethyl-1-methyl-2-nitroimidazole (20): Nitroimidazole **37** (50 mg, 0.318 mmol) was dissolved in 1 mL of $SOCl_2$ (1 mL, 13.8 mmol) and was stirred at room temperature for 15 minutes, after which the reaction was quenched by the addition of ice, and extracted with EtOAc (5 × 10 mL). The EtOAc layer was washed with water and brine, dried over $MgSO_4$, filtered, and dried under reduced pressure to give the imidazole chloride (**20**) as a yellow oil (55.9 mg, 95%). R_f = 0.70 (EtOAc); IR (film): 2092, 1767, 1302, 720 cm^{-1}; ^1H NMR (500 MHz, $CDCl_3$) δ 7.19 (s, 1H, H-4), 4.63 (s, 2H, H-6a & H-6b), 4.07 (s, 3H, N-Me); ^{13}C NMR (125 MHz, $CDCl_3$): δ 146.5 (C-2), 133.1 (C-5), 128.6 (C-4), 34.3 (N-Me), 33.9 (C-6); HRMS(ESI) *m/z* calcd. For $[C_5H_6ClN_3O_2+H]^+$: 176.0221, obsd.: 176.0218.

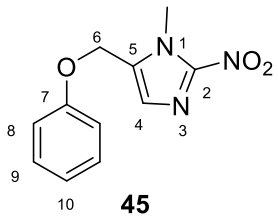

45

1-Methyl-2-nitro-5-(phenoxymethyl)-1*H*-imidazole (45): Bromide **19** (50 mg, 0.23 mmol) was coevaporated three times with DMF and dissolved in DMF (0.5 mL). This solution was added dropwise to a mixture of phenol (64 mg, 0.68 mmol), K_2CO_3 (94 mg, 0.68 mmol), and TBAI (1 mg, 0.003 mmol) in DMF (2 mL) at 0 °C. The resulting mixture was stirred at room temperature for 16 hours. After TLC analysis (R_f = 0.25, EtOAc:PE, 2:3, *v/v*) showed reaction completion, the reaction mixture was concentrated *in vacuo* and purified by column chromatography on silica gel (PE:EtOAc, 10:1, *v/v*) to yield a brown solid (32 mg, 61%). R_f = 0.25 (EtOAc:PE, 2:3, *v/v*); IR (film): 3029, 1647, 1520 cm^{-1}; ^1H NMR (500 MHz, $CDCl_3$): δ 7.33 (t, $J_{8,9} = J_{9,10}$ = 7.1 Hz, 2H, H-9), 7.21 (s, 1H, H-4), 7.04 (t, $J_{9,10}$ = 5.5 Hz, 1H, H-10), 6.97 (d, $J_{8,9}$ = 7.8 Hz, 2H, H-8), 5.06 (s, 2H, H6a & 6b), 4.06 (s, 3H, N-Me); ^{13}C NMR (125 MHz, $CDCl_3$): δ 157.5 (C-7), 146.4 (C-2), 132.8 (C-5), 129.9 (C-9), 129.0 (C-4), 122.3 (C-10), 114.8 (C-8), 59.6 (C-6), 34.6 (N-Me); HRMS(ESI) *m/z* calcd. For $[C_{11}H_{11}N_3O_3+H]^+$: 234.0873, obsd.: 234.0885.

6-chloroformate-1,2:3,4-Di-*O*-isopropylidene-α-D-galactopyranose (51):

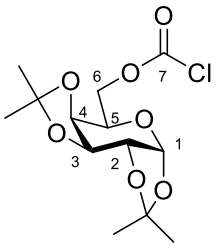

51

1,2:3,4-Di-*O*-isopropylidene-α-D-galactopyranose (**42**, 50 mg, 0.19 mmol) was coevaporated three times with toluene and then dissolved in THF (0.8 mL). To this solution, triethylamine (0.032 mL, 0.23 mmol) was added dropwise and the resulting mixture was cooled to 0 °C. Triphosgene (19 mg, 0.064 mmol) in THF (1 mL) was then added dropwise to this solution and the resulting suspension was left to stir for 1 hour at room temperature before being concentrated under reduced pressure to yield a yellow oil, which was purified using silica gel column chromatography (PE:EtOAc, 3:1, *v/v*) to give a clear oil (57 mg, 92%). R_f = 0.7 (EtOAc:PE, 1:1, *v/v*); $[\alpha]^{25}_D$ = - 7.6 (c = 1, DCM); IR (film): 2983, 1698, 1381, 1071, 1006, 770 cm^{-1}; ^{1}H NMR (500 MHz, $CDCl_3$): δ 5.53 (d, $J_{1,2}$ = 5.0 Hz, 1H, H-1), 4.63 (dd, $J_{3,4}$ = 1.4, $J_{3,2}$ = 7.7 Hz, 1H, H-3), 4.42-4.45 (m, 2H, H-6a &6b), 4.33-4.35 (m, 1H, H-2), 4.23 (d, $J_{4,3}$ = 8.0 Hz, 1H, H-4), 4.08 (t, $J_{5,6a/b}$ = 6.2 Hz, 1H, H-5), 1.52 (s, 3H, CH_3), 1.44 (s, 3H, CH_3), 1.33 (s, 6H, 2× CH_3); ^{13}C NMR (125 MHz, $CDCl_3$): δ 151.0 (C-7), 109.9 (C_q), 108.9 (C_q), 96.3 (C-1), 70.7 (C-4), 70.6 (C-3), 70.3 (C-2), 70.2 (C-6), 65.4 (C-5), 26.0 (CH_3), 25.9 (CH_3), 24.9 (CH_3), 24.4 (CH_3).

6-*O*-(1-methyl-2-nitro-1*H*-imidazol-5-yl)methyl-1,2:3,4-Di-*O*-isopropylidene-α-D-galactopyranose (52):

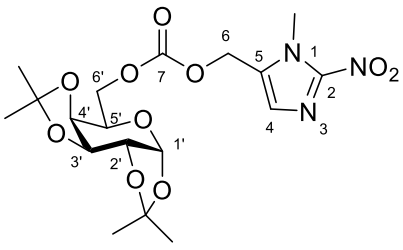

52

Nitroimidazole **37** (12 mg, 0.074 mmol) was dissolved in a mixture of THF (0.8 mL) and triethylamine (0.01 mL, 0.074 mmol), and cooled to 0 °C. Galacotse chloroformate **51** (20 mg, 0.062 mmol) was coevaporated with toluene (three times), dissolved in THF (0.4 mL), and added dropwise to the nitroimidazole solution. The resulting mixture was warmed to room temperature and allowed to stir for 3 hours before being concentrated under reduced pressure to yield an orange oil, which was purified using gradient silica gel flash chromatography (DCM:EtOAc, 18:1 to 9:1, *v/v*) to give a pale yellow oil (9.6 mg, 35%). R_f = 0.53 (DCM:EtOAc, 1:1, *v/v*); $[\alpha]^{25}_D$ = - 3.9 (c = 0.3, DCM); IR(film): 2988, 2934, 1749, 1540, 1372, 1252 cm^{-1}; ^{1}H NMR (500 MHz, $CDCl_3$): δ 7.27 (s, 1H, H-4), 5.51 (d, $J_{1',2'}$ = 5.18 Hz, 1H, H-1),

5.19 (s, 2H, H-6a & 6b), 4.62 (dd, $J_{3',4'}$ = 1.7 Hz, $J_{3',2'}$ = 7.8 Hz, 1H, H-3′), 4.33-4.39 (m, 3H, H-2′, H-6a′ & H-6b′), 4.22 (d, $J_{3',4'}$ = 8.4 Hz, H-4′), 4.05 (bs, 4H, *N*-Me & H-5′), 1.48 (s, 3H, CH_3), 1.44 (s, 3H, CH_3), 1.33 (s, 3H, CH_3), 1.32 (s, 3H, CH_3); ^{13}C NMR (125 MHz, $CDCl_3$): δ 154.3 (C-7), 146.3 (C-2), 131.2 (C-5), 130.0 (C-4), 109.8 (C_q), 108.8 (C_q), 96.2 (C-1′), 70.8 (C-4′), 70.7 (C-3′), 70.3 (C-2′), 67.4 (C6′), 65.7 (C-5′), 58.0 (C-6), 34.4 (N-Me), 26.0 (CH_3), 25.9 (CH_3), 24.9 (CH_3), 24.5 (CH_3); HRMS(ESI) calcd. For $[C_{18}H_{25}N_3O_{10}+H]^+$: 444.1613, obsd.: 444.1612.

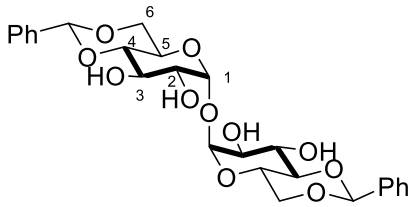

18

4,6:4',6'-Di-*O*-benzylidene-α,α′-trehalose (18): Trehalose **18** prepared according to the adapted procedure of Baddeley and Wardell (2009).[95] Trehalose dihydrate (1.2 g, 3.17 mmol) was coevaporated with ethanol (4 x 5 mL), and toluene (1 x 5 mL), and dissolved in dry DMF (10 mL). To this solution, benzaldehyde dimethyl acetal (0.47 mL, 3.17 mmol) in dry DMF (3.75 mL), and a catalytic amount (0.01 g) of camphorsulfonic acid were added. The reaction mixture was heated at 100˚C for 45 minutes, during which time two additional portions of benzaldehyde dimethyl acetal (0.94 mL, 6.34 mmol) were added. The reaction mixture was concentrated *in vacuo* and the product crystallised from toluene and water to yield the title compound (1.27 g, 2.44 mmol, 78%) as white crystals. R_f = 0.80 (MeOH:EtOAc, 1:4, *v/v*); Mp. 196-198 °C; lit.[95] Mp 197-198 °C; $[\alpha]^{19}_D$ = + 78 (c = 1, MeOH); lit. $[\alpha]^{25}_D$ = + 81.3 (c = 1, MeOH); IR (film):3445, 3212, 2360, 1656, 1071 cm^{-1}; ^{1}H NMR (500MHz, CD_3OD): δ = 7.48-7.51 (m, 4H, Ar), 7.33-7.35 (m, 6 H; Ar), 5.57 (s, 2 H, C<u>H</u>-Ph), 5.13 (d, $J_{1,2}$ = 4.0 Hz, 2 H; H-1), 4.22 (dd, $J_{6,6'}$ = 4.8 Hz, $J_{5,6}$ = 9.9 Hz, 2 H; H-6), 4.12 (m, 2 H, H-5), 4.03 (t, $J_{2,3}$ = $J_{3,4}$ = 9.6 Hz, 2 H; H-3), 3.73 (t, $J_{5,6'}$ = $J_{6,6'}$ = 10.3 Hz, 2 H, H-6'), 3.63 (dd, $J_{1,2}$ = 3.9 Hz, $J_{2,3}$ = 9.4 Hz, 2 H; H-2), 3.49 (t, $J_{3,4}$ = $J_{4,5}$ = 9.6 Hz, 2 H, H-4); ^{13}C NMR (125 MHz, CD_3OD): δ = 126.1-137.8 (Ar), 101.8 (CH-Ph) 95.1 (C-1), 81.6 (C-3), 72.4 (C-2), 70.1 (C-4), 68.5 (C-6), 62.8 (C-5); HRMS(ESI) calcd. For $[C_{26}H_{30}O_{11}+H]^+$: 519.1861, obsd.: 519.1877.

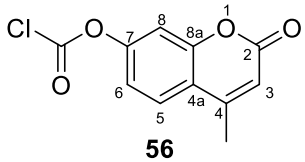

56

4-methyl-2-oxo-2*H*-chromen-7-yl carbonochloridate (56) To a solution of 4-methyl-umbelliferone (**55**) (80 mg, 0.45 mmol) in dry THF (1 mL) was added triethylamine (0.08 mL, 0.55 mmol). The resulting solution was cooled to 0 °C followed by the dropwise addition of triphosgene (44.9 mg, 0.15 mmol) in dry THF (1 mL). The reaction mixture was warmed to room temperature and stirred for 4 hours. After TLC analysis revealed the absence of starting materials (PE:EtOAc, 1:1, *v/v*), the solvent was removed *in vacuo*, and the resulting solid was purified by silica gel column chromatography (DCM:EtOAc, 1:1, *v/v*) to yield the title compound as a white solid (148.6 mg, 92%). R_f = 0.24 (DCM:EtOAc, 1:1, *v/v)*; Mp = 145.2–146.3 °C; IR (film): 3102, 1735, 1388, 847 cm^{-1}; ^1H NMR (500 MHz, $CDCl_3$): δ 7.68 (d, $J_{5,6}$ = 8.5 Hz, 1H, H-5), 7.33 (s, 1H, H-8), 7.28 (d, $J_{5,6}$ = 8.8Hz,1H, H-6), 6.32 (s, 1H, H-4), 2.46 (s, 3H, C<u>H</u>$_3$); ^{13}C NMR (125 MHz, $CDCl_3$): δ 160.2 (C-2), 154.2 (C-7), 152.7 (C-8a), 151.7 (C-4a), 150.6 (O-<u>C</u>OCl), 125.7 (C-6), 118.5 (C-4), 117.1 (C-5), 115.0 (C-3), 109.8 (C-8), 18.7 (<u>C</u>H$_3$).

(1-methyl-2-nitro-1*H*-imidazol-5-yl)methyl (4-methyl-2-oxo-2*H*-chromen-7-yl) carbonate (53): Imidazole **37** (45 mg, 0.18 mmol) was coevaporated three times with toluene, dissolved in pyridine (1 mL), and cooled to 0 °C. To this solution, chloroformate **56** (26.4 mg, 0.17 mmol) in pyridine (1.5 mL) was added dropwise. The solution was warmed to 70 °C, and stirred for 14 hours. The reaction mixture was allowed to cool and the solvent was removed under reduced pressure. The resulting brown solid was purified by gradient flash chromatography (PE:EtOAc, 4:1 to 1:1, *v/v*) to yield the title compound as a brown solid (16.2 mg, 25%). R_f = 0.32 (EA:PE, 7:3, *v/v*); IR(film): 3069, 2921, 1717, 1604, 1517, 1343 cm^{-1}; UV λ_{ex} = 317 nm, λ_{em} = 383 nm; ^1H NMR (500 MHz, $CDCl_3$): δ 7.63 (d, $J_{5,6}$ = 8.8 Hz, 1H, H-5), 7.32 (s, 1H, H-4′), 7.22 (s, 1H, H-8), 7.15 (d, $J_{5,6}$ = 8.4 Hz, 1H, H-6), 6.30 (s, 1H, H-3), 5.34 (s, 2H, H-6a′ & H-6b′), 4.12 (s, 3H, N-Me), 2.44 (s, 3H, C<u>H</u>$_3$); ^{13}C NMR (125 MHz, $CDCl_3$): δ 160.2 (C-2), 154.1 (C-7), 152.8 (C-8a), 152.3 (-OCOO-), 151.7 (C-4a), 146.5 (C-2′), 130.5 (C-4′), 130.4 (C-5′), 125.7 (C-6), 118.4 (C-4), 117 (C-5), 115.0 (C-3),

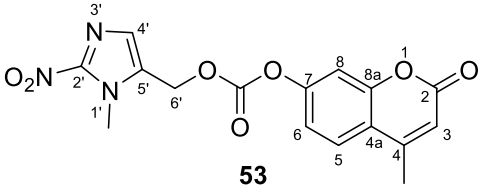

53

109.8 (C-8), 59.0 (C-6′), 34.5 (N-Me), 18.9 (<u>C</u>H$_3$); HRMS(ESI) *m/z* calcd. For [$C_{16}H_{13}N_3O_7$+H]$^+$: 360.0826, obsd.: 360.0836.

4-methyl-7-((1-methyl-2-nitro-1*H*-imidazol-5-yl)methoxy)-2*H*-chromen-2-one (57): Imidazole bromide **19** (60 mg, 0.27 mmol) was coevaporated three times with DMF, dissolved in DMF (1 mL) and added dropwise to a solution of 4-methylumbelliferone (**55**) (192 mg, 1.09 mmol), K_2CO_3 (150.6 mg, 1.09 mmol), and TBAI (1 mg, 0.002 mmol) in DMF (5 mL) at 0 °C. The reaction mixture was allowed to warm to room temperature and stirred for 2 hours, after which TLC analysis (EtOAc) revealed the absence of imidazole bromide **19**. The solvent was removed under reduced pressure and the resulting solid was purified by gradient silica gel column chromatography (PE:EtOAc, 1:9 to 3:2, *v/v*) to yield ether-linked fluoroprobe **57** (47 mg, 55%). **57**

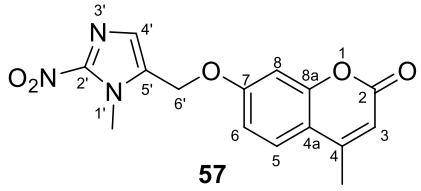

R_f = 0.3 (EtOAc); IR(film): 3084, 1709, 1613, 1537, 1351 cm^{-1}; UV λ_{ex} = 319 nm, λ_{em} = 380 nm; ^{1}H NMR (500 MHz, $CDCl_3$): δ 7.55 (d, $J_{5,6}$ = 9.7 Hz, 1H, H-5), 7.28 (s, 1H, H-4′), 6.92 (bs, 2H, H-6 & H-8), 6.19 (s, 1H, H-3), 5.13 (s, 2H, H-6a′ & H6b′), 4.08 (s, 3H, N-Me), 2.42 (s, 3H, 4-Me); ^{13}C NMR (125 MHz, $CDCl_3$): δ 160.8 (C-2), 160.1 (C-7), 155.2 (C-8a), 152.2 (C-4a), 146.6 (C-2′), 131.5 (C-5′), 129.3 (C-4′), 126.6 (C-6), 114.8 (C-4), 112.9 (C-3), 112.4 (C-5), 101.9 (C-8), 59.8 (C-6′), 34.6 (N-Me), 18.8 (4-Me); HRMS(ESI) calcd. For [$C_{15}H_{13}N_3O_5$+H]$^+$: 316.0928, calcd.: 316.0917.

4-methyl-2-oxo-2*H*-chromen-7-yl acetate (60): Acetic anhydride (1.6 mL, 1.7 mmol) was added dropwise to a solution of 7-hydroxy-4-methyl-coumarin (**55**) (200 mg, 1.1 mmol) and DMAP (0.01 g, 0.08 mmol) in dry dichloromethane (5 mL). The resulting solution was allowed to stir at room temperature for 3 hours. After TLC analysis revealed the absence of starting material, the reaction was poured into water, and the resulting white solid was filtered to yield the title compound (221 mg, 92%). **60**

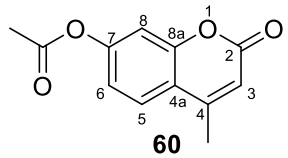

R_f = 0.39 (PE:EtOAc, 1:1, *v/v*); IR(film): 3052, 1758, 1620, 1507, 1331 cm^{-1}; UV λ_{ex} = 311 nm, λ_{em} = 376 nm; ^{1}H NMR (500 MHz, CD_3OD): δ 7.80 (d, $J_{5/6}$ = 8.6 Hz, 1H, H-5), 7.18 (s, 1H, H-8),

7.15 (d, $J_{5,6}$ = 8.8 Hz, 1H, H-6), 6.31 (s, 1H, H-3), 2.48 (s, 3H, 4-Me), 2.31 (s, 3H, OAc CH_3); ^{13}C NMR (125 MHz, CD_3OD): δ 169.0 (OAc), 161.2 (C-2), 153.9 (C-7), 153.5 (C-8a), 153.5 (C-4a), 125.7 (C-6), 118.2 (C-5), 117.7 (C-4), 113.4 (C-3), 109.9 (C-8), 19.5 (OAc CH_3), 17.3 (4-Me); HRMS(ESI) calcd. For $[C_{12}H_{10}O_4+H]^+$: 219.0652, obsd.: 219.0657.

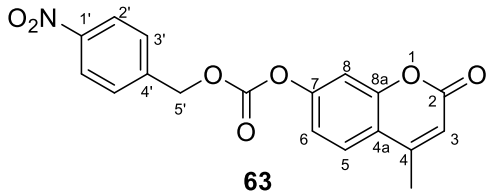

63

4-Methyl-7-(*p*-nitrobenzyloxycarboxy)-2*H*-chromen-2-one (63): *p*-Nitrobenzylalcohol (**61**) (45 mg, 0.18 mmol) was coevaporated with DMF and dissolved in a mixture of DMF (1 mL) and triethylamine (0.05 mL, 0.354 mmol). To this solution, chloroformate **56** (32.5 mg, 0.212 mmol) was added dropwise, and the resulting suspension was warmed to 40 °C and allowed to stir for 12 hours. The solvent was removed *in vacuo* and the resulting solid was purified by gradient column chromatography (PE:EtOAc, 9:1 to 9:2, *v/v*) to yield the title compound **63** as a brown solid (15 mg, 24%). R_f = 0.60 (PE:EtOAc, 1:1, *v/v*); IR(film):3078, 1714, 1608, 1517, 1389 cm^{-1}; UV λ_{ex} = 312 nm, λ_{em} = 384 nm; ^{1}H NMR (500 MHz, $CDCl_3$): δ 8.28 (d, $J_{5/6}$ = 8.0 Hz, 1H, H-5), 7.62 (d, $J_{2',3'}$ = 8.6 Hz, 4H, H-2a′, H-2b′, H-3a′ & H-3b′), 7.23 (s, 1H, H-8), 7.17 (d, $J_{5,6}$ = 8.9 Hz, 1H, H-6), 6.29 (s, 1H, H-3), 5.39 (s, 2H, H-5a′ & H-5b′), 2.44 (s, 3H, CH_3); ^{13}C NMR (125 MHz, $CDCl_3$): δ 160.3 (C-2), 154.2 (C-7), 153.0 (C-8a), 152.6 (-OCOO-), 151.7 (C-4a), 148.2 (C-1′), 141.4 (C-4′), 128.7 (C-3′), 125.7 (C-6), 124.0 (C-2′), 118.3 (C-4a), 117.2 (C-5), 114.9 (C-3), 109.9 (C-8), 69.0 (C-6′), 18.8 (4-Me); HRMS(ESI) calcd. For $[C_{18}H_{13}NO_7+H]^+$: 356.0765, obsd. 356.0769.

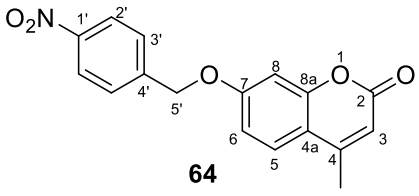

64

4-methyl-7-((4-nitrobenzyl)oxy)-2*H*-chromen-2-one (64): To a mixture 4-methylumbelliferone **55** (400 mg, 2.2 mmol) and *p*-nitrobenzyl bromide (**62**) (540 mg,2.5 mmol) in DMF (20 mL) was added sodium hydride (136.3 mg, 3.4 mmol), and the resulting suspension was stirred for 2 hours, before being diluted with water (50 mL), and extracted with EtOAc (5 × 50 mL). The combined organic fractions were washed with brine, dried over $MgSO_4$, filtered, and concentrated under reduced

pressure to yield the title compound (613 mg, 87%) as a white solid. R_f = 0.29 (EtOAc:PE, 2:3, *v/v*); IR(film): 3091, 2920,1715, 1601, 1514, 1340 cm^{-1}; UV λ_{ex} = 319 nm, λ_{em} = 379 nm; ^{1}H NMR (500 MHz, $CDCl_3$): δ 8.27 (d, $J_{2',3'}$ = 8.5 Hz, 2H, H-2a′ & H-2b′), 7.62 (d, $J_{2',3'}$ = 8.1 Hz, 2H, H-3a′ & H-3b′), 7.53 (d, $J_{5,6}$ = 9.2 Hz, 1H, H-5), 6.94 (d, $J_{5,6}$ = 9.4 Hz, 1H, H-6), 6.87 (s, 1H, H-8), 6.17 (s, 1H, H-3), 5.24 (s, 2H, H6a′ & H6′), 2.41 (s, 3H, 4-Me); ^{13}C NMR (125 MHz, $CDCl_3$) δ 161.0 (C-2), 160.9 (C-7), 155.2 (C-8a), 152.3 (C-4a), 147.8 (C-1′), 143.2 (C-4′), 127.7 (C-3a′ & C-3b′), 125.8 (C-6), 124.0 (C-2a′ & C-2b′), 114.3 (C-4), 112.7 (C-5), 112.5 (C-3), 102.0 (C-8), 69.1 (C-6′), 18.7 (4-Me); HRMS(ESI) calcd. For $[C_{18}H_{13}NO_7+H]^+$: 312.0866, obsd. 312.0865.

4.3 Biological methods

NTR activation of reporter fluoroprobes in E. coli[121]

SOS-R2 pUCX:*ntr* strains (including the pUCX empty plasmid control) were seeded into 96-well microplates containing 200 μL LB + Amp + glycose (0.4%) and grown overnight (16 hours) at 30 °C, 200 rpm. The next morning, 15 μL of each culture was added to 200 μL of assay media (LB + Amp + 0.05 mM IPTG + 0.2% *v/v* glucose) in a 96-well microplate, and cultures were grown for 3.5 hours at 30 °C, 200 rpm. The cultures were then split and100 μL aliquots were pipetted into two fresh microplates, one with 100 μL assay media + reporter fluoroprobe (2 × concentration) and the other with 100 μL assay media + DMSO control. The cultures were then incubated (30 °C, 200 rpm) for approximately 3 hours, with fluorescence measured every 20 minutes (λ_{ex} = 345 nm, λ_{em} = 460 nm) using the EnSpire 2300 Multilabel Reader (*Perkin Elmer, Waltham, MA, USA*).

Statistical analysis

Statistical significance was analysed using one-way analysis of variance (ANOVA) followed by post-hoc analysis using the Tukey's Multiple Comparison Test to compare means of every treatment group. Statistical calculations were performed using IBM SPSS Statistics 2.0 (*IBM, Armonk, NY, USA*)

Cell culture

RAW 264.7 cells were revived from frozen liquid nitrogen stocks (1×10^6 cells/mL [DMSO]) by quickly thawing them in a 37 °C water bath and immediately transferring them into 10 mL of pre-warmed complete culture media (CTCM) (Dulbecco's Modified Eagle's Medium (DMEM); 1 × Penicillin-streptomycin, 25 mM HEPES buffer solution, 10% Foetal Calf Serum (FCS) in basal media Gibco®DMEM; Invitrogen) and centrifuged for 5 minutes (300 rpm). The supernatant (containing DMSO) was discarded and the cells were resuspended in 7 mL CTCM and seeded into a CELLSTAR® 75 cm^2 cell culture flask, and incubated for 72 hours at 37 °C, 5% CO_2.

Cell maintenance

RAW 264.7 cells were maintained every 72 hours:

Once the RAW 264.7 cells reached 80% confluency, the media was removed aseptically, and the adherent cells were washed with 100 × Dulbecco's Phosphate Buffered Saline (DPBS), mechanically disrupted, and centrifuged for 5 minutes (at 300 rmp). The cellular pellet was resuspended in 1 mL of DPBS, counted, and seeded into a new CELLSTAR®75 cm^2 cell culture flask at 1×10^6 cells per 13 mL of CTCM.

Hypoxia induced cell death

RAW 264.7 cells were seeded at 1×10^6 cells/mL (DPBS) to a total of 2 mL/well. Cells were then incubated under either hypoxic (1.2% O_2, 5% CO_2) or normoxic (20% O_2, 5% CO_2) for 3 hours. After incubation, cells were mechanically disrupted and counted using trypan blue staining as a measure of cellular viability.

Normoxia experiments

RAW 264.7 cells were seeded at an appropriate concentration (2×10^5 -1×10^6 cells/mL[DPBS/CMEM]) into a 96-well plate (100 μL/well), and left to incubate (37 °C, 5% CO_2) for 2 hours. Reporter fluoroprobes and controls were added at a range of concentrations (0-250 μM, 100 μL/well), and left to

incubate (37 °C, 5% CO_2) for approximately 3 hours. Fluorescence measurements were made at half hour time points (λ_{ex} = 345 nm, λ_{em} = 460 nm) using the EnSpire 2300 Multilabel Reader (*Perkin Elmer, Waltham, MA, USA*).

Hypoxia experiments

RAW 264.7 cells were seeded at an appropriate concentration (2×10^5 -1×10^6 cells/mL[DPBS/CMEM]) into two 96-well plates (100 μL/well), and left to incubate (37 °C, 5% CO_2) for 2 hours. Reporter fluoroprobes and controls were added at a range of concentrations (0-250 μM) to each of the plates (100 μL/well), and left to incubate under either hypoxic (1.2% O_2, 5% CO_2) or normoxic (20% O_2, 5% CO2) for approximately 3 hours. Fluorescence measurements were taken prior to and after incubation (λ_{ex} = 345 nm, λ_{em} = 460 nm) using the EnSpire 2300 Multilabel Reader (*Perkin Elmer, Waltham, MA, USA*).

Fluoroprobe stability studies:

Aqueous stability:

DPBS was added to a 96-well microplate (100 μL/well). The fluoroprobes were then added at a range of concentrations (0-250 μM) to the 96-well plate (100 μL/mL) and left to incubate for 3 hours (37 °C, 5% CO_2). Fluorescence measurements were made at half hour time points (λ_{ex} = 345 nm, λ_{em} = 460 nm) using the EnSpire 2300 Multilabel Reader (*Perkin Elmer, Waltham, MA, USA*).

Cellular stability:

RAW 264.7 cells were seeded into a 96-well microplate at a concentration of 2×10^5 cells/mL (1×10^4 cells/well) in DPBS, and left to incubate (37 °C, 5% CO_2) for 2 hours. Reporter fluoroprobes and controls in DPBS were added at a range of concentrations (0 μM - 250 μM) to each of the plates (100 μL/well), and left to incubate for 3 hours. Fluorescence measurements were made at half hour time points (λ_{ex} = 345 nm, λ_{em} = 460 nm) using the EnSpire 2300 Multilabel Reader (*Perkin Elmer, Waltham, MA, USA*).

References:

1. David, A. R. Z., M. R., Cancer: an old disease, a new disease or something in between? *Nat. Rev. Cancer* **2010,** *10*, 728-733.
2. Siegel, R., Zou, Z.,Jemal, A., Cancer statistics, 2014. *CA Cancer J. Clin.* **2014,** *64*, 9-29.
3. Ministry of Health., Mortality: Historical summary 1948-2010. New Zealand Ministry of Health publications: 2014.
4. Chabner, B. A. R., T. G., Chemotherapy and the war on cancer. *Nat. Rev. Cancer* **2005,** *5*, 65-72.
5. DeVita, V. T.,Chu, E., A History of Cancer Chemotherapy. *Cancer Res.* **2008,** *68*, 8643-8653.
6. Papac, R. J., Origins of Cancer Therapy. *Yale J. Biol. Med.* **2001,** *74*, 391-398.
7. Gilman, A.,Philips, F., The Biological Actions and Therapeutic Applications of the B-Chloroethyl Amines and Sulfides. *Science* **1946,** *103*, 409-436.
8. Denny, W. A., Tumor-activated Prodrugs-A New Approach to Cancer Therapy. *Cancer Invest.* **2004,** *22*, 604-619.
9. Frei, E., Teicher, B. A., Holden, S. A., Preclinical studies and clinical correlation of the effect of alkylating dose. *Cancer Res.* **1988,** *48*, 6417 - 23.
10. Thomlinson, R. H., Gray, L. H., The histological structure of some human lung cancers and the possible implications for radiotherapy. *Brit. J. Cancer* **1955,** *9*, 539-549.
11. Brown, J. M., Giaccia, A. J., The unique physiology of solid tumors: opportunities (and problems) for cancer therapy. *Cancer Res.* **1998,** *58*, 1408-16.
12. Denny, W. A., The role of hypoxia-activated prodrugs in cancer therapy. *Lancet Oncol.* **2000,** *1*, 25-29.
13. Ryan, H. E., Poloni, M., McNulty, W., Elson, D., Gassmann, M., Arbeit, J. M., Johnson, R. S., Hypoxia-inducible factor-1alpha is a positive factor in solid tumor growth. *Cancer Res.* **2000,** *60*, 4010-5.
14. Semenza, G. L., HIF-1 and tumor progression: pathophysiology and therapeutics. *Trends. Mol. Med.* **2002,** *8*, 62-67.
15. Semenza, G. L., Targeting HIF-1 for cancer therapy. *Nat. Rev. Cancer* **2003,** *3*, 721 - 732.
16. Harris, A. L., Hypoxia - a key regulatory factor in tumour growth. *Nat. Rev. Cancer* **2002,** *2*, 38-47.
17. Cockman, M. E., Masson, N., Mole, D. R., Jaakkola, P., Chang, G., Clifford, S. C., Maher, E. R., Pugh, C. W., Ratcliffe, P. J., Maxwell, P. H., Hypoxia Inducible Factor-α Binding and Ubiquitylation by the von Hippel-Lindau Tumor Suppressor Protein. *J. Biol. Chem.* **2000,** *275*, 25733-25741.
18. Tanimoto, K., Makino, Y., Pereira, T., Poellinger, L., Mechanism of regulation of the hypoxia-inducible factor -1alpha by the von Hippel-Lindau tumor suppressor protein. *EMBO J.* **2000,** *19*, 4298 - 4309.
19. Ivan, M., Kondo, K., Yang, H., Kim, W., Valiando, J., Ohh, M., Salic, A., Asara, J. M., Lane, W. S., Kaelin, W. G., HIFα Targeted for VHL-Mediated Destruction by Proline Hydroxylation: Implications for O2 Sensing. *Science* **2001,** *292*, 464 -8.

20. Denny, W. A., The Design of Drugs that Target Tumor Hypoxia. *Aust. J. Chem.* **2004,** *57*, 821-828.
21. Brown, J. M., Wilson, W. R., Exploiting tumour hypoxia in cancer treatment. *Nat. Rev. Cancer* **2004,** *4*, 437 - 447.
22. Jaffar, M., Williams, K. J., Stratford, I. J., Bioreductive and gene therapy approaches to hypoxic diseases. *Adv. Drug Delivery Rev.* **2001,** *53*, 217-228.
23. Grigoryan, R., Keshelava, N., Anderson, C., Reynolds, C. P., In vitro testing of chemosensitivity in physiological hypoxia. *Methods Mol. Med.* **2005,** *110*, 87-100.
24. Denny, W. A., Hypoxia-activated prodrugs in cancer therapy: progress to the clinic. *Future Oncol.* **2010,** *6*, 419-428.
25. Kizaka-Kondoh, S., Konse-Nagasawa, H., Significance of nitroimidazole compounds and hypoxia-inducible factor-1 for imaging tumor hypoxia. *Cancer Sci.* **2009,** *100*, 1366-1373.
26. Belcourt, M. F., Hodnick, W. F., Rockwell, S., Sartorelli, A. C., Exploring the mechanistic aspects of mitomycin antibiotic bioactivation in Chinese hamster ovary cells overexpressing NADPH:cytochrome C (P-450) reductase and DT-diaphorase. *Adv. Enzyme Regul.* **1998,** *38*, 111-133.
27. Brown, J. M., Exploiting the hypoxic cancer cell: mechanisms and therapeutic strategies. *Mol. Med. Today* **2000,** *6*, 157-162.
28. Denny, W. A., Wilson, W. R., Hay, M. P., Recent developments in the design of bioreductive drugs. *Br. J. Cancer, Suppl.* **1996,** *74*, S32-S38.
29. Palmer, B. D., Wilson, W. R., Pullen, S. M., Denny, W. A., Hypoxia-selective antitumor agents. 3. Relationships between structure and cytotoxicity against cultured tumor cells for substituted N,N-bis(2-chloroethyl)anilines. *J. Med. Chem.* **1990,** *33*, 112-121.
30. Groot, F. M. H., Damen, E. W. P., Scheeren, H. W., Anticancer Prodrugs for Application in Monotherapy Targeting Hypoxia, Tumor-Associated Enzymes, and Receptors. *Curr. Med. Chem.* **2001,** *8*, 1093-122.
31. McKeown, S. R., Cowen, R. L., Williams, K. J., Bioreductive drugs: from concept to clinic. *Clin. Oncol.* **2007,** *19*, 427-42.
32. Zeman, E. M., Brown, J. M., Lemmon, M. J., Hirst, V. K., Lee, W. W., SR-4233: A new bioreductive agent with high selective toxicity for hypoxic mammalian cells. *Int. J. Radiat. Oncol.* **1986,** *12*, 1239-1242.
33. Brown, J. M., SR 4233 (tirapazamine): a new anticancer drug exploiting hypoxia in solid tumours. *Brit. J. Cancer* **1993,** *67*, 1163 - 1170.
34. Wang, J., Biedermann, K. A., Brown, J. M., Repair of DNA and Chromosome Breaks in Cells Exposed to SR 4233 under Hypoxia or to Ionizing Radiation. *Cancer Res.* **1992,** *52*, 4473-4477.
35. Rischin, D., Peters, L., Hicks, R., Hughes, P., Fisher, R., Hart, R., Sexton, M., D'Costa, I., von Roemeling, R. , Phase I Trial of Concurrent Tirapazamine, Cisplatin, and Radiotherapy in Patients With Advanced Head and Neck Cancer. *J. Clin. Oncol.* **2001,** *19*, 535-542.
36. Williamson, S. K., Crowley, J. J., Lara, P. N., McCoy, J., Lau, D. H. M., Tucker, R. W., Mills, G. M., Gandara, D. R., Phase III Trial of Paclitaxel Plus Carboplatin With or Without Tirapazamine in Advanced Non–Small-Cell Lung Cancer: Southwest Oncology Group Trial S0003. *J. Clin. Oncol.* **2005,** *23*, 9097-9104.

37. Bedikian, A. Y., Legha, S. S., Eton, O., Buzaid, A. C., Papadopoulos, N., Plager, C., Mclntyre, S., Viallet, J. , Phase II trial of escalated dose of tirapazamine combined with cisplatin in advanced malignant melanoma. *Anti-Cancer Drug.* **1999,** *10*, 735-740.
38. Brown, J. M., Siim, B. G., Hypoxia-specific cytotoxins in cancer therapy. *Semin. Radiat. Oncol.* **1996,** *6*, 22-36.
39. Albertella, M. R., Loadman, P., Jones, P. H., Phillips, R. M., Rampling, R., Burnet, N., Alcock, C., Anthoney, A., Vjaters, E., Dunk, C. R., Harris, P. A., Wong, A., Lalani, A. S., Twelves, C. J., Hypoxia-Selective Targeting by the Bioreductive Prodrug AQ4N in Patients with Solid Tumors: Results of a Phase I Study. *Clin. Cancer Res.* **2008,** *14*, 1096-1104.
40. Steward, W. P., Middleton, M., Benghiat, A., Loadman, P. M., Hayward, C., Waller, S., Ford, S., Halbert, G., Patterson, L. H., Talbot, D., The use of pharmacokinetic and pharmacodynamic end points to determine the dose of AQ4N, a novel hypoxic cell cytotoxin, given with fractionated radiotherapy in a phase I study. *Ann. Oncol.* **2007,** *18*, 1098-1103.
41. Papadopoulos, K. P., Goel, S., Beeram, M., Wong, A., Desai, K., Haigentz, M., Milián, M. L., Mani, S., Tolcher, A., Lalani, Alshad S., Sarantopoulos, J. , A Phase 1 Open-Label, Accelerated Dose-Escalation Study of the Hypoxia-Activated Prodrug AQ4N in Patients with Advanced Malignancies. *Clin. Cancer Res.* **2008,** *14*, 7110-7115.
42. Wilson, W. R., Hay, M. P., Targeting hypoxia in cancer therapy. *Nat. Rev. Cancer* **2011,** *11*, 393-410.
43. Chen, Y., Hu, L., Design of anticancer prodrugs for reductive activation. *Med. Res. Rev.* **2009,** *29*, 29-64.
44. Siegel, D., Ross, D., Immunodetection of NAD(P)H:quinone oxidoreductase 1 (NQO1) in human tissues. *Free Radical Bio. Med.* **2000,** *29*, 246-253.
45. Jaffar, M., Phillips, R. M., Williams, K. J., Mrema, I., Cole, C., Wind, N. S., Ward, T. H., Stratford, I. J., Patterson, A. V., 3-Substituted-5-aziridinyl-1-methylindole-4,7-diones as NQO1-directed antitumour agents: mechanism of activation and cytotoxicity in vitro. *Biochem. Pharmacol.* **2003,** *66*, 1199-1206.
46. Sartorelli, A. C., Therapeutic Attack of Hypoxic Cells of Solid Tumors: Presidential Address. *Cancer Res.* **1988,** *48*, 775-778.
47. Blower, P. J., Dilworth, J. R., Maurer, R. I., Mullen, G. D., Reynolds, C. A., Zheng, Y., Towards new transition metal-based hypoxic selective agents for therapy and imaging. *J. Inorg. Biochem.* **2001,** *85*, 15-22.
48. Reisner, E., Arion, V. B., Keppler, B. K.,Pombeiro, A. J. L., Electron-transfer activated metal-based anticancer drugs. *Inorg. Chim. Acta.* **2008,** *361*, 1569-1583.
49. Gabrilovich, D. I., Ostrand-Rosenber, S., Bronte, V., Coordinated regulation of myeloid cells by tumours. *Nat. Rev. Immunol.* **2012,** *12*, 253 - 268.
50. Mosser, D. M., Edwards, J. P. , Exploring the full spectrum of macrophage activation. *Nat. Rev. Immunol.* **2008,** *8*, 958 - 969.
51. Gordon, S., Alternative activation of macrophages. *Nat. Rev. Immunol.* **2003,** *3*, 23-35.
52. Biswas, S. K., Mantovani, A., Macrophage plasticity and interaction with lymphocyte subsets: cancer as a paradigm. *Nat. Immunol.* **2010,** *11*, 889 - 896.

53. Allavena, P., Sica, A., Solinas, G., Porta, C.,Mantovani, A., The inflammatory micro-environment in tumor progression: the role of tumor-associated macrophages. *Crit. Rev. Oncol. Hematol.* **2008,** *66*, 1-9.
54. Balkwill, F. A., Inflammation and cancer: back to Virchow? *Lancet* **2001,** *357*, 539.
55. Mantovani, A., Allavena, P., Sozzani, S., Vecchi, A., Locati, M.,Sica, A., Chemokines in the recruitment and shaping of the leukocyte infiltrate of tumors. *Semin. Cancer Biol.* **2004,** *14*, 155-160.
56. Mantovani, A., Sozzani, S., Locati, M., Allavena, P.,Sica, A., Macrophage polarization: tumor-associated macrophages as a paradigm for polarized M2 mononuclear phagocytes. *Trends. Immunol.* **2002,** *23*, 549-555.
57. Kelly, P. M., Macrophages in human breast disease: a quantitative immunohistochemical study. *Brit. J. Cancer* **1988,** *57*, 174 - 177.
58. Murdoch, C., Giannoudis, A.,Lewis, C. E., Mechanisms regulating the recruitment of macrophages into hypoxic areas of tumors and other ischemic tissues. *Blood* **2004,** *104*, 2224-2234.
59. Sica, A., Schioppa, T., Mantovani, A., Allavena, P., Tumour-associated macrophages are a distinct M2 polarised population promoting tumour progression: Potential targets of anti-cancer therapy. *Eur. J. Cancer* **2006,** *42*, 717 - 727.
60. Allavena, P., Sica, A., Garlanda, C., Mantovani, A., The Yin-Yang of tumor-associated macrophages in neoplastic progression and immune surveillance. *Immunol. Rev.* **2008,** *222*, 155 - 161.
61. Sica, A.,Mantovani, A., Macrophage plasticity and polarization: in vivo veritas. *J. Clin. Invest.* **2012,** *122*, 787-95.
62. Klimp, A. H., de, V. E. G. E., Scherphof, G. L.,Daemen, T., A potential role of macrophage activation in the treatment of cancer. *Crit. Rev. Oncol. Hematol.* **2002,** *44*, 143-61.
63. Nagarajan, R., Clohisy, D.,Weigel, B., New paradigms for therapy for osteosarcoma. *Curr. Oncol. Rep.* **2005,** *7*, 410-414.
64. Nardin, A., Lefebvre, M. L., Labroquere, K., Faure, O.,Abastado, J. P., Liposomal Muramyl Tripeptide Phosphatidylethanolamine: Targeting and Activating Macrophages for Adjuvant Treatment of Osteosarcoma. *Curr. Cancer Drug Tar.* **2006,** *6*, 123-133.
65. Leifler, K. S., Svensson, S., Abrahamsson, A., Bendrik, C., Robertson, J., Gauldie, J., Olsson, A.-K.,Dabrosin, C., Inflammation Induced by MMP-9 Enhances Tumor Regression of Experimental Breast Cancer. *J. Immunol.* **2013,** *190*, 4420-4430.
66. Hoption, C. S. A., van, N. J. P.,van, N. C., Dr William Coley and tumour regression: a place in history or in the future. *Postgrad. Med. J.* **2003,** *79*, 672-80.
67. McCarthy, E. F., The toxins of William B. Coley and the treatment of bone and soft-tissue sarcomas. *Iowa Orthop. J.* **2006,** *26*, 154-158.
68. Old, L. J., Tumor Necrosis Factor (TNF). *Science* **1985,** *230*, 630-632.
69. Bassi, P., BCG (Bacillus of Calmette Guerin) therapy of high-risk superficial bladder cancer. *Surg. Oncol.* **2002,** *11*, 77-83.
70. Nepple, K. G., Aubert, H. A., Braasch, M. R.,O'Donnell, M. A., Combination of BCG and interferon intravesical immunotherapy: an update. *World J. Urol.* **2009,** *27*, 343-346.

71. Witjes, J. A., Management of BCG Failures in Superficial Bladder Cancer: A Review. *European Urology* **2006,** *49*, 790-797.
72. Hu, H.-M., Urba, W. J.,Fox, B. A., Gene-Modified Tumor Vaccine with Therapeutic Potential Shifts Tumor-Specific T Cell Response from a Type 2 to a Type 1 Cytokine Profile. *J. Immunol.* **1998,** *161*, 3033-3041.
73. Bloch, H., STUDIES ON THE VIRULENCE OF TUBERCLE BACILLI. *J. Exp. Med.* **1950,** *91*, 197-218.
74. Ishikawa, E., Ishikawa, T., Morita, Y. S., Toyonaga, K., Yamada, H., Takeuchi, O., Kinoshita, T., Akira, S., Yoshikai, Y.,Yamasaki, S., Direct recognition of the mycobacterial glycolipid, trehalose dimycolate, by C-type lectin Mincle. *J. Exp. Med.* **2009,** *206*, 2879-2888.
75. Khan, A. A., Stocker, B. L.,Timmer, M. S. M., Trehalose glycolipids—synthesis and biological activities. *Carbohyd. Res.* **2012,** *356*, 25-36.
76. Barry Iii, C. E., Lee, R. E., Mdluli, K., Sampson, A. E., Schroeder, B. G., Slayden, R. A.,Yuan, Y., Mycolic acids: structure, biosynthesis and physiological functions. *Prog. Lipid Res.* **1998,** *37*, 143-179.
77. Chatterjee, D., The mycobacterial cell wall: structure, biosynthesis and sites of drug action. *Curr. Opin. Chem. Biol.* **1997,** *1*, 579-588.
78. Pimm, M. V., Baldwin, R. W., Polonsky, J.,Lederer, E., Immunotherapy of an ascitic rat hepatoma with cord factor (trehalose-6, 6′-dimycolate) and synthetic analogues. *Int. J. Cancer* **1979,** *24*, 780-785.
79. Bekierkunst, A., Wang, L., Toubiana, R.,Lederer, E., Immunotherapy of Cancer with Nonliving BCG and Fractions Derived from Mycobacteria: Role of Cord Factor (Trehalose-6, 6′-Dimycolate) in Tumor Regression. *Infect. Immun.* **1974,** *10*, 1044-1050.
80. Yarkoni, E.,Rapp, H. J., Tumor Regression after Intralesional Injection of Mycobacterial Components Emulsified in 2,6,10,15,19,23-Hexamethyl-2,6,10,14,18,22-tetracosahexaene (Squalene), 2,6,10,15,19,23-Hexamethyltetracosane (Squalane), Peanut Oil, or Mineral Oil. *Cancer Res.* **1979,** *39*, 1518-1520.
81. Watanabe, R., Yoo, Y. C., Hata, K., Mitobe, M., Koike, Y., Nishizawa, M., Garcia, D. M., Nobuchi, Y., Imagawa, H., Yamada, H.,Azuma, I., Inhibitory effect of trehalose dimycolate (TDM) and its stereoisometric derivatives, trehalose dicorynomycolates (TDCMs), with low toxicity on lung metastasis of tumour cells in mice. *Vaccine* **1999,** *17*, 1484-1492.
82. Nolibe, D., Masse, R., Tenu, J.-P., Lepoivre, M.,Petit, J.-F., Activation of rat alveolar macrophages and protection against i.v. injected tumor cells by intratracheal administration of trehalose dimycolate. *Cancer Immunol. Immun.* **1986,** *23*, 200-206.
83. McLaughlin, C. A., Strain, S. M., Bickel, W. D., Goren, M. B., Azuma, I., Milner, K., Cantrell, J. L.,Ribi, E., Regression of line-10 hepatocellular carcinomas following treatment with water-soluble, microbial extracts combined with trehalose or arabinose mycolates. *Cancer Immunol. Immun.* **1978,** *4*, 61-68.
84. Schoenen, H., Bodendorfer, B., Hitchens, K., Manzanero, S., Werninghaus, K., Nimmerjahn, F., Agger, E. M., Stenger, S., Andersen, P., Ruland, J., Brown, G. D., Wells, C.,Lang, R., Cutting Edge: Mincle Is Essential for Recognition and Adjuvanticity of the Mycobacterial Cord Factor and its Synthetic Analog Trehalose-Dibehenate. *J. Immunol.* **2010,** *184*, 2756-2760.

85. Geisel, R. E., Sakamoto, K., Russell, D. G.,Rhoades, E. R., In Vivo Activity of Released Cell Wall Lipids of Mycobacterium bovis Bacillus Calmette-Guérin Is Due Principally to Trehalose Mycolates. *J. Immunol.* **2005,** *174*, 5007-5015.
86. Sakamoto, K., Kim, M. J., Rhoades, E. R., Allavena, R. E., Ehrt, S., Wainwright, H. C., Russell, D. G.,Rohde, K. H., Mycobacterial Trehalose Dimycolate Reprograms Macrophage Global Gene Expression and Activates Matrix Metalloproteinases. *Infect. Immun.* **2013,** *81*, 764-776.
87. Khan, A. A., Chee, S. H., McLaughlin, R. J., Harper, J. L., Kamena, F., Timmer, M. S. M.,Stocker, B. L., Long-Chain Lipids Are Required for the Innate Immune Recognition of Trehalose Diesters by Macrophages. *ChemBioChem* **2011,** *12*, 2572-2576.
88. Furukawa, A., Kamishikiryo, J., Mori, D., Toyonaga, K., Okabe, Y., Toji, A., Kanda, R., Miyake, Y., Ose, T., Yamasaki, S.,Maenaka, K., Structural analysis for glycolipid recognition by the C-type lectins Mincle and MCL. *P. Natl. Acad. Sci. USA.* **2013,** *110*, 17438-17443.
89. Lobato-Pascual, A., Saether, P. C., Fossum, S., Dissen, E.,Daws, M. R., Mincle, the receptor for mycobacterial cord factor, forms a functional receptor complex with MCL and FcεRI-γ. *Eur. J. Immunol.* **2013,** *43*, 3167-3174.
90. Miyake, Y., Toyonaga, K., Mori, D., Kakuta, S., Hoshino, Y., Oyamada, A., Yamada, H., Ono, K.-i., Suyama, M., Iwakura, Y., Yoshikai, Y.,Yamasaki, S., C-type Lectin MCL Is an FcRγ-Coupled Receptor that Mediates the Adjuvanticity of Mycobacterial Cord Factor. *Immunity* **2013,** *38*, 1050-1062.
91. Matsunaga, I.,Moody, D. B., Mincle is a long sought receptor for mycobacterial cord factor. *J. Exp. Med.* **2009,** *206*, 2865-2868.
92. Yamasaki, S., Ishikawa, E., Sakuma, M., Hara, H., Ogata, K., Saito, T., Mincle is an ITAM-coupled activating receptor that senses damaged cells. *Nat. Immunol.* **2008,** *9*, 1179-1188.
93. Feinberg, H., Jégouzo, S. A. F., Rowntree, T. J. W., Guan, Y., Brash, M. A., Taylor, M. E., Weis, W. I.,Drickamer, K., Mechanism for Recognition of an Unusual Mycobacterial Glycolipid by the Macrophage Receptor Mincle. *J. Biol. Chem.* **2013,** *288*, 28457-28465.
94. Jiao, H., Lewis, J., Matteucci, M.,Sun, D., Antineoplastic agent-heteroarylmethylammonium salt derivatives as hypoxia activated prodrugs and their preparation, pharmaceutical compositions and use in the treatment of cancer. *PCT Int. Appl.* **2008**, 74pp.
95. Baddeley, T. C.,Wardell, J. L., Synthesis of Per- and Poly-Substituted Trehalose Derivatives: Studies of Properties Relevant to Their Use as Excipients for Controlled Drug Release. *J. Carbohydr. Chem.* **2009,** *28*, 198-221.
96. Matteucci, M., Duan, J.-X., Jiao, H., Kaizerman, J.,Ammons, S., Phosphoramidate alkylator prodrugs and their preparation, pharmacokinetics and use in the treatment of cancer and hyperproliferative diseases. *PCT Int. Appl.* **2007**, 213pp.
97. Clayden, J., Greeves, N., Warren, S., *Organic Chemistry*. Oxford University Press: 2001.
98. Matteucci, M., Jian-Xin, D., Hypoxia-Activated Anti-Cancer Agents. **2008**.
99. Denny, W. A., The role of hypoxia-activated prodrugs in cancer therapy. *Lancet ONcol.* **2000,** *1*, 25-29.

100. Carl, P. L., Chakravarty, P. K.,Katzenellenbogen, J. A., A novel connector linkage applicable in prodrug design. *J. Med. Chem.* **1981,** *24*, 479-480.
101. de Groot, F. M. H., Loos, W. J., Koekkoek, R., van Berkom, L. W. A., Busscher, G. F., Seelen, A. E., Albrecht, C., de Bruijn, P.,Scheeren, H. W., Elongated Multiple Electronic Cascade and Cyclization Spacer Systems in Activatible Anticancer Prodrugs for Enhanced Drug Release. *J. Org. Chem.* **2001,** *66*, 8815-8830.
102. D'Souza, A. J. M.,Topp, E. M., Release from polymeric prodrugs: Linkages and their degradation. *J. Pharm. Sci.* **2004,** *93*, 1962-1979.
103. Chakrabarty, S. P., Ramapanicker, R., Mishra, R., Chandrasekaran, S., Balaram, H., Development and characterisation of lysine based tripeptide analogues as inhibitors of Sir2 activity. *Bioorgan. Med. Chem.* **2009,** *17*, 8060-8072.
104. Goren, Z., Heeg, M. J.,Mobashery, S., Facile chloride substitution of activated alcohols by triphosgene: application to cephalosporin chemistry. *J. Org. Chem.* **1991,** *56*, 7186-7188.
105. Frenette, M., Coenjarts, C.,Scaiano, J. C., Mapping Acid-Catalyzed Deprotection in Thin Polymer Films: Fluorescence Imaging Using Prefluorescent 7-Hydroxycoumarin Probes. *Macromol. Rapid Comm.* **2004,** *25*, 1628-1631.
106. Jacks, T. J., Kircher, H. W. , Fluorometric assay for the hydrolytic activity of lipase using fatty acyl esters of 4-methylumbelliferone. *Anal. Biochem.* **1967,** *21*, 279-285.
107. Guilbault, G. G.,Hieserman, J., Fluorometric substrate for sulfatase and lipase. *Anal. Chem.* **1969,** *41*, 2006-2009.
108. Prosser, G. A., Copp, J. N., Mowday, A. M., Guise, C. P., Syddall, S. P., Williams E. M., Horvat, C. N., Swe, P. M., Ashoorzadeh, A., Denny, W. A., Smaill, J. B., Patterson, A. V., Ackerley, D. F., Creation and screening of a multi-family bacterial oxidoreductase library to discover novel nitroreductases that efficiently activate the bioreductive prodrugs CB1954 and PR-104A. *Biochem. Pharmacol.* **2013,** *85*, 1091-1103.
109. Green, L., Storey, M., Williams, E., Patterson, A., Smaill, J., Copp, J.,Ackerley, D., The Flavin Reductase MsuE Is a Novel Nitroreductase that Can Efficiently Activate Two Promising Next-Generation Prodrugs for Gene-Directed Enzyme Prodrug Therapy. *Cancers* **2013,** *5*, 985-997.
110. Lewis, J. S., Lee, J. A., Underwood, J. C., Harris, A. L.,Lewis, C. E., Macrophage responses to hypoxia: relevance to disease mechanisms. *J. Leukocyte Biol.* **1999,** *66*, 889-900.
111. Hu, J., Handisides, D. R., Valckenborgh, E. V., De Raeve, H., Menu, E., Vande Broek, I., Liu, Q., Sun, J. D., Van Camp, B., Hart, C. P., Vanderkerken, K. , Targeting the multiple myeloma hypoxic niche with TH-302, a hypoxia-activated prodrug. *Blood* **2010,** *116*, 1524-1527.
112. Sun, J. D., Liu, Q., Wang, J., Ahluwalia, D., Ferraro, D., Wang, Y., Duan, J., Ammons, W. S., Curd, J. G., Matteucci, M. D., Hart, C. P. , Selective Tumor Hypoxia Targeting by Hypoxia-Activated Prodrug TH-302 Inhibits Tumor Growth in Preclinical Models of Cancer. *Clin. Cancer Res.* **2012,** *18*, 758-70.
113. Meng, F., Evans, J. W., Bhupathi, D., Banica, M., Lan, L., Lorente, G., Duan, J.-X., Cai, X., Mowday, A. M., Guise, C. P., Maroz, A., Anderson, R. F., Patterson, A. V., Stachelek, G. C., Glazer, P. M., Matteucci, M. D.,Hart, C. P.,

Molecular and Cellular Pharmacology of the Hypoxia-Activated Prodrug TH-302. *Mol. Cancer Ther.* **2012,** *11*, 740-751.
114. Hua, L., Wu, X., Han, J., Chen, L. Vass, S. O., Browne, P., Hall, B. S., Bot, C., Gobalakrishnapillai, V., Searle, P. F., Knox, R. J. Wilinson, S. R., Synthesis and structure–activity relationships of nitrobenzyl phosphoramide mustards as nitroreductase-activated prodrugs. *Bioorg. Med. Chem. Lett.* **2011,** *21*, 3986-3991.
115. Denny, W. A., Prodrug strategies in cancer therapy. *Eur. J. Med. Chem.* **2001,** *36*, 577-595.
116. Kwon, D. H., Osato, M. S., Graham, D. Y.,El-Zaatari, F. A. K., Quantitative RT-PCR analysis of multiple genes encoding putative metronidazole nitroreductases from Helicobacter pylori. *Int. J. Antimicrob. Ag.* **2000,** *15*, 31-36.
117. Abdel-Mottaleb, M. S. A., El-Sayed, B. A., Abo-Aly, M. M.,El-Kady, M. Y., Fluorescence-properties and excited state interactions of 7-hydroxy-4-methylcoumarin laser dye. *J. Photoch. Photobio. A.* **1989,** *46*, 379-390.
118. Li, X., Wang, J., Zhang, L.,Xu, W., Design, Synthesis, and Preliminary Activity Evaluation of Novel Peptidomimetics as Aminopeptidase N/CD13 Inhibitors. *Arch. Pharm.* **2011,** *344*, 494-504.
119. McElvain, S. M.,Laughton, P. M., Piperidine Derivatives. XXIV. 1-Methyl-4-phenyl-3-piperidone and Related Products. *J. Am. Chem. Soc.* **1951,** *73*, 448-452.
120. Hay, M. P., Wilson, W. R.,Denny, W. A., Design, Synthesis and Evaluation of Imidazolylmethyl Carbamate Prodrugs of Alkylating Agents. *Tetrahedron* **2000,** *56*, 645-657.
121. Prosser, G. A., Copp, J. N., Syddall, S. P., Williams, E. M., Smaill, J. B., Wilson, W. R., Patterson, A. V.,Ackerley, D. F., Discovery and evaluation of Escherichia coli nitroreductases that activate the anti-cancer prodrug CB1954. *Biochem. Pharmacol.* **2010,** *79*, 678-687.

Appendix

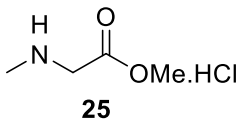

25

^{1}H NMR

CD_3OD, 500 MHz

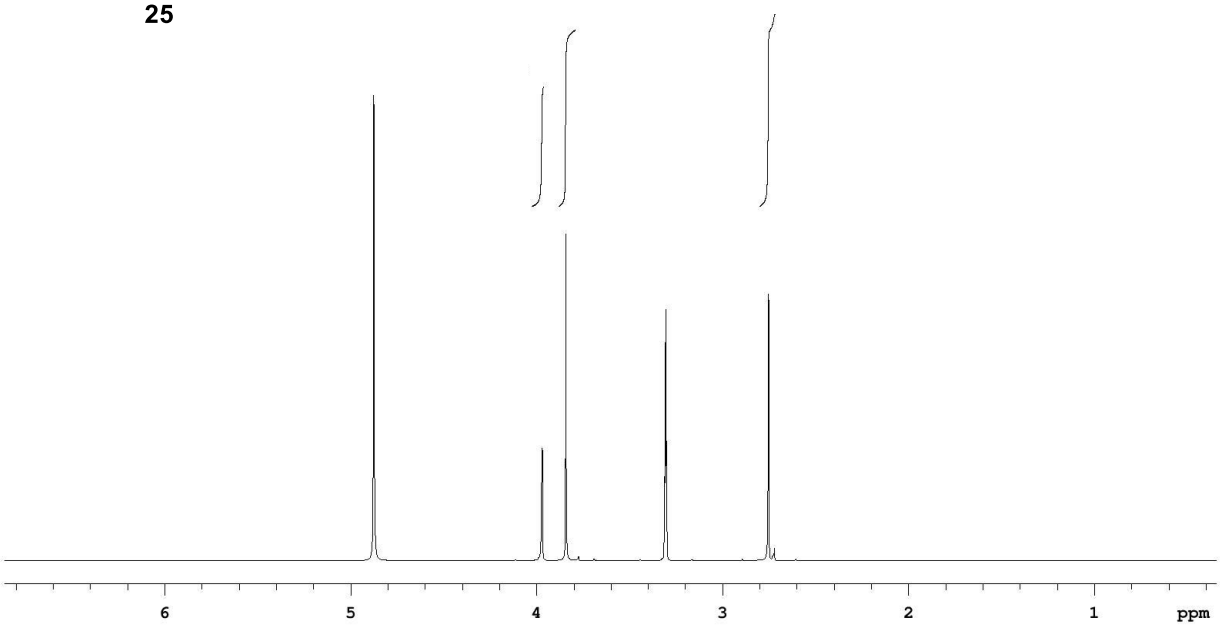

^{13}C NMR

CD_3OD, 125 MHz

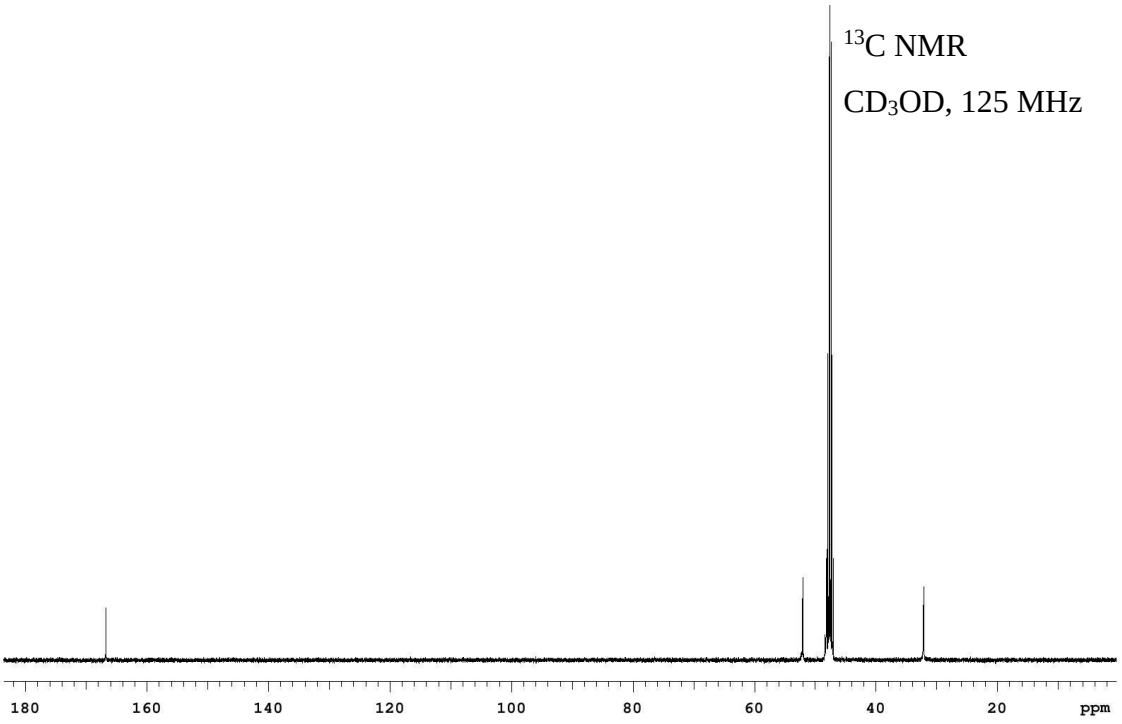

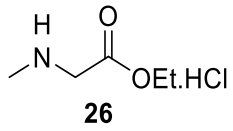

26

^{1}H NMR

CD_3OD, 500 MHz

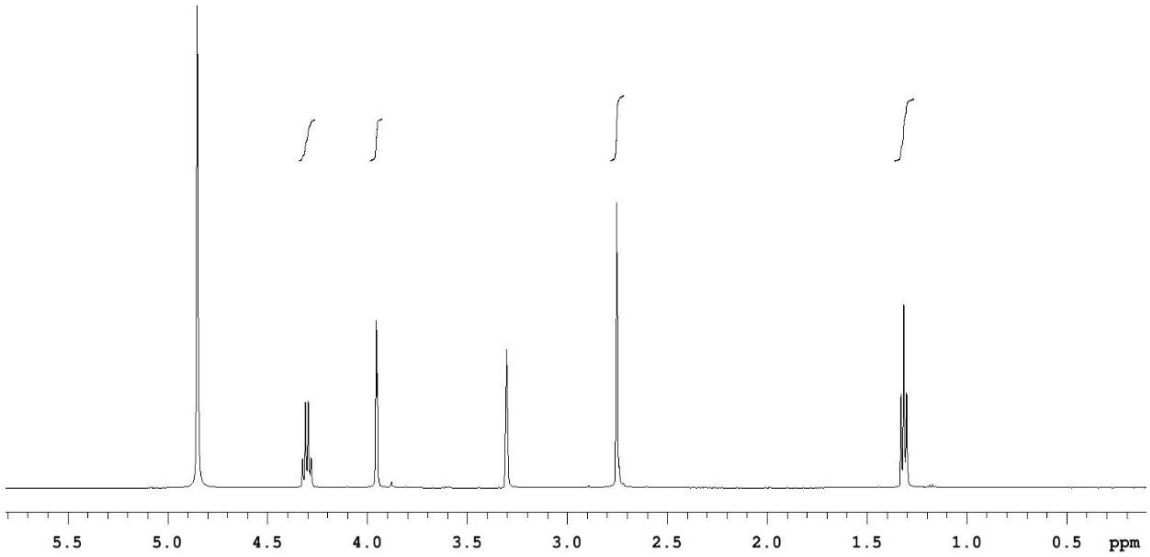

^{13}C NMR

CD_3OD, 125 MHz

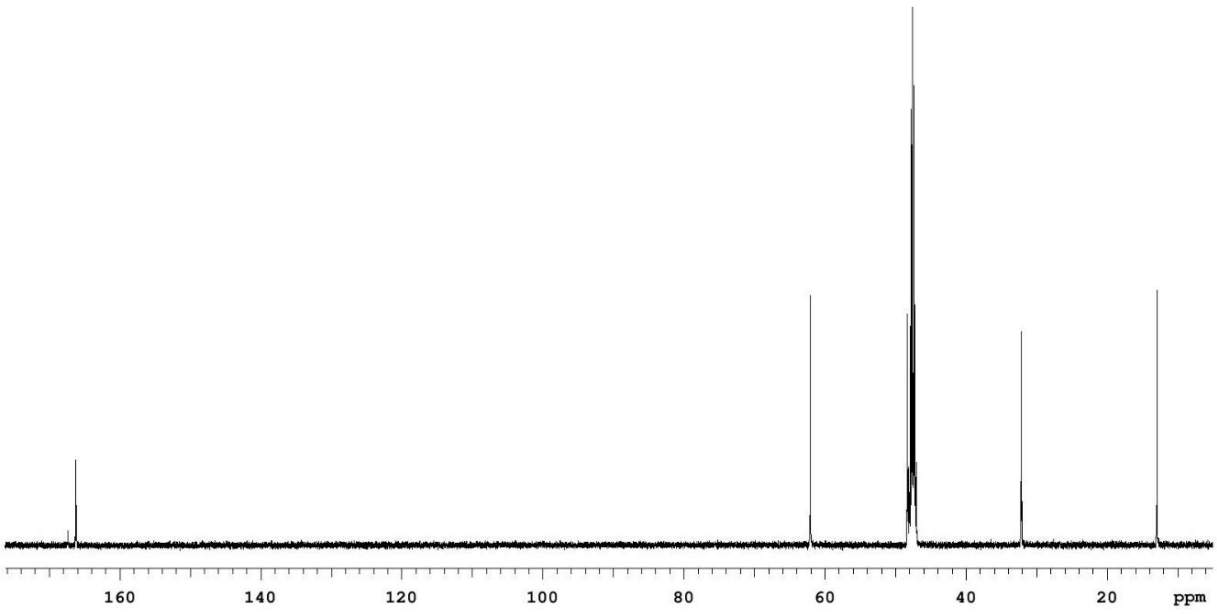

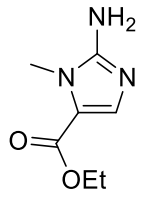

22

^{1}H NMR

CD_3OD, 500 MHZ

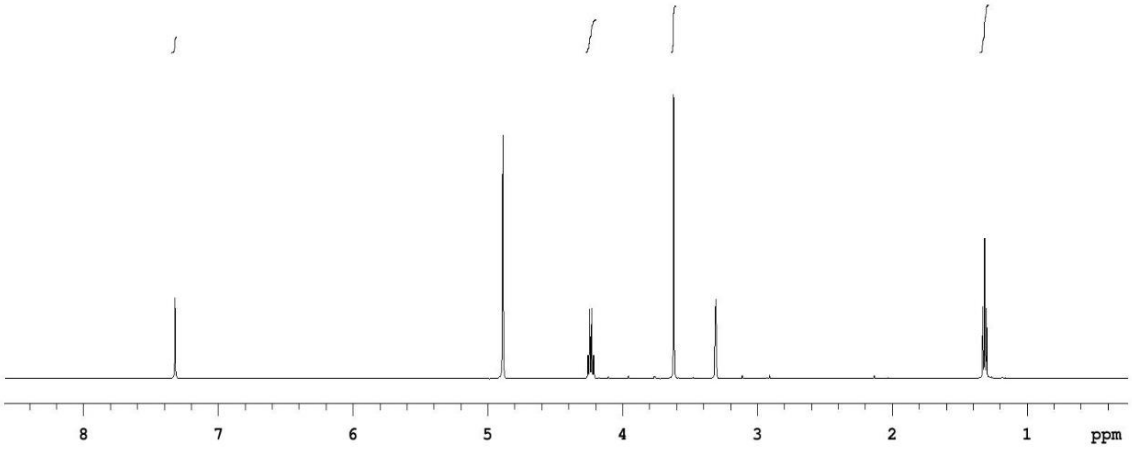

^{13}C NMR

CD_3OD, 125 MHz

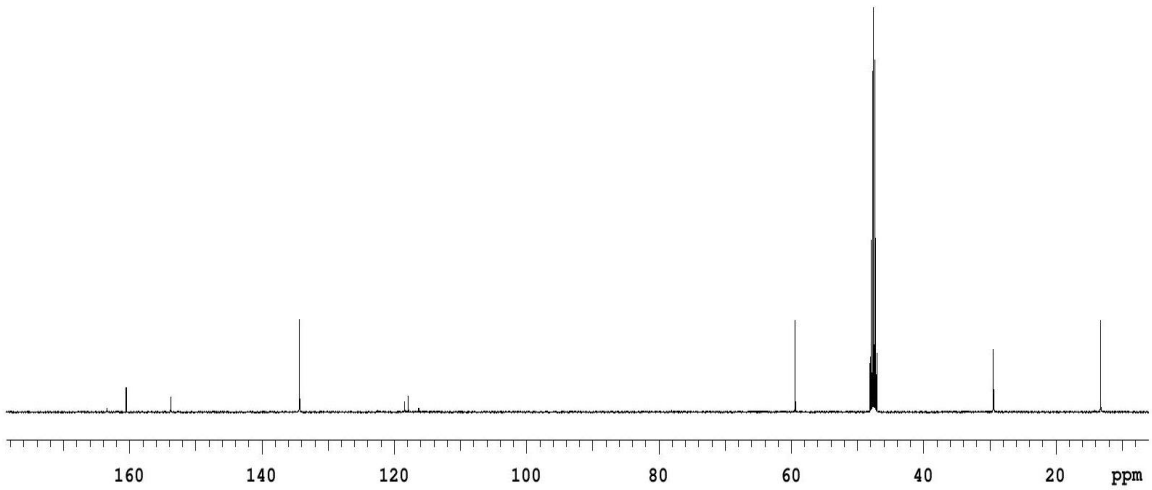

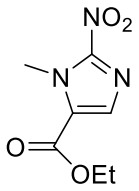

35

^{1}H NMR

CD_3OD, 500 MHz

^{13}C NMR

CD_3OD, 125 MHz

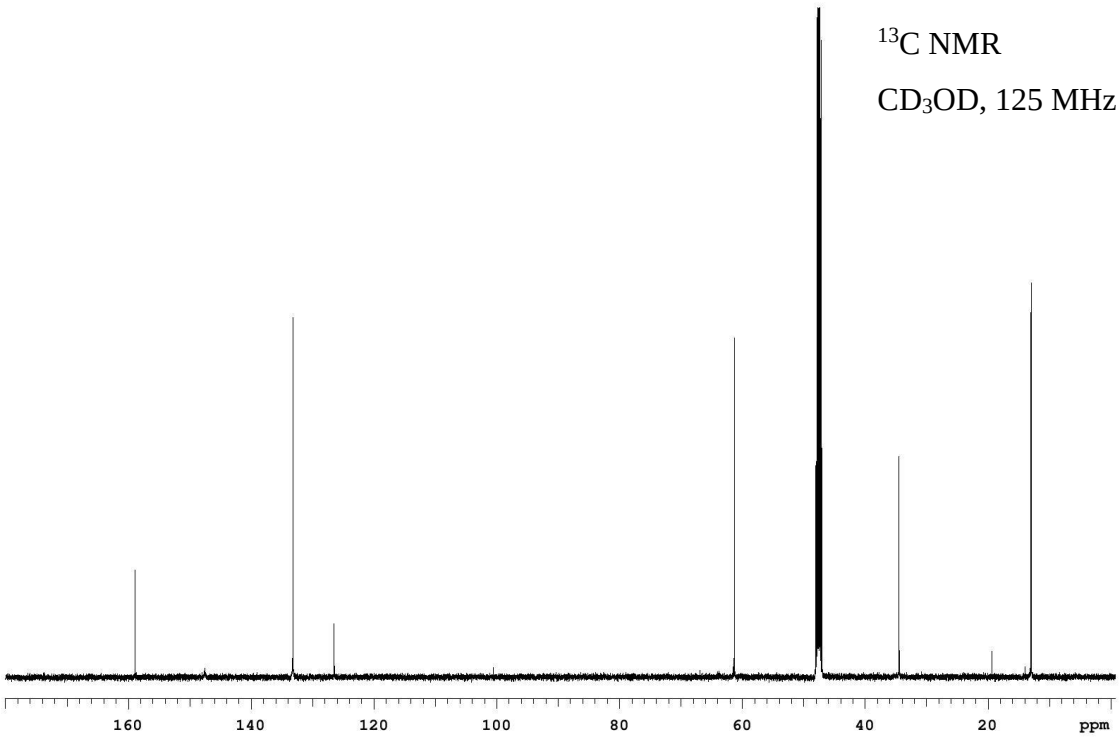

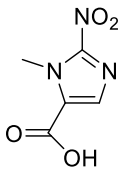

36

^{1}H NMR

CD_3OD, 500 MHz

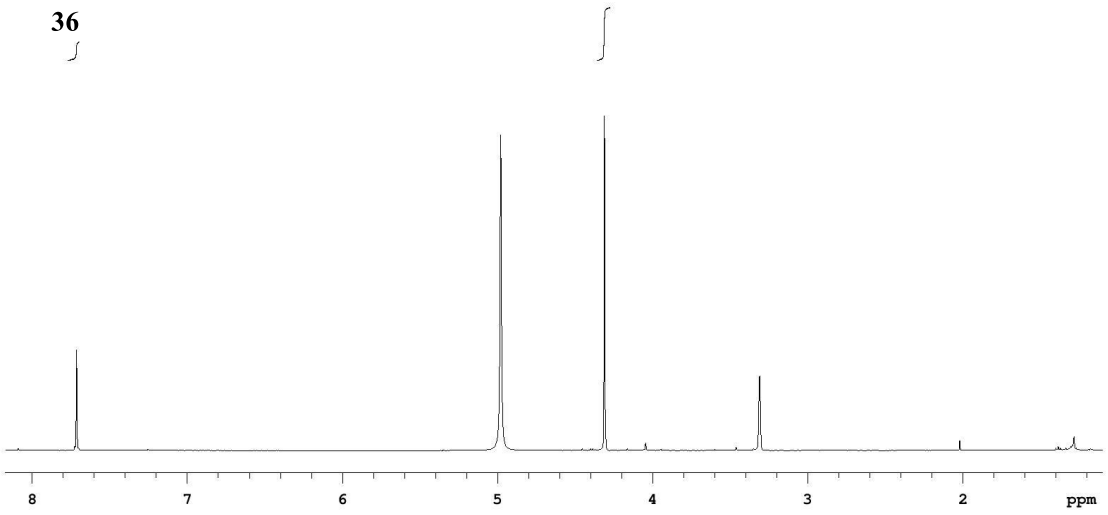

^{13}C NMR

CD_3OD, 125 MHz

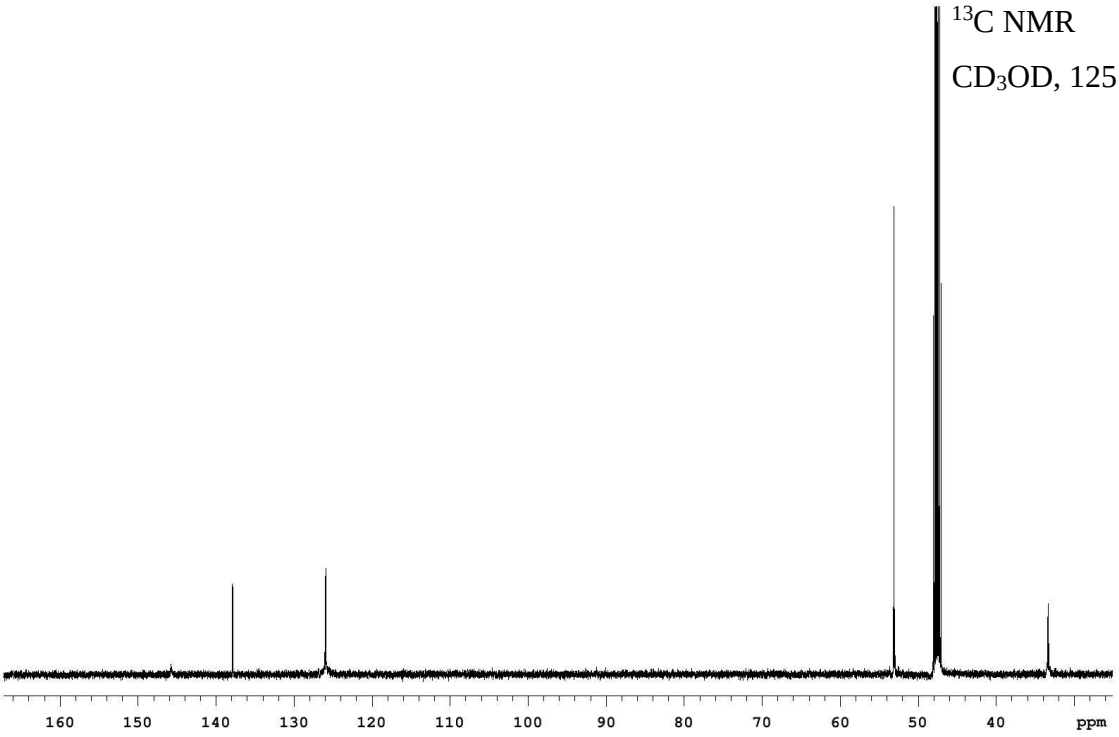

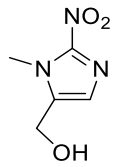

37

^{1}H NMR

CD_3OD, 500 MHz

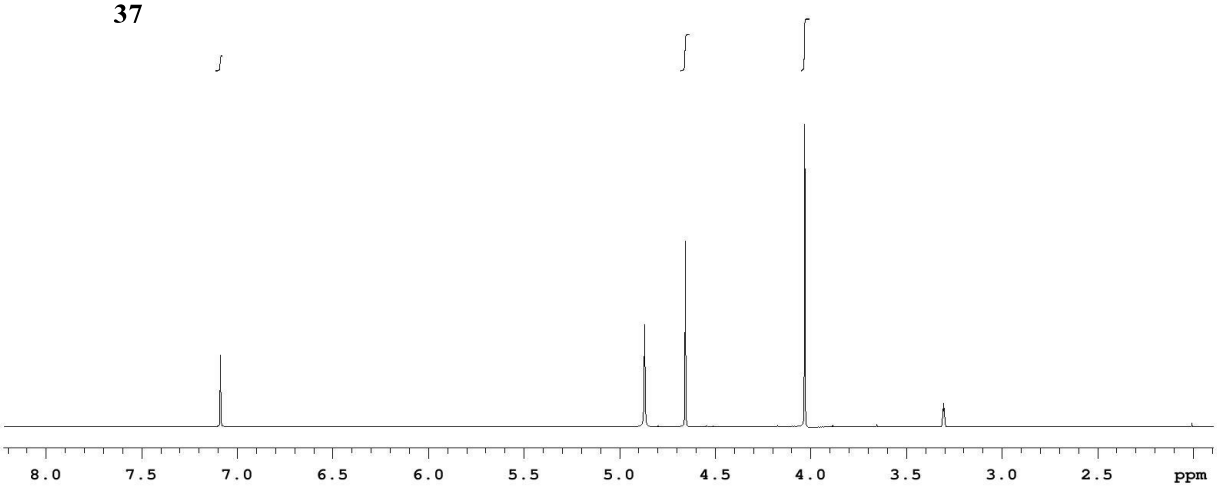

^{13}C NMR

CD_3OD, 125 MHz

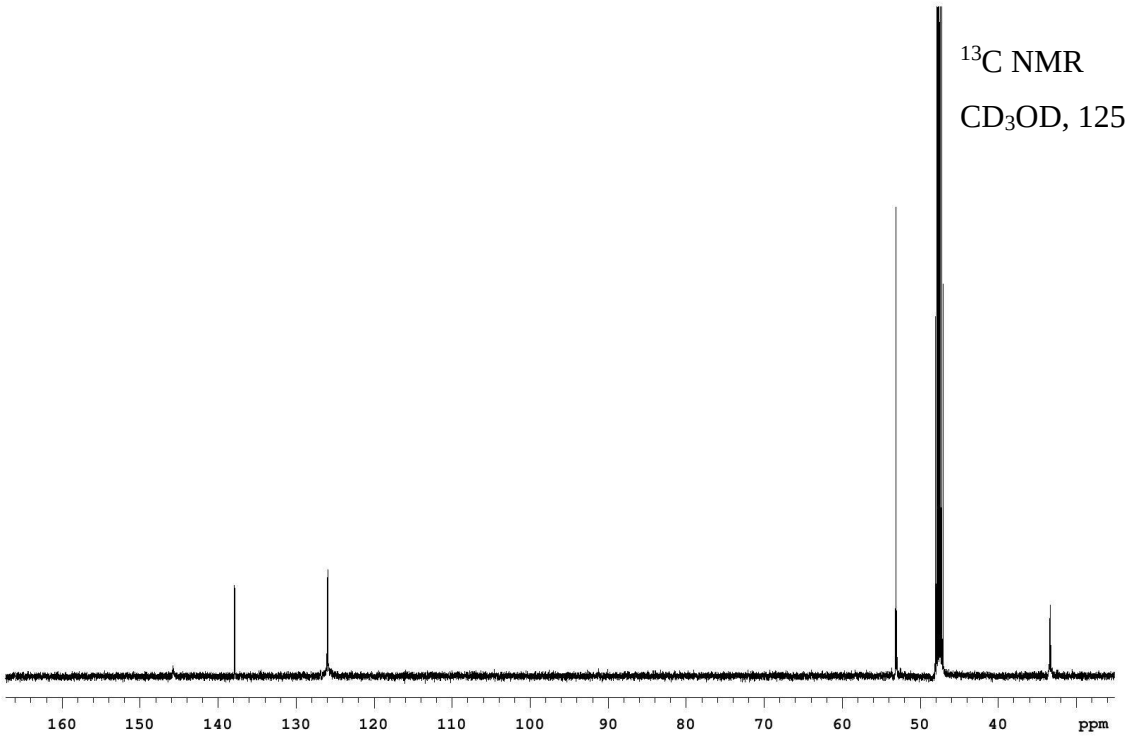

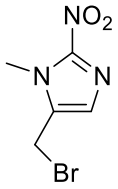

19

^{1}H NMR

$CDCl_3$, 500 MHz

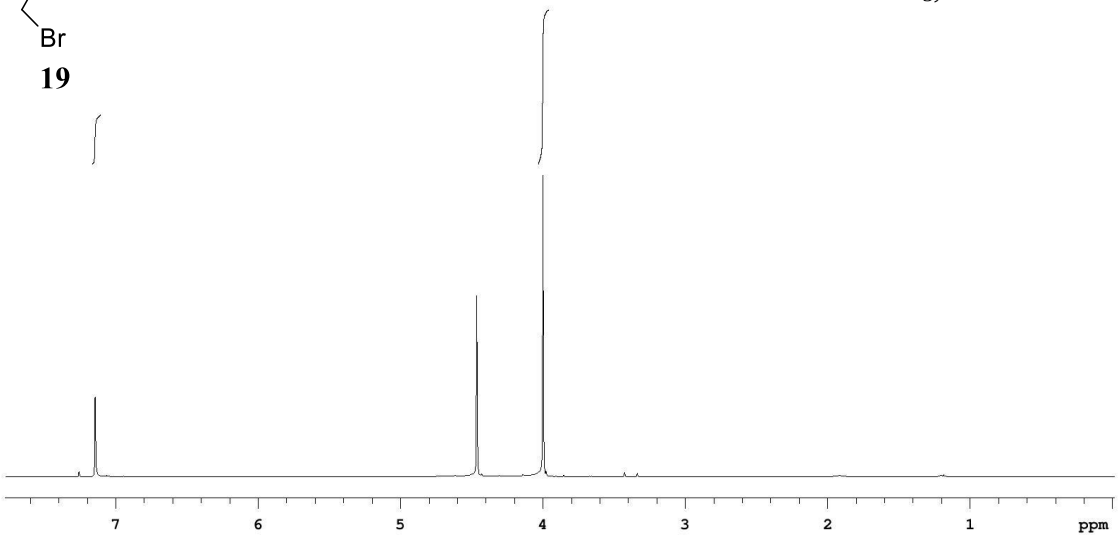

^{13}C NMR

$CDCl_3$, 125 MHz

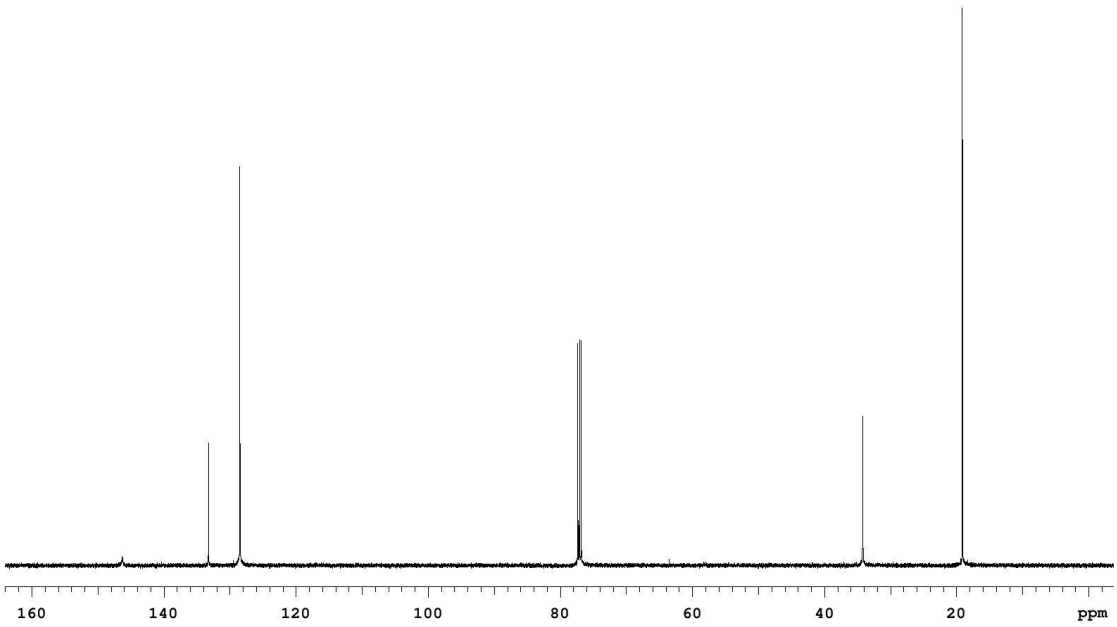

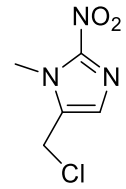

20

^{1}H NMR

$CDCl_3$, 500 MHz

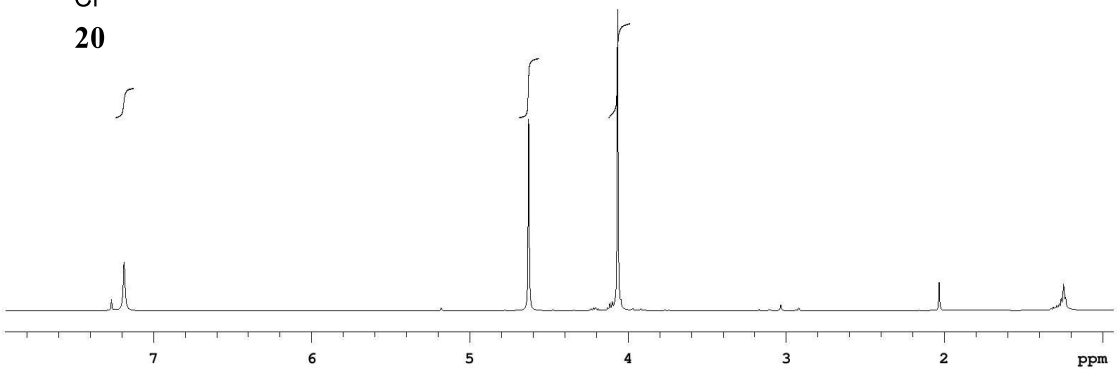

^{13}C NMR

$CDCl_3$, 125 MHz

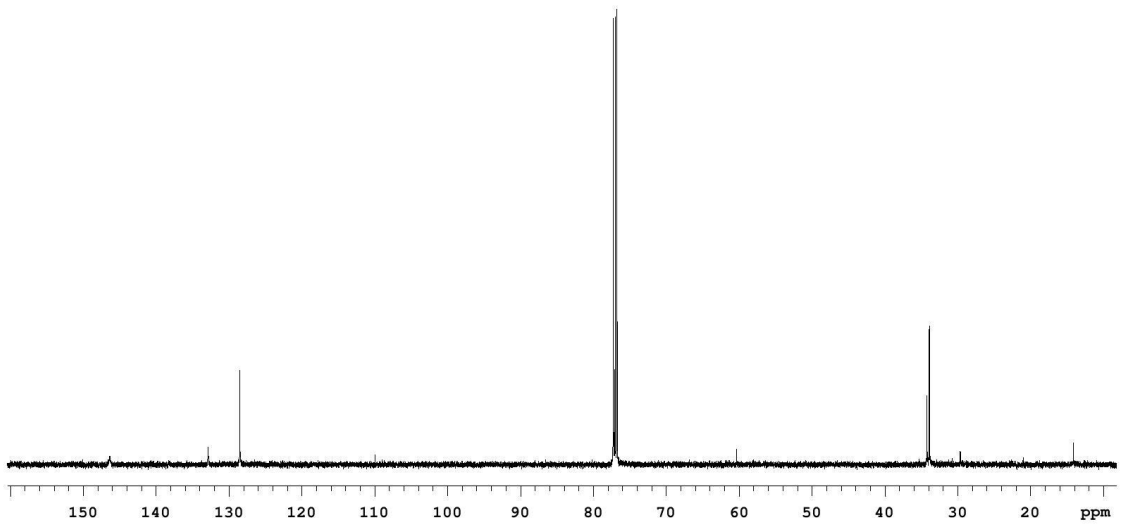

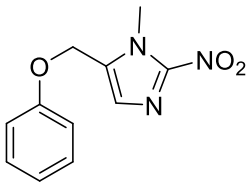

45

^{1}H NMR

$CDCl_3$, 500 MHz

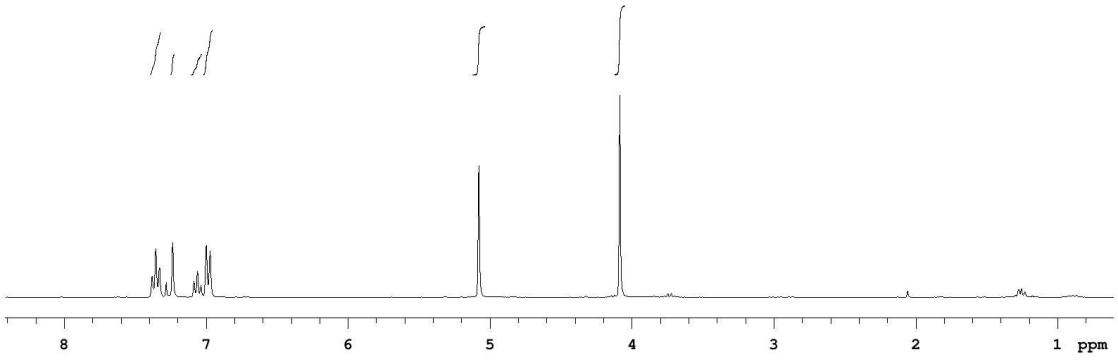

^{13}C NMR

$CDCl_3$, 125 MHz

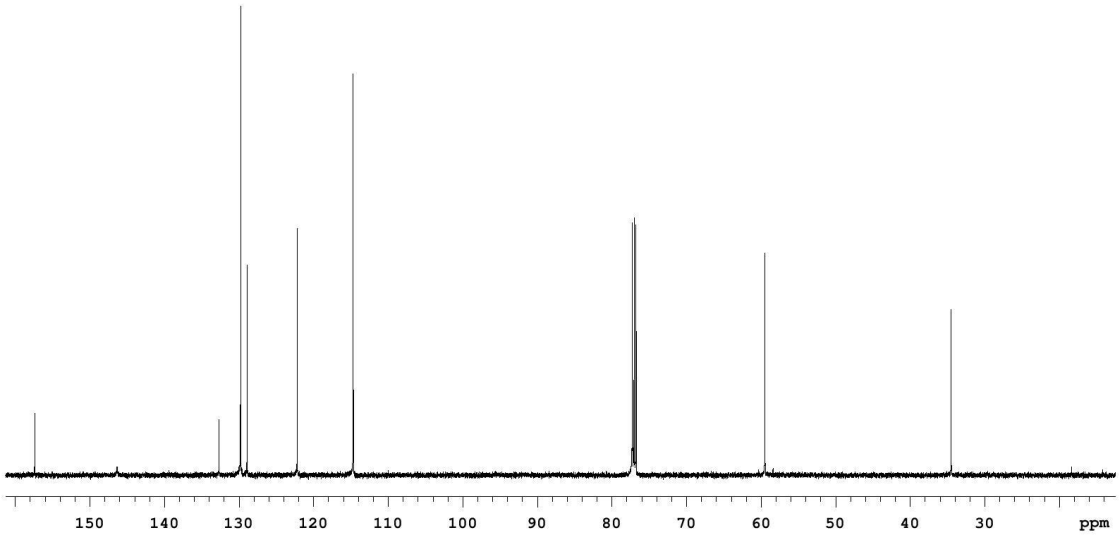

^{1}H NMR

$CDCl_3$, 500 MHz

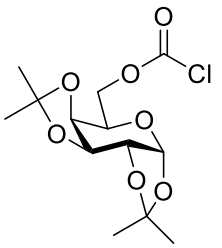

51

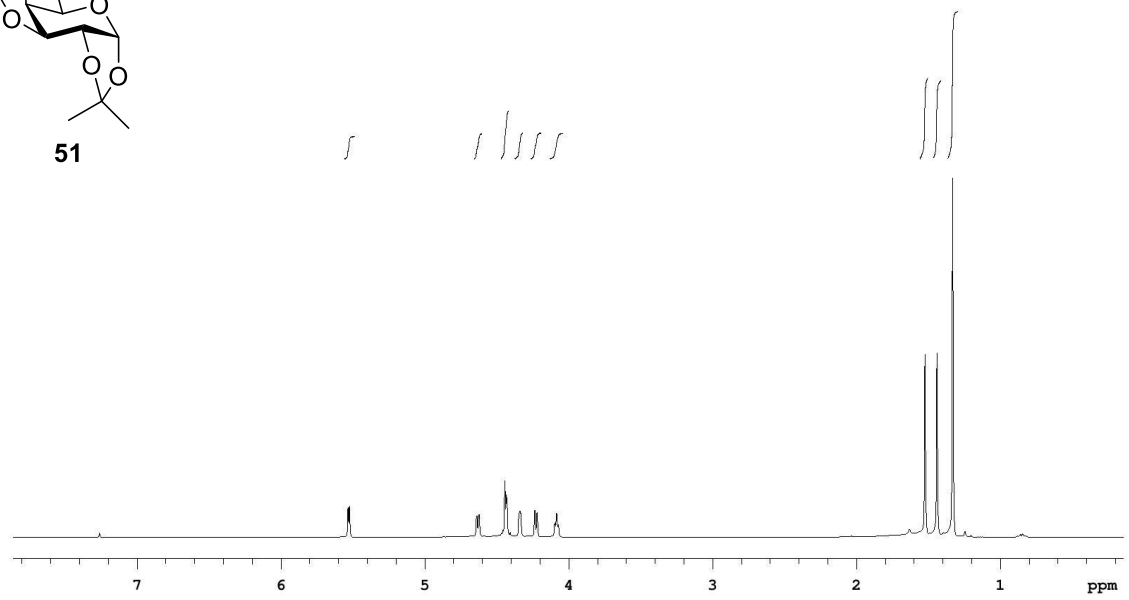

^{13}C NMR

$CDCl_3$, 125 MHz

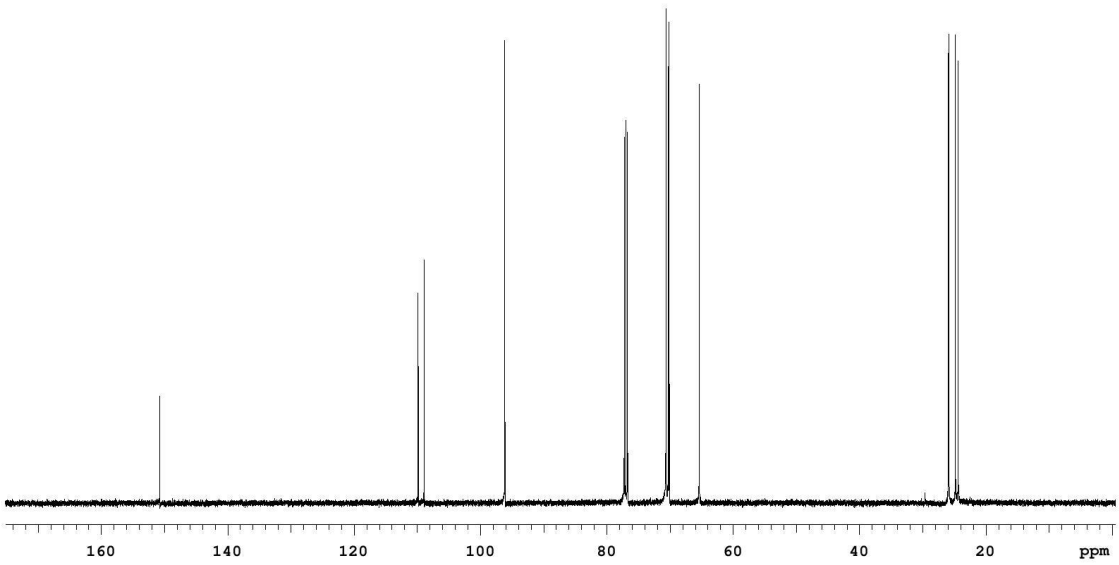

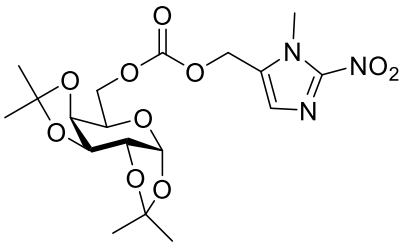

52

^{1}H NMR

$CDCl_3$, 500 MHz

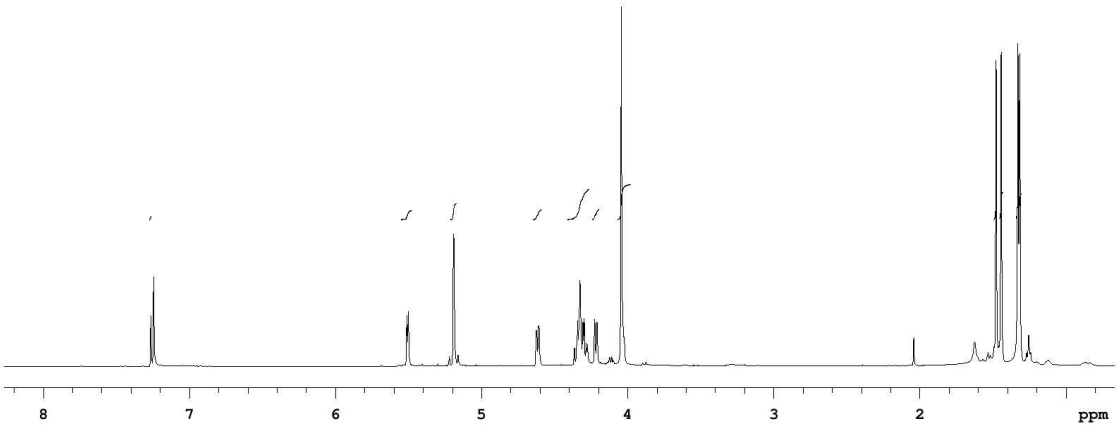

^{13}C NMR

$CDCl_3$, 125 MHz

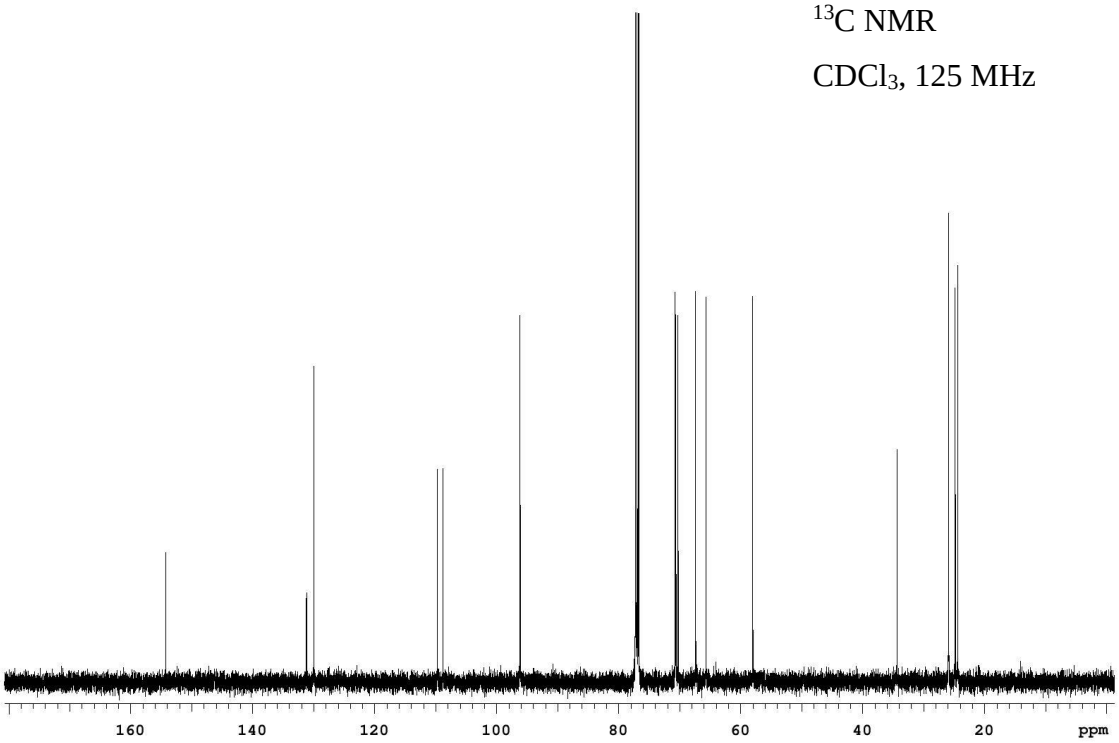

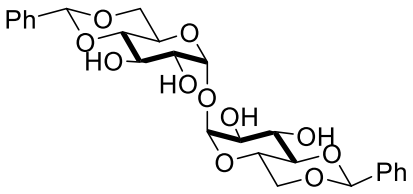

18

^{1}H NMR

CD_3OD, 500 MHz

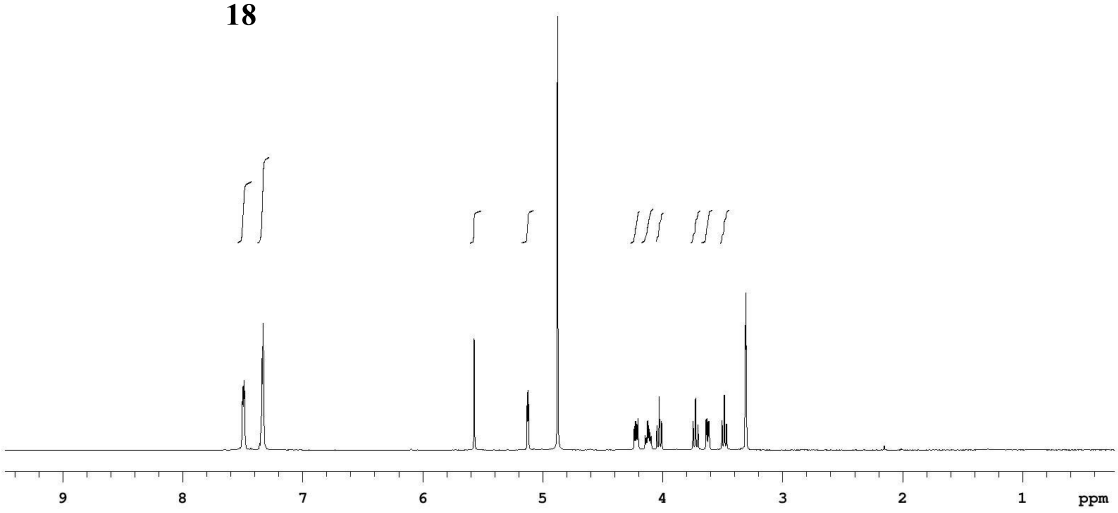

^{13}C NMR

CD_3OD, 125 MHz

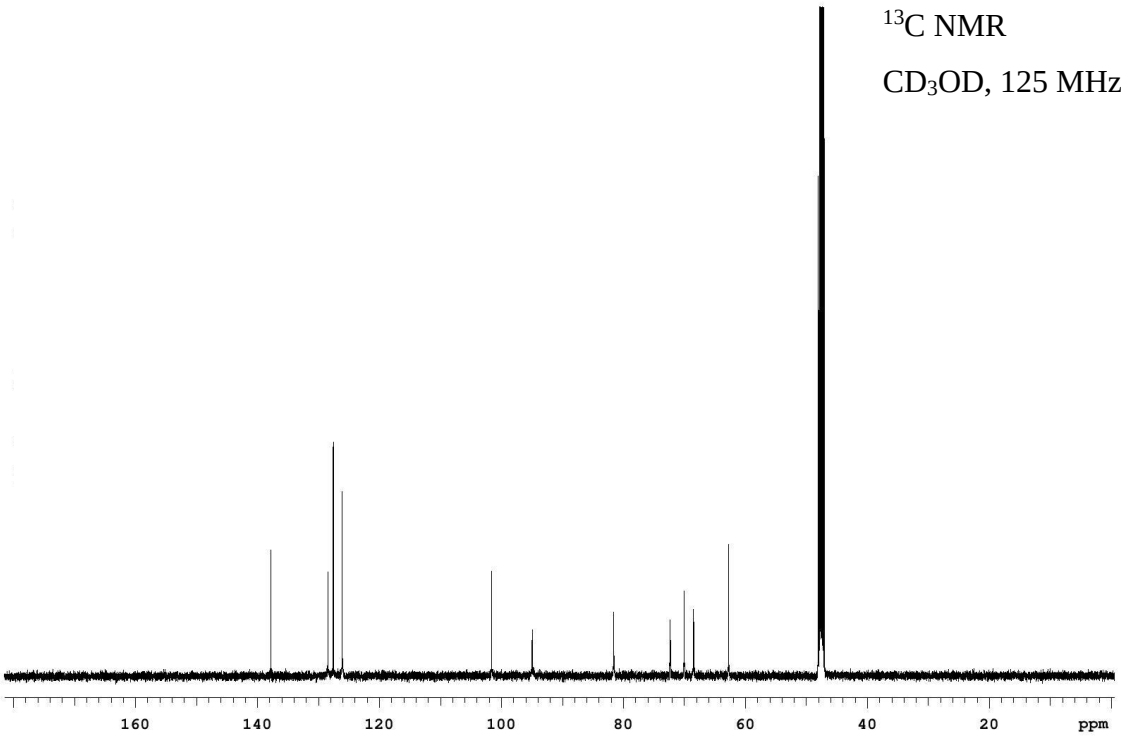

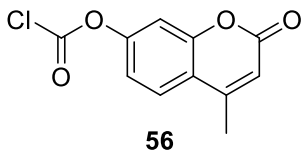

56

^{1}H NMR

$CDCl_3$, 500 MHz

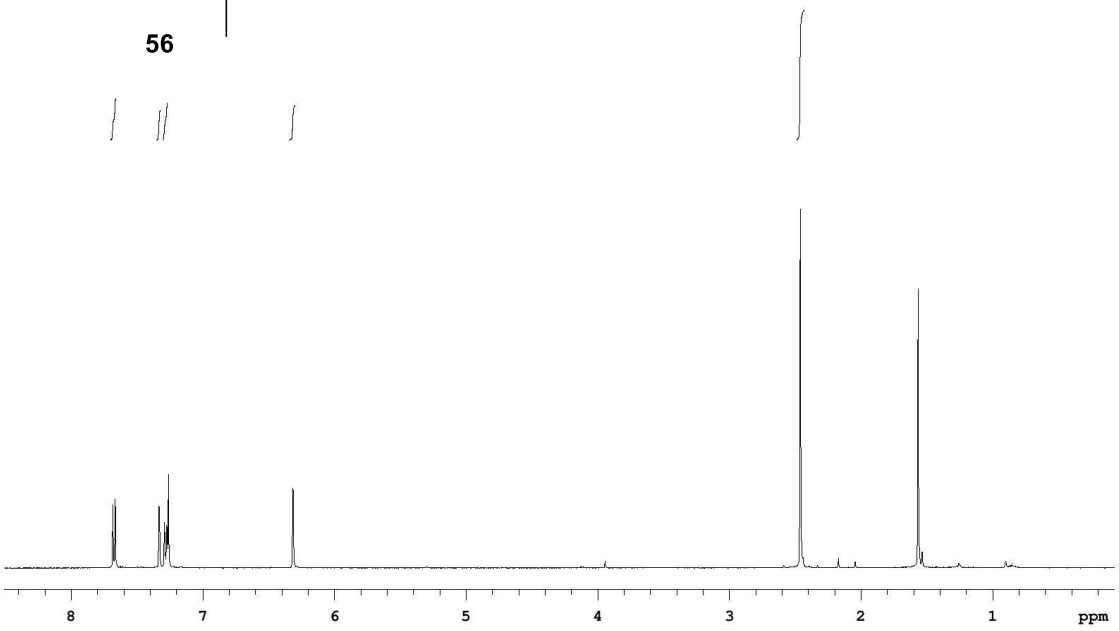

^{13}C NMR

$CDCl_3$, 125 MHz

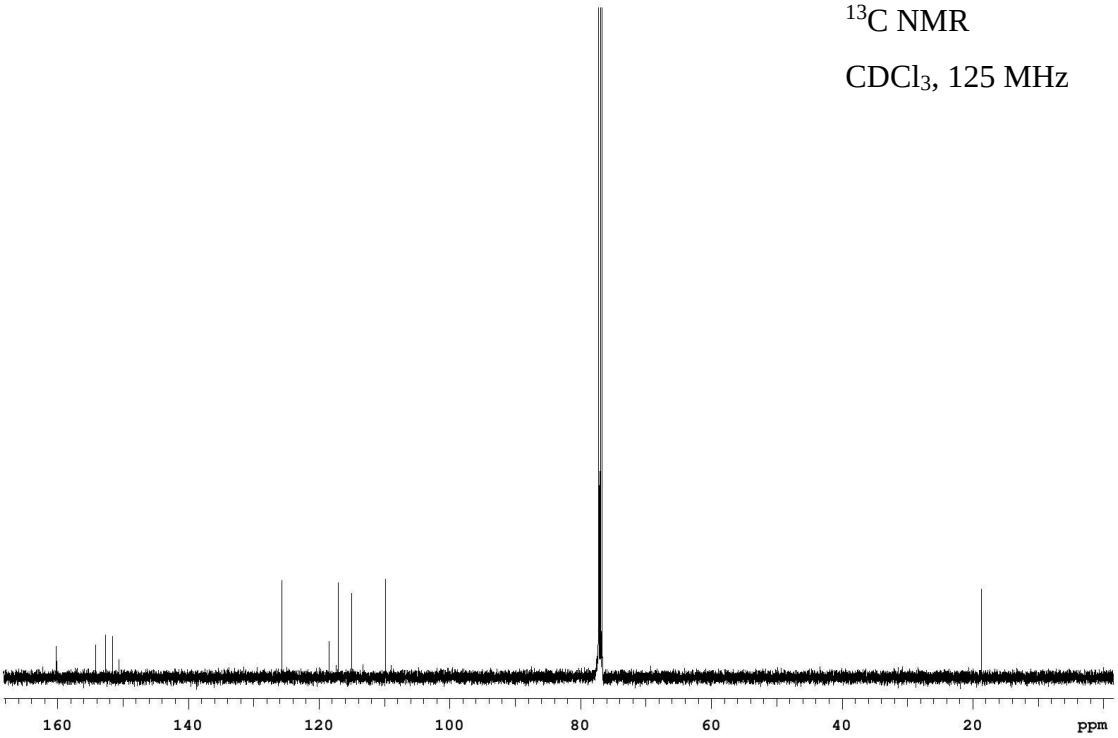

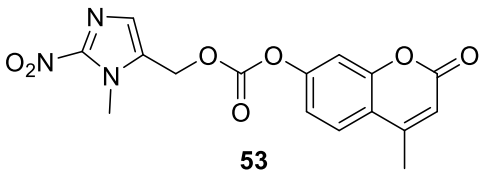

53

^{1}H NMR

$CDCl_3$, 500 MHz

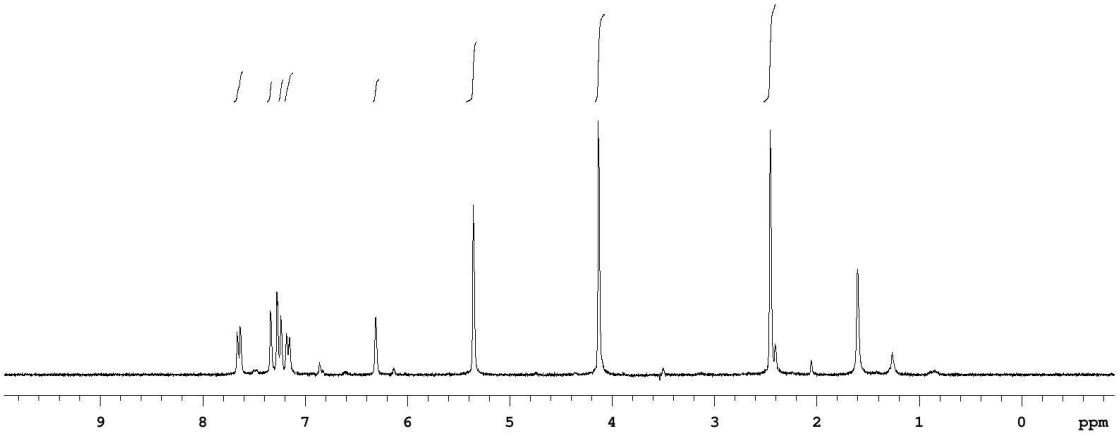

^{13}C NMR

$CDCl_3$, 125 MHz

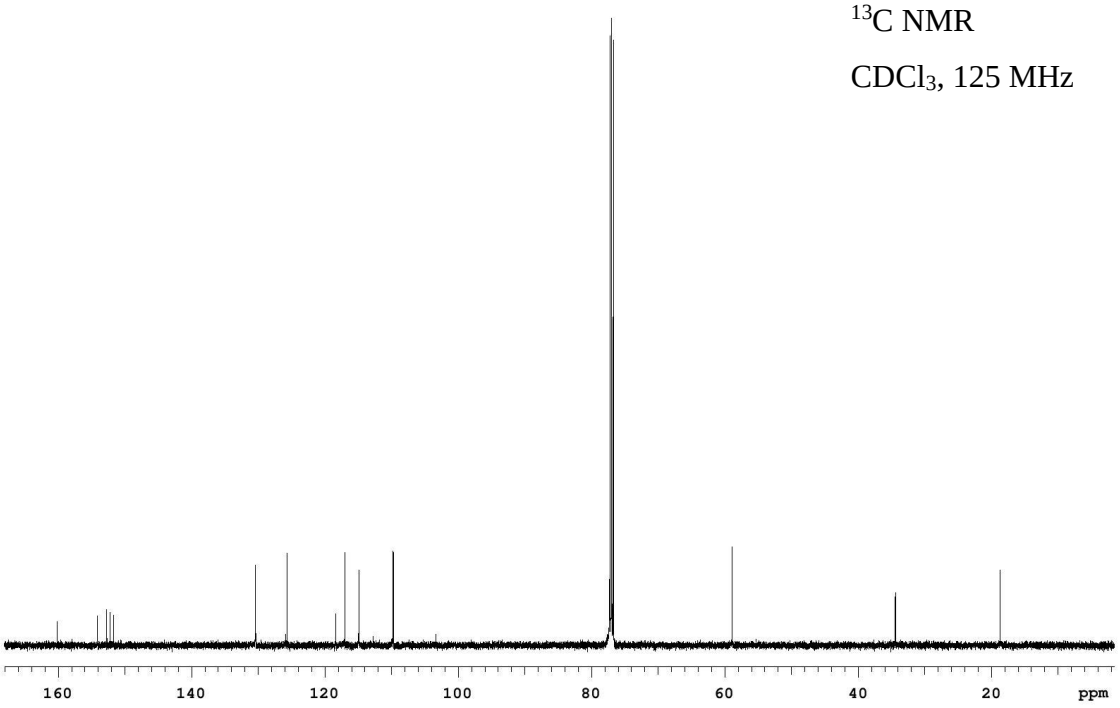

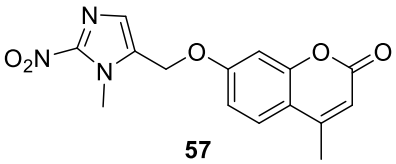

57

^{1}H NMR

$CDCl_3$, 500 MHz

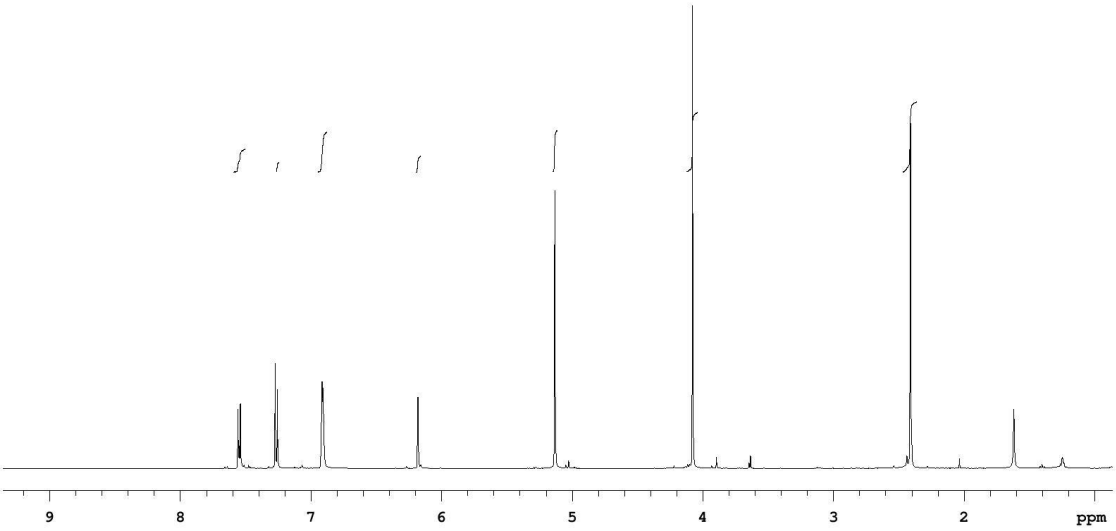

^{13}C NMR

$CDCl_3$, 125 MHz

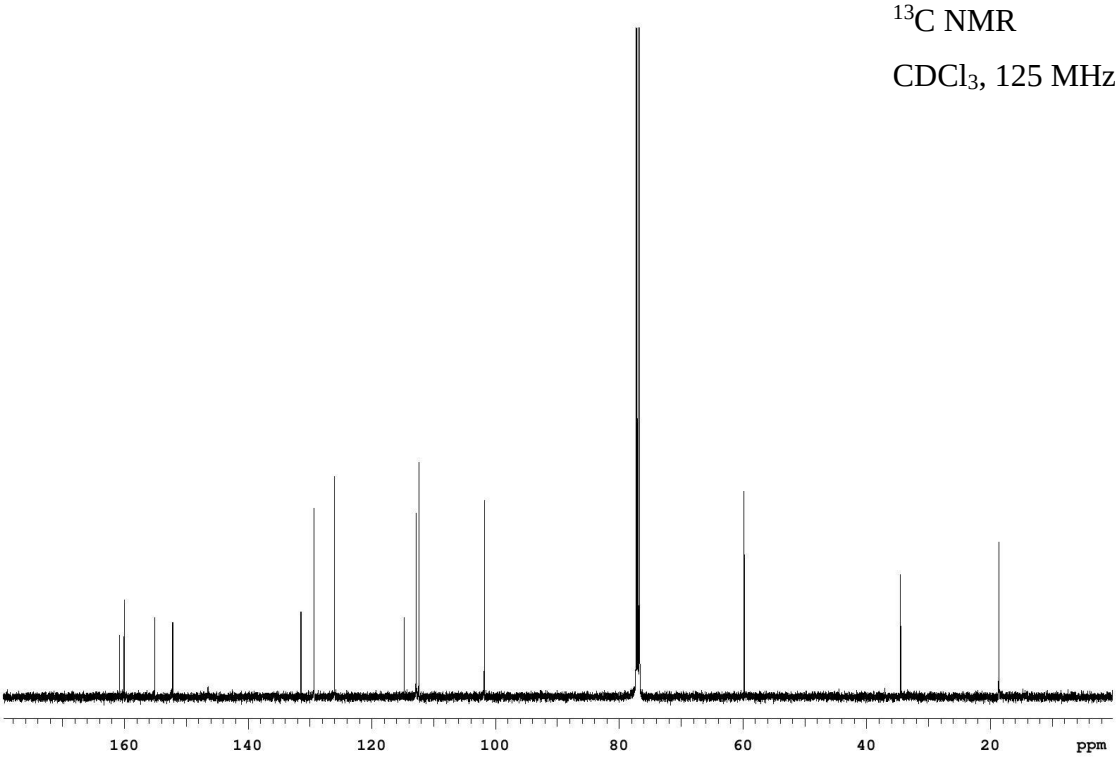

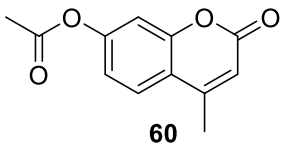

60

^{1}H NMR

CD_3OD, 500 MHz

^{13}C NMR

CD_3OD, 125 MHz

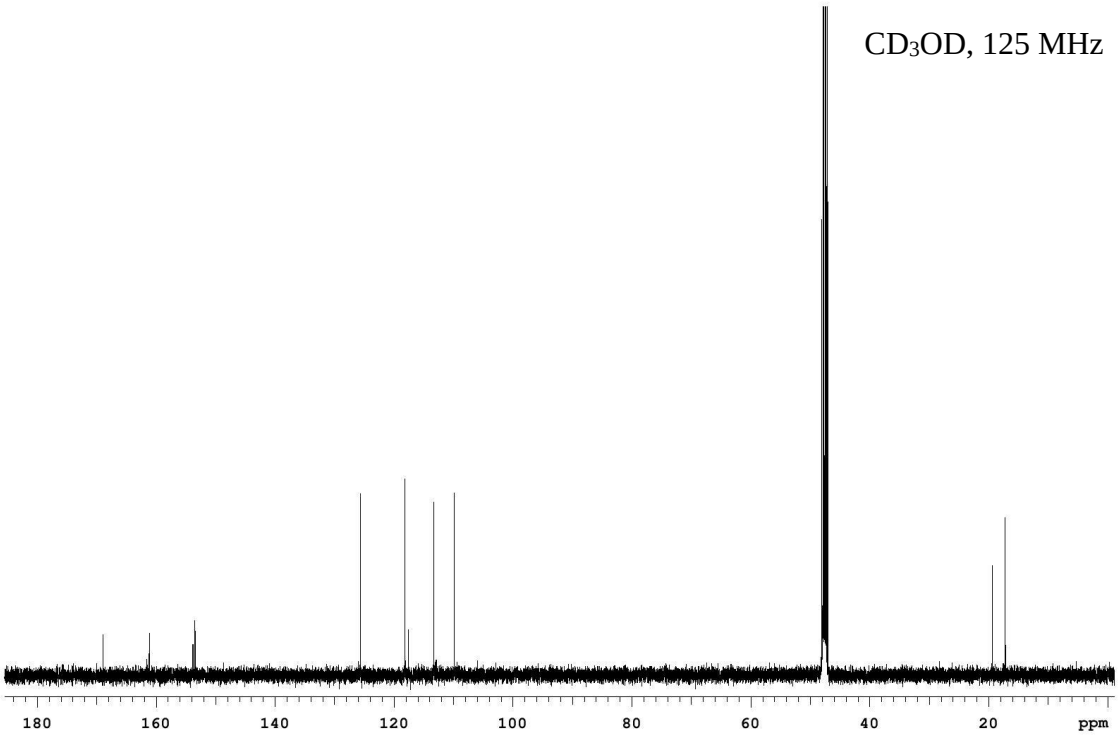

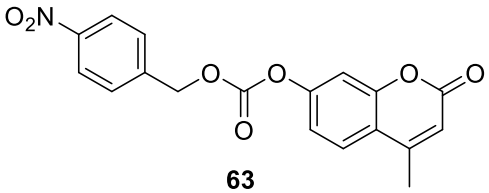

63

^{1}H NMR

$CDCl_3$, 500 MHz

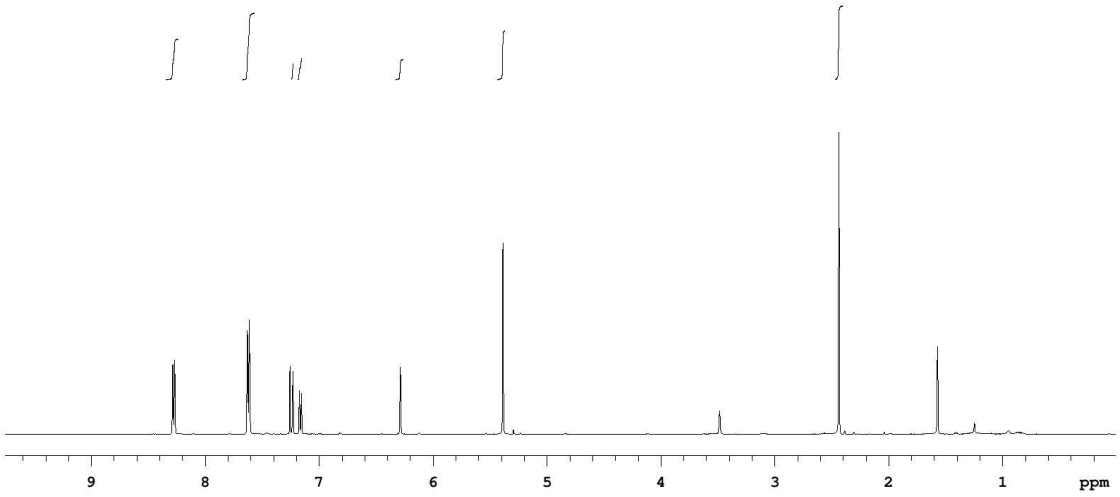

^{13}C NMR

$CDCl_3$, 125 MHz

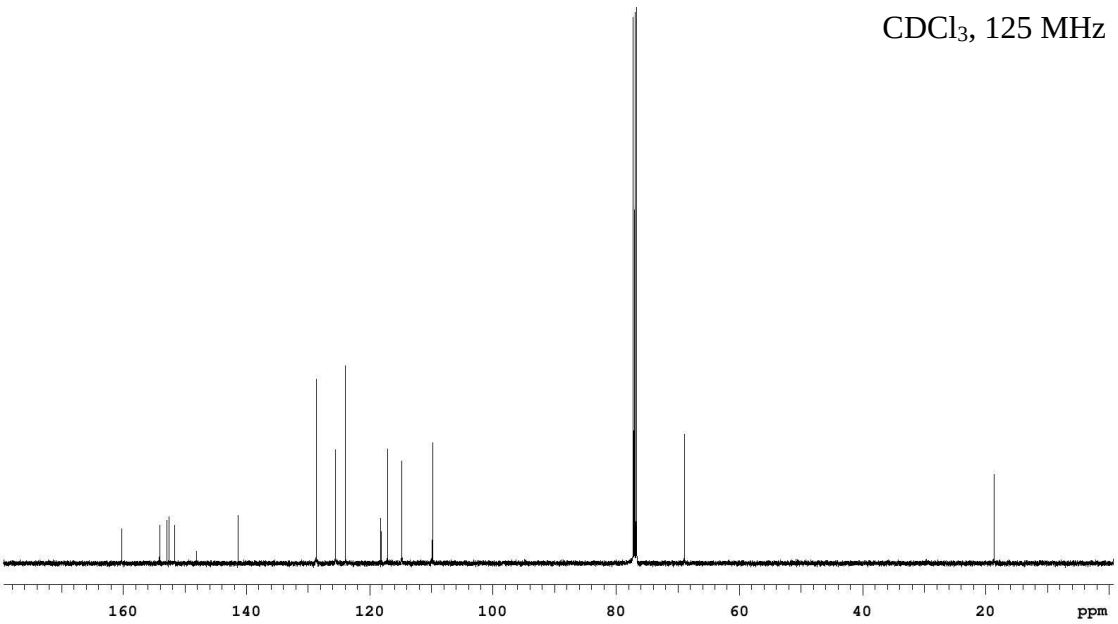

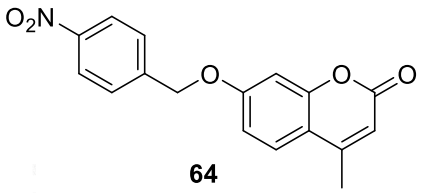

64

^{1}H NMR

$CDCl_3$, 500 MHz

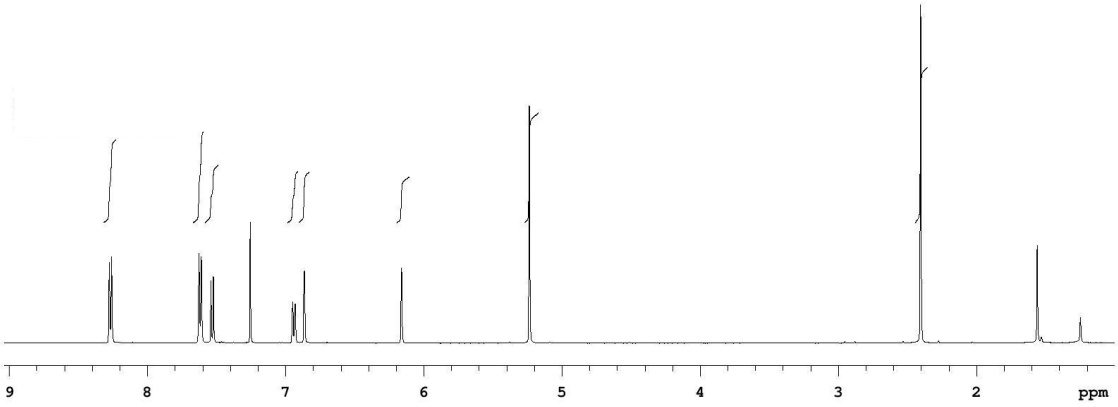

^{13}C NMR

$CDCl_3$, 125 MHz